FLUORESCENT NOBLE METAL NANODOTS FOR BIOLOGICAL APPLICATIONS

A Dissertation
Presented to
The Academic Faculty

By

Sungmoon Choi

In Partial Fulfillment
Of the Requirements for the Degree
Doctor of Philosophy in the
School of Chemistry & Biochemistry

Georgia Institute of Technology
December 2010

FLUORESCENT NOBLE METAL NANODOTS
FOR BIOLOGICAL APPLICATIONS

Approved by:

Professor Robert M. Dickson,
Advisor
School of Chemistry and
Biochemistry
Georgia Institute of Technology

Professor Mostafa A. El-Sayed
School of Chemistry and
Biochemistry
Georgia Institute of Technology

Professor Christoph Fahrni
School of Chemistry and
Biochemistry
Georgia Institute of Technology

Professor L. Andrew Lyon
School of Chemistry and
Biochemistry
Georgia Institute of Technology

Professor Niren Murthy
Wallace H. Coulter Department of
Biomedical Engineering and
School of Chemistry and
Biochemistry
Georgia Institute of Technology

Date Approved: October, 22nd, 2010

Acknowledgements

Time is so fast. I feel like yesterday I started Ph.D. course. During the course, I have learned a lot in class and in the Dickson lab. However, not all days were good. Sometimes, I was so frustrated and could not sleep well. Sometimes, I was so excited to do my research to make new materials and did not realize that the time was close to midnight. Before I started Ph.D. course, my old advisor told me that Ph.D. is not the degree itself, but a gold medal after wining a battle with myself. Now, I can absolutely understand that.

I would like to thank my advisor, Prof. Robert M. Dickson, to give me good opportunity to extend my knowledge and freedom which I can creatively think and do research. Also, I would like to thank my committee; Prof. L. Andrew Lyon, Prof. Niren Murthy, Prof. Christoph J. Fahrni, Prof. Mostafa A. El-Sayed to give me a lot comments and advices. Especially, I would like to thank the past and present members; Jeng-Cheng Hsiang, Sandeep Patel, Dulal Senapati, Chris Richards, Rusty Nicovich, Soonkyo Jung, Amy Jablonski, Chaoyang Fan, Nathan Hull, Parveen Sood, Andrew Khalil, and Aaron Danberry. Additinally, I would like to thank coworkers; Sungmun Lee, Bart Blackburn, and Michael Smith.

Finally, I would like to thank, but this word is not enough to express my heart to my parents, cousins, and my husband, Junhua Yu, for all the support, their constant understanding, endless patience, and unlimited encouragement.

TABLE OF CONTENTS

LIST OF TABLES

LIST OF SCHEMES

LIST OF FIGURES

LIST OF SYMBOLS AND ABBREVIATIONS

Φ	Quantum yield
S_0	Ground state
S_1	1st Excited state
σ	Absorption cross section
I	Intensity
τ_{on}	On time
τ_{off}	Off time
FCS	Fluorescence correlation spectroscopy
HOMO	Highest occupied molecular orbital
LUMO	Lowest unoccupied molecular orbital
k_{et}	Energy transfer rate
r	Radius
R_0	Hydrodynamic radius
FRET	Fluorescence resonance energy transfer
TCSPC	Time-correlated single photon counting
PEG	Poly ethylene glycol
APD	Avalanche photo diode
PMT	Photo multiplier tube
CCD	Charge coupled device
TCEP	Tris(2-carboxyethyl)phosphine
Sulfo-SMCC	4-(N-Maleimidomethyl) cyclohexane-1-carboxylic acid 3-sulfo-N-hydroxy succinimide ester sodium salt
DMEM	Dulbecco'sModified Eagle's Medium
PBS	Phosphate buffered saline
EDTA	Ethylenediaminetetraacetic acid
MWCO	Molecular Weight Cut-Off
GM	Goppert-Mayer units
PAMAM	Poly(amidoamine)
PG-*b*- PAA	polyglycerol-*block*-poly(acrylic acid)
PSS	Poly(styrene sulfonate)
anti-OP	Anti-OxPhos complex IV subunit Va mouse IgG2a
anti-HS	Anti-heparin/heparansulfate mouse IgG1
PLGA	Poly(D,L-lactic-co-glycolic acid)
DOTAP	1,2-Dioleoyl-3-Trimethylammonium Propane
MRI	Magnetic resonance imaging
BSA	Bovine serum albumin

SUMMARY

Commercial organic dyes are widely used for cellular staining due to their small size, high brightness, and chemical functionality. However, their brightness and photobleaching are not ideal for studying dynamics inside live cells. As an improvement over organics and much larger quantum dots, silver nanodots exhibit low cytotoxicity and excellent brightness and photostability, while retaining small size. We have utilized single strand DNA hairpin structures to encapsulate Ag nanodots. Compared to encapsulation within non-hair pin single strand DNA, Ag nanodots are dramatically improved with excellent spectral purity, high concentration, and good photophysical properties such as higher quantum yields and excellent extinction coefficients.

In addition, chemical and thermal stability of Ag nanodots is remarkably improved by modifying DNA hairpin structures. Their applications for multi-color staining were demonstrated by conjugating antibodies with several Ag nanodots respectively and staining the targets of interest in fixed cells. These new nanodots exhibit dramatically improved stability in live cells as well, when delivered into cells by microinjection. It suggests that Ag nanodots have great potential as an alternative to commercial organic dyes and quantum dots for cellular staining with excellent photophysical properties.

The great brightness and photostability of Ag nanodots indicate that they might be outstanding imaging agents for *in vivo* studies when encapsulated in delivery vehicles. Moreover, Ag nanodots can be optically modulated, which will improve the signal to noise ratio of optical imaging in high background environments. These good

characteristics are combined with delivery vehicles such as PLGA and nanogels. After encapsulation, Ag nanodots still retain their good photophysical properties and modulation. It might be useful for *in vivo* applications in the near future.

As another noble metal nanodot, gold nanodots are produced in single strand DNA as well and show red emission with high quantum yield, large Stokes shift, excellent chemical and photophysical stability. Their potential application as cellular staining agent was illustrated by co-staining with a commercial organic dye, in which Au nanodots displayed bright imaging and novel photostability. It could be a powerful cellular marker for biological application when time-gated imaging techniques are applied.

CHAPTER I

Introduction

1-1. Modern imaging and biological studies require better fluorophores.

Cellular staining/molecular imaging have been developing in divergent directions: Either towards macroscopic deep tissue *in vivo* imaging transmitted from the microscopic fluorescence imaging, or towards single molecule imaging to obtain information at much smaller scale and much more specific details.

Researchers continue to improve visualization and quantitation of molecular processes as they occur *in vivo* in their intact and native physiological states. [1-4] In the early 1960s, Winkelman performed the first quantitative study of fluorescence *in vivo* with exogenous fluorophores (porphyrin) using fluorometry and spectrophotometry.[5] Subsequently, more techniques and equipments were developed, such as fluorescence bronchoscope which use a mercury arc lamp or a CW (continuous wave) krypton-ion laser source and image target with an intensifier to amplify the faint fluorescence.[6, 7] However, some biological chromophores, such as hemoglobin, strongly absorb visible light, thereby limiting depth penetration at short wavelengths to a few tens of microns. There are also various fluorescent substances in various tissues, for instance, tryptophan, collagen, elastin, nicotineamide adenine dinucleotide, reduced form (NADH), flavin

mononucleotide (FMN) and porphyrins, obstructing the detection efficiency of target signals.[8] These noise sources for signal detection come to a minimum above 600 nm.[3] Other biological components are optically transparent from the visible to the near IR (NIR) but strongly absorb light in the infrared. Accordingly, for *in vivo* imaging, fluorophores that emit in the near infrared (NIR) window (600 – 1000 nm) are needed, as hemoglobin and water absorb minimally so as to allow photons to penetrate in tissue up to a few millimeters.[9, 10] Appropriate fluorophores were developed intensively, but their availabilities are still limited. A good *in vivo* fluorophore requires not only proper excitation/emission wavelength and high quantum yield, but also depends on several parameters to define the effectiveness of imaging agents in vivo, such as probe targeting, activation, pharmacokinetics and biocompatibility.[9] Among the NIR fluorophores, indocyanine green,[11, 12] methylene blue,[13] the polypentaemethine series,[14-16] as well as newly developed semiconductor quantum dots[17, 18] are frequently used.

Besides developing better fluorophores to yield higher signal intensity, there are also techniques to avoid autofluorescence and increase the signal to noise ratio. Time-gated imaging is one of them.[19, 20] Fluorescence from target is collected before or after autofluorescence becomes dominant.[21] Otherwise, a chromophore with long lifetime is used. After excitation, autofluorescence decays in a few nanoseconds and then emission from this chromophore is obtained.[22, 23] Either ways avert the co-occurrence of target emission and autofluorescence. Recently, Dickson group reported a new technique to increase signal to noise ratio.[24] Fluorescence of silver nanodots under primary excitation can be fluorescently enhanced under a secondary laser irradiation. However, most of the fluorophores show little such fluorescence enhancement. When the fluorescence of silver

nanodots is modulated at a certain frequency by the on/off of the secondary laser, a mixture of emission from both autofluorescence and silver nanodots is collected. Since only silver nanodots are modulatable, the signal from silver nanodots is recovered by demodulation to remove the high autofluorescence background, yielding much higher signal to noise ratio. This technique is potentially useful for further *in vivo* imaging application.

The other dramatic trend for molecular imaging is single molecule imaging. Thanks to the development of imaging technology, fluorophores and imaging method, single molecule imaging has been improved from just imaging particles at low temperature[25, 26] to room temperature,[27, 28] and finally applied to the investigation of individual events in biology, such as enzyme activities, protein-DNA interactions, as well as bioactive particle trafficking.[29-35] Contrary to ensemble measurements in which only average information of heterogenerous population is observed, single molecule imaging can real-time identify unique subpopulations and individual reaction intermediates with high spatial (nm) and temporal (ms) resolution, and obtain reaction rates, forces generated, stochastic fluctuations as well as enzyme conformations.[36-42]

The key to successful single molecule imaging is to obtain adequate signal to noise ratio. Background photon noise, as part of the total noise, poses the fundamental limit to the S/N ratio. To decrease the background noise, smaller excitation and detection volume also improve signal to noise ratio.[43] Near-field scanning optical microscopy (NSOM) which enables simultaneously topographic and single-molecule fluorescence imaging, has been applied on live cell membranes studies.[44] In addition, total internal

reflection (TIR) excitation of fluorophore also decrease the excitation volume to avoid the unnecessary excitation of surrounding fluorophore.[45, 46]

Nevertheless, a good fluorophore will benefit single molecule imaging. Some regular organic dyes are commonly applied to single molecule imaging, for instance, Cy3, Cy5, Cy 5.5, Cy7 from The cyanine family,[47-52] tetramethylrhodamine, rhodamine 6G, Texas Red from The rhodamine family,[26, 27, 53-57] and other commercial dyes from The Alexa® series.[58, 59] Moreover, fluorescent proteins[60-63] and semiconductor quantum dots[64-66] are also utilized as single molecule imaging fluorophores.

As mentioned, the key to molecular and fluorescence imaging is qualified fluorophores. Besides a proper excitation and emission wavelength, high fluorescence quantum yield is essential. To obtain more detected photons from fluorophores in some conditions, e.g. extremely low fluorophore concentration in single molecule imaging, or dim light excitation in *in vivo* imaging, maximizing the photon emission rate also requires shorter fluorescence lifetime and higher molar extinction coefficient of the fluorophore so that even at weak light excitation, there are still a lot photons absorbed by the fluorophore.[35] The ability to emit light at a certain circumstance is referred as brightness (B_e), which is determined by the molar extinction coefficient (ε, M^{-1} cm^{-1}) and the fluorescence quantum yield (Φ_F) at certain excitation/emission wavelength:

$$B_e = \Phi_F \cdot \varepsilon$$

At the single molecule level or any other level, the brightness can be modeled as

$$B_s = \Phi_F \cdot \sigma = \Phi_F \cdot \frac{2.303\varepsilon}{N_A}$$

Where σ is the absorption cross section of the fluorophores in unit of cm^2, and N_A is Avogadro number.

In the limit of low excitation intensity (I_{ex}, in unit of photon cm^{-2} s^{-1}), the photon emission rate (I_{em}, in unit of photon s^{-1} $molecule^{-1}$) of a single fluorophore can be calculated from the product of its brightness and excitation intensity:

$$I_{em} = I_{ex} \cdot B_s = I_{ex} \cdot \Phi_F \cdot \frac{2.303\varepsilon}{N_A}$$

Obviously, higher fluorescence quantum yield and molar extinction coefficient will boost the brightness of the fluorophore. For a typical organic fluorophore, $\sim 6 \times 10^4$ photons/s can be reached at a few hundred Watt cm^{-2} excitation.[67] Even with a 5% detection efficiency, 300 photons/100 ms can be obtained, which is enough for efficient imaging. The brightness/photon emission rate is a key parameter of qualified fluorophores for single molecule imaging as well as *in vivo* imaging.

However, brightness of a fluorophore is not the only consideration in choosing a fluorophore for molecular imaging. It should be also chemically and photophysically stable during the imaging, which enables long time, reliable data acquisition.[1, 68] However, photobleaching happens to most of organic fluorophores[69-71] as well as fluorescent proteins.[72-74] The photostability of a fluorophore is described by photobleaching quantum yield (Φ_B):[75]

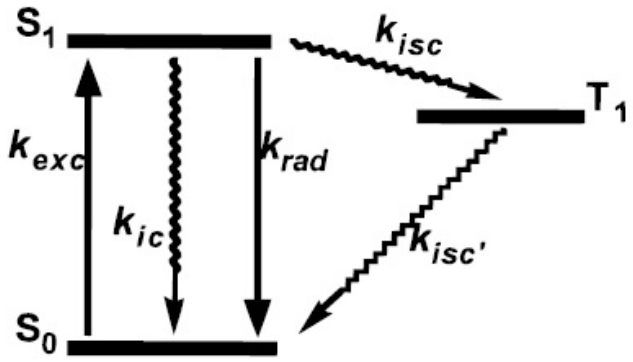

Scheme 1-1. Three-electronic-state diagram. k_{exc} : excitation rate, k_{rad} : radiative rate constant, k_{IC} : internal conversion rate constant, k_{ISC} : intersystem crossing rate constant, $k_{ISC'}$: triplet depopulation rate constant.

$$\Phi_B = \frac{k_{bleach}}{k_{rad}+k_{ic}+k_{isc}+k_{bleach}} \cong \frac{k_{bleach}}{k_{exc}}$$

where k_{exc} is the excitation rate, k_{rad} : radiation, k_{IC} : internal conversion, k_{ISC} : intersystem crossing, k_{bleach} : bleaching rate constant. Φ_B indicates the probability of photobleaching per photon absorbed. It depends on the structure of fluorophores and the environments the fluorophores are in, but neither on the excitation intensity nor excitation mode in the limit of low excitation intensity. For fluorescent proteins, it is around 10^{-5},[72, 76] whereas for organic fluorophores, it ranges from 10^{-7} to 10^{-4}.[77-80] In other words, good single molecule fluorophores typically emit only about 10^7 photons before photobleaching.[81]

The emission of organic dyes typically originates either from an optical transition delocalized over the whole chromophore (resonant dyes) or from intramolecular charge transfer transitions (CT dyes).[82] Most common fluorophores, such as fluoresceins, rhodamines, most 4,4′-difluoro-4-bora-3a,4a-diaza-s-indacenes(BODIPY dyes) and most cyanines are resonant dyes with high molar absorption coefficients, and moderate-to-high fluorescence quantum yields and characteristic narrow absorption and emission bands at a small solvent polarity–insensitive Stokes shift. However, the CT dyes have large Stokes shift, high sensitivity to solvent polarity due to their charge-transfer appearance. Generally, they also exhibit lower quantum yield and lower molar extinction coefficient.[83] Whereas, some near IR fluorophores are CT dyes per se, and typically have low fluorescence quantum yield. Since quantum yield, extinction coefficient, and photobleaching quantum yield are major criteria to select fluorophores, some dyes, such as cyanines, are chosen for *in vivo* and single molecule studies, especially in the near IR region. [47-52]

There are groups trying to improve fluorophore quality, especially on brightness and photostability. Willets *et al*. synthesized a series of fluorophores consisting of an amine donor and a dicyanodihydrofuran (DCDHF) acceptor linked by a conjugated unit to replace some fluorophores for single molecule imaging to achieve high extinction coefficient, high quantum yield, and photostability.[84-86] It is also reported that polyfluorination of cyanine dyes can improve photostability and fluorescence properties.[87] Otherwise, antioxidants were introduced to delay the photobleaching.[88]

Semiconductor quantum dots show not only excellent photostability, but also very large molar extinction coefficients on the order of 0.5–5 × 10^6 $M^{-1}cm^{-1}$, resulting in 10 -

100 fold increase in fluorescence brightness. [89-92] However, quantum dots have drawbacks as well, such as large size and potential toxicity. Our group developed a new class of fluorophore, water soluble fluorescent silver nanodots, showing excellent photophysics and reasonably small size. Before illustrating the advantages of the silver nanodots, fluorophores commonly used will be discussed.

1-2. Major fluorophores in use

There are a variety of emissive materials for cellular imaging. In addition to the most widely used fluorophores, organic dyes, metal-centered complexes are also used, such as d^6 or d^8 transition metal complexes, often based on Ru(II), Os(II), Re(I), Ir(III) and Pt(II), with metal-to-ligand-charge-transfer (MLCT) emission,[93-95] as well as lanthanide(III) complexes (Sm, Eu, Tb, Dy, Yb) with characteristic sharp emissions from f-f electronic states transition.[96-98] They usually have long luminescence lifetime (> μs), and their emission is sensitive to oxygen, suggesting their application only in bulk cellular staining, with high chromophore loading concentration.[99-103] However, as mentioned above, organic fluorophores have small size (< 1 nm), the most variety of excitation/emission choices, short fluorescence lifetimes, high fluorescence quantum yields and reasonable molar extinction coefficients. They are widely commercially available, with countless applications, and still under improvement, which are represented by rhodamine family,[104] cyanine family,[105, 106] BODIPY dyes[107] and Alexa series.[108]

Live cell imaging imposes challenges for the application of organic dyes. In some cases, a few copies of proteins need to be marked in live cells, which requires highly specific labeling in real time. However, it is rare for a general organic dye to react selectively with such particular proteins. The loading of organic dyes in bulk also leads to high background dye concentration and non-specific staining, resulting in strong fluorescence background. Fortunately, the discovery and utilization of fluorescent proteins in live cells solved this problem.[109-112] A protein of interest can be genetically

encoded with a fluorescent protein tag. When the protein is expressed, the fluorescent protein tag will also be expressed simultaneously, and consequently the location of the protein of interest can be traced. Moreover, fluorescent proteins can also be expressed in a particular type of cell and the expressed cells are used for cell trafficking in *in vivo* system by their fluorescence.[113, 114] Stemming from green fluorescent protein, several fluorescent proteins with varied emissions, functions and photostabilities have been developed.[115-117] While fluorescent proteins yield excellent specificity in labeling, they exhibit similar photophysics as organic fluorophores, e.g. fluorescence quantum yields of more than 60% and photobleaching quantum yield of around 10^{-5}.[72, 76] When recognizing the contribution of fluorescent proteins to live cell imaging, we have also realized their limitations, i.e., the relatively large fluorescent protein size (more than 3 nm) which brings in possible steric hindrance to the protein of interest and, more or less fewer choices of emission wavelength than commercial organic dyes.

Inspired by genetically encoded tags, some small size protein/peptides were developed, which show highly specific binding or reaction to a certain substrate specially modified with an organic fluorophore with or without the help of an enzyme. The protein/peptide genetically tagged to the protein of interest is also expressed simultaneously together with this protein of interest. The organic fluorophore is then reacting with the protein/peptide and the protein of interest gets fluorescently labeled.[118, 119] There are several systems following this protocol, including the biarsenical dyes such as FIAsH or ReAsH bind to the tetracysteine tag,[120] Ni ions bind to the hexahistidine tag,[121] and O^6-alkylguanine–DNA alkyltransferase that self-catalyzes the reaction between itself and enzymatic substrate derivatives.[122] The Ting group developed

exogenous enzymes, such as lipoic acid or biotin ligase, to link fluorophore modified lipoic acid or biotin to a small specific protein.[123-125] Other than fluorophore modified substrate, Nolan screened a 38 amino acid peptide that binds with a K_d of 25 pM to Texas red fluorophore.[126] These protocols take advantage of both wide variety of organic fluorophores and the highly specific labeling powered with genetic encoding. However, there are still limits on the intracellular availability of organic fluorophore modified substrate in living cells, restricting the wide applications.

No matter organic fluorophores or fluorescent proteins, they suffer from low brightness and photobleaching. On the contrary, quantum dots have complementary properties, with excellent photostability and 10 to 100-fold increase in fluorescence brightness due to very large molar extinction coefficients while maintaining high fluorescence quantum yields. These advantages attract numerous applications in cellular imaging, single molecule imaging as well as *in vivo* imaging.[83, 92, 127-133] However, the stability and photophysics of quantum dots highly depend on their surface protection which increases the quantum dot nanoparticle diameter, mostly more than 25 nm. The large size of such heavily protected nanocrystalline appendages further sterically hinders the target of interest, and they can aggregate because of non-optimal surface chemistry. Moreover, several biomolecules are typically attached to a single QD, leading to difficulty to control biomolecule orientation. The size also makes the dots cell-membrane-non-permeant.[83] Therefore, quantum dots are more or less good for cell surface staining,[134] otherwise, they have to be delivered into cells physically by microinjection,[135] electroporation,[136] or by conjugating to cell penetrating peptide and passing through cell membrane via endocytosis.[137] Concerns over their potential toxicity

in *in vivo* application are increasing, likely due to the release of toxic heavy metal building up the nanocrystalline, such as free cadmium. It is reported that CdS quantum dots degrade upon illumination,[138] oxidation,[139, 140] or in the presence of hypochlorous acid, a common biological oxidant present in many inflamed tissues.[141]

1-3. Improved gold nanodot emission

Tremendous applications of gold have been published.[142] Although it is much easier to find gold nanoparticles in the literature, emissive gold nanodots were reported at times. Similar to silver, defined gold nanodots, as referred as gold clusters then, were first prepared in rare-gas matrices.[143-147]. Au_2 in Ar matrices exhibits emissions at 286, 325, and 757 nm, with absorption at UV region. Whereas compared to Au_2, Au_3 in Ar matrices displays red-shifted emission at 529, 579, and 809 nm.[145] Emissive gold nanodots stable in ambient environments were synthesized later, mostly with the protection of thiol-rich derivatives, such as gluthathione (Au_{28}),[148] *meso*-2,3-dimercaptosuccinic acid,[149] alkanethiol[150, 151] or phenylethylthiolate[152]. Blue emission was reported with high quantum yields under the protection of dendrimer.[153-155] However, most of the emissions locate in red to near-IR region, with less than 3% quantum yields, depending on the nanodot size and the protection ligand.[149, 150, 152, 156-158] Recently, gold nanodots with higher emission quantum yields (>7%) were prepared under the protection of proteins[159] or carbohydrates.[160] The lifetime of such nanodots depends on scaffolds as well. For example, dendrimer protected gold nanodots exhibit nanosecond-scale lifetime, however, some monolayer-protected gold nanodots show microsecond-scale lifetime.

Though great improvement of their photophysical properties, gold nanodots are not yet as useful biological tools as gold nanoparticles. It is not clear that such properties are intrinsic and could not be better, or just because the better condition is not discovered yet. The photophysics of gold nanodots suggest their application may be limited in bulk imaging.

1-4. Silver nanodots emerging as promising fluorophores

It has been long ago found that bulk noble metal could be photoluminescent, but with very low luminescence quantum yield.[161] Fluorescent silver nanodots or silver clusters, as biological labels became applicable only after the synthesis of water-soluble, stable silver nanodots under the protection of dendrimer.[162] Many silver nanodots have been created in various scaffolds; the single stranded DNA (ssDNA) scaffold results in so far the best photophysical properties of silver nanodots with accessible tunability.[21, 163-173] They present spectrally pure emissions ranging from blue to near IR, showing up to 40% fluorescent quantum yields, mostly more than 120,000 M^{-1} cm^{-1} molar extinction coefficient, and small size (~ 2 nm) which largely results from the protection groups. In polyvinyl alcohol film, single silver nanodots display excellent photostability, > 60-fold more stable than general organic dyes.[167]

Moreover, they have single-component, nanosecond fluorescence lifetimes that are shorter than those of larger multiexponentially decaying semiconductor quantum dots.[83] Another advantage of silver nanodots is that they exhibit two photon absorption cross sections comparable to that of quantum dots, as large as 50,000 GM (Goppert-Mayer units, 10^{-50} cm^4 photon s^{-1}) while maintaining nearly an order of magnitude smaller hydrodynamic diameter.[174] In addition, the ssDNA or peptide scaffolds also afford mono-covalent link point to other bioactive target, resulting in more accurate conjugation and decreasing cross-linking and non-specific staining. All these excellent photophysical properties suggest that silver nanodots may be strong alternatives to

current fluorophores, combining merits of the outstanding photophysics from semiconductor quantum dots and reasonably small size of organic dyes.

1-5. A brief history of silver nanodots

Prior to creating bright, stable, water-soluble fluorescent silver nanodots, several emissive species made from silver or gold had been investigated. One such class of species is ligand-protected Ag(I) complexes. Reaction between silver bis(triphenylphosphine) nitrate with thiourea derivatives yields Ag(I) luminescent complexes, with blue emission only at low temperature (10 K).[175] However, luminescence of Ag(I) in silver-doped $NaY(PO_3)_4$ crystal is much stable, exhibiting similar but detectible emission at room temperature.[176] Another well-studied field is complexes of Ag(I),[177-179] Ag(I)/Cu(I),[180] Ag(I)/Au(I),[181] Ag(I)/Sb(V)[182] or Ag(I)/Re(VII)[183] in which more than one Ag(I) ion or a combination of the above metal ions form weak metal-metal bonds, and the silver in these complexes are called clusters. The number of silver(I) atoms in such silver clusters varies from 2 to 6, and most of them are prepared in organic solvents with emissions ranging from violet to near-IR, and exhibit sub-microsecond to sub-millisecond luminescence lifetimes.[177, 178, 180, 181, 184-192]

Besides Ag(I) clusters, Ag^0 clusters have also been produced on or within solid supports. Since reduced silver are quite vulnerable in ambient environment, with reduction potential decreasing from 0.799 V of the conventional silver electrode to -1.8 V of free silver atom,[193] it is important to apply an inert environment, or a protection group to stabilize the clusters. For example, silver clusters are generated in famous silver halide microcrystals used for photography. A few photons absorbed by these microcrystals create silver clusters from which green and red emission can be observed at low temperatures.[194, 195] Graphite has also been used as substrate for production of silver

clusters.[196] Moreover, atomic silver clusters reduced from silver oxide thin films to by UV light or femtosecond-laser irradiation have been also identified as the origin of strong luminescence observed.[197-199] Some silver salt clusters adsorbed on zeolite surface, for example, AgI on zeolite-Y[200, 201] or Ag_2S on zeolite-A,[202-204] can be also luminescent.[203-206] some groups ascribe the emission to Ag^0,[200, 201] while some still consider the emission is from silver salt clusters with long luminescence lifetime of microsends to miliseconds.[202-204]

Nano-sized metal particle, especially from silver and gold has drawn much more attentions.[207-211] Among the classified three size domains of these particles, i.e. large nanoparticles, small nanoparticles, and clusters (nanodots),[153] clusters were studied to understand the dependence of electronic, magnetic, structural, bonding, and reactivity properties on particle size bridging between isolated metal atoms and the bulk metals.[212, 213] Active metal clusters can be stabilized in rare-gas matrices by cryogenic matrix trapping techniques by which gaseous atomic or molecular species condense together with a large excess of an inert gas matrix on a suitable substrate at cryogenic temperatures.[214] Encapsulation by a rare-gas shell is essential to generate stable metal clusters with these methods.[215] Tremendous efforts have been applied to spectroscopic investigation of noble metal clusters in such rare-gas matrices, particularly silver[144, 145, 212, 213, 215-236] and gold clusters[143-147]. It affords data from ligand-free metal clusters to explore intrinsic chemical and physical properties of a few atom clusters. Silver clusters have also been generated in other rigid matrices, such as glass. Silver ion-doped glass is irradiated with light and silver clusters are then formed.[237] Similarly, the silver clusters exhibit UV

absorption. On the other hand, their emission is quite broad, spanning the whole visible region.[238]

The difference in the emission bands indicates that environments of the clusters are important. The rare-gas wrapped clusters only reflect the"true" properties of ligand-free silver clusters. However, for more complicated system, the proper building unit of clusters is the cluster plus surrounding interface region. Silver clusters should be produced in solutions and this is fulfilled by γ-radiolysis of silver ions.[239] Henglein and coworkers were the first to find that long-lived (for minutes and hours) intermediate clusters were formed in the γ-irradiation of $AgClO_4$ solutions containing polyphosphates at the early steps of the reduction process. These clusters included a few silver atoms and were the precursors of the colloidal metal.[227, 240] Water[241, 242] and other organic solvents, such as methanol,[243] ethanol,[244] 2-propanol,[239] supercritical ethane,[245] are applied as media. As expected, the lifetimes of such active species in ambient environments are quite short, just a few seconds to a few minutes due to lack of proper protection.[241] The polyanions, such as polyphosphate,[246] poly(acrylic acid),[247] polyacrylate,[248-250] are then added into the aqueous silver ion solution to prevent the cluster agglomeration due to the repulsion between the polymer chains, and the lifetimes are extended to hours or even weeks at room temperature.[246]

1-6. Current synthesis methods

Fluorescent silver nanodots generated in rare-gas, graphite, glass or zeolite are of interest to study the basic properties of metal clusters, to develop photoresponsive materials and catalytic materials,[206] but it is not likely to be applied to molecular staining since the lack of good compatibility. Moreover, an ideal fluorophore for such staining should be chemically and photophysically stable, bright, sterically invisible, less-toxic and manipulatable to conjugate to targets. As mentioned previously, it is easy to create silver nanodots by reduction or photoactivation, but to keep these vulnerable nanodots stable in ambient environments, a "strong" protection group is indispensable, not only to prevent these nanodots from agglomeration, but also to afford a platform for the formation of silver nanodots. Silver ions are bound to the protection group, followed by reduction. The reduced silver atoms merge to form silver nanodots.[246] The Dickson group for the first time prepared stable, water soluble, fluorescent silver nanodots with dendrimer protection.[162] Thereafter, numerous efforts have been attracted in this field. Currently, there are mainly a few scaffolds to prepare silver nanodots.

A. <u>Dendrimer protected silver nanodots</u>

Dendrimers are repeatedly branched large molecules. The specific construction of dendrimer, particularly poly(amidoamine) (PAMAM), presenting roughly spherical space with amino groups indenting inside the whole molecule, offers excellent capability to protect metal ions as well as nanoparticles.[251, 252] In the first generation of stable, water soluble, fluorescent silver nanodots, fourth- and second-generation OH-terminated

PAMAM and silver ions at were mixed a 1:2 molar ratio and irradiated with blue light from a band-pass-filtered mercury lamp through a standard epifluorescence microscope. Stable silver nanodots were observed with emission maxima at 533, 553, 589, 611, and 648 nm. These clusters are bright and photostable. Even with weak mercury lamp excitation (30 W/cm^2), they are readily observed at the single molecule level.[162]

Other dendrimers, for example, amine-terminated, ethylenediamine core generation 5 poly(amidoamine) dendrimer (PAMAM_E5.NH2) and its succinamic acid (PAMAM_E5.NSAH) and glycidol derivatives (PAMAM_E5.NGly), are also used to protect silver nanodots.[165] A dendrimer:silver ion molar ratio of 1:25 was used and, similarly, reduced silver atoms were created with UV light photoactivation, as referred by the authors as [$(Ag0)_{25}$-PAMAM_E5.NH_2] nanocomposites, which display blue emission in the range of 400-500 nm.

B. Polyelectrolyte protected silver nanodots

Similar to dendrimers, polymers have also been applied for the protection of reduced metal, but mostly result in nanoparticle formation when reducing agent is used.[253-257] However, when silver ions are photoactivated, silver nanoparticle remains small, and in some cases, silver nanodots are formed, likely due to the strong protection of polymer and slow reaction rate (lower local concentration of reduced silver atoms). In those reported polyelectrolyte protected silver nanodots, acrylic acid acts as a core component.

Sodium polyacrylate was used by Ershov *et al*. to protect silver clusters generated by exposure to a pulse of high-energy radiation. Though absorption from silver clusters (Ag_2^+) was observed, emission from these clusters was not reported.[249, 250] Treguer *et al*.[258] observed silver nanodot emission adsorbed on colloidal silver nanoparticles stabilized with polyacrylate, while it might be difficult to assign where the emission came from. Zhang *et al*.[259] synthesized poly(N-isopropylacrylamide-acrylic acid-2-hydroxyethyl acrylate) (poly(NIPAM-AA-HEA)) microgel particles. After mixing the microgel dispersion and silver ions at a molar ratio [Ag^+]:[COOH] of 1:1 for 30 min, mixture was subjected to UV-irradiation. Fluorescent silver nanodots were then created with an emission maximum of 610 nm. In this report, longer irradiation led to the final generation of non-emissive, large size nanoparticles.

Quite similar to the above hydrogel particles, polyglycerol-*block*-poly(acrylic acid) (PG-*b*- PAA) copolymers were recently prepared and silver nanodots were created by keeping molar ratio of acrylic acid groups to Ag^+ ions at 2:1.[170] The emission from these silver nanodots displays a broad peak spanning the wavelength range of 450–750 nm, while centered at about 590 nm. Analogs of poly(acrylic acid), such as poly(methacrylic acid) with a smaller molecular weight of 10kDa, were also utilized as silver nanodot protection groups.[163, 169, 260]

Both polyelectrolyte protection and photoactivation are not prerequisites to generate stable fluorescent silver nanodots. Poly(styrene sulfonate) (PSS) was used as protection group and mixed with silver ions. However, only silver nanoparticles were produced even though UV/Vis irradiation was used as the reduction method.[261] Interestingly, when silver ion forms complexes with 3-(2-

aminoethylamino)propyltrimethoxy silane before it is added into poly(acrylic acid) solution, fluorescent silver nanodots can be created by chemical reduction of a mixture of poly(acrylic acid) and the silver-silane complexes.[172] The chelation of amino silane might prevent fast nucleation of reduced silver atoms. Silver nanodots in such polyelectrolyte protection exhibit mainly red emission, with a few percent fluorescence quantum yield.

C. Peptide/protein protected silver nanodots

Silver ions have long been used for cellular staining to reveal nucleoli in which silver ions bind to some argyrophilic proteins in these nucleoli, such as nucleolin.[262-264] Yu *et al*. incubated silver ions with formaldehyde-fixed cells and fluorescent silver nanodots were generated in nucleoli. Inspired by the strong binding ability of nucleolin to silver ions, they also created short peptides based on nucleolin to protected silver nanodots.[21] These peptides are less than 18 amino acids long, with a molecular weight of < 2.5 kDa – much smaller than quantum dots. However, similar to polyelectrolyte-protected silver nanodots, their fluorescence quantum yields are low, about 3% with red emission.

Another protein, bovine pancreatic R-chymotrypsin, was also utilized for protection of silver nanodots.[265] The size of nanodots as observed with high resolution TEM (HRTEM) was about 1 nm, larger than the reported less than 10 silver atoms in fluorescent silver nanodots. However, it is hard to verify the emission was derived from such silver nanoparticles or from some small, invisible clusters.

However, when a smaller peptide is applied as protection group, other extra procedures have to be performed to obtain stable silver nanodots. Thiol-rich peptide, glutathione, has strong affinity to silver ion. It has also been used as a protection group.[266] The nanodots were prepared by repeated reduction of glutathione/Ag^+ mixture in oxidative conditions. However, the quantum yield was not reported, but indicated that, interestingly, red emission was produced as well. It is not clear why the red emission was created with peptide protection.

D. Oligomer ssDNA protected silver nanodots

ssDNA was for the first time applied for silver nanodots synthesis by Petty *et al*. in our group.[166] With single stranded 5′-AGGTCGCCGCCC-3′ as a template, a mixture of several emitters was prepared with red-centered emissions. The creation of silver nanodots in a ssDNA scaffold is both nucleotide- and time-dependent. This phenomenon was more recently also reported by Gwinn *et al*.[173] Hairpins with C or G bases as loop bases created about 10-fold higher emission compared to that of A as loop bases. Interestingly, the hairpin with T as loop bases could not produce any emissive species. In this report, they also found that, both with C as protection group, single strand oligo C produces brighter silver nanodots emission than C bases in hairpin loop. The number of C bases in the hairpin loop also influences the yield of fluorescence intensity from silver nanodots.[267] The concentration of ssDNA is another factor to influence the generation of silver nanodots. Higher ssDNA concentration favors a red-emitting species.[268] However,

in the above cases, multi-emitters with emissions in blue, green, red region, as a mixture in the DNA-Ag solutions, are generated.

The synthesis of silver nanodots was greatly improved when DNA microarrays were used to screen ssDNA sequence being able to protect silver nanodots.[167] Based on this technique, a few sequences were selected and for the first time too, the spectrally pure silver nanodots were reported, with emissions ranging from blue to near IR. These emitters possess up to 40% fluorescent quantum yields, high molar extinction coefficient, and less than 3 nm hydrodynamic radius. The photostability of one of the red emitters was 60-fold better, compared to Cy3 in polyvinyl alcohol film. The two-photon absorption features of these pure emitters were then investigated.[174] All of the three emitters studied show more than 30,000 GM two photon absorption cross section; especially a 710 emitter with 5′-CCCTAACTCCCC-3′ protection reaches 50,000 GM, more than 100-fold higher than that of a popular fluorophore, Cy5 (400 GM).

1-7. Major challenges for noble metal nanodot applications

Noble metals have been successfully shifted from nanoparticles to nanodots, and consequently quantum confinement results in molecular characteristics. Though gold nanodots are still waiting for intense investigation, the dramatic improvement on photophysical properties of silver nanodots promotes such emitters as excellent candidates for cellular staining, particularly, single molecule imaging and *in vivo* imaging, thanks to their high extinction coefficient, high quantum yield and outstanding photostability. It has been demonstrated that silver nanodots display these photophysical properties in fixed cell staining, e.g. better brightness and photostability than general organic dyes.[172] When it comes to live cell imaging, we have to circumvent the oxidative stability of Ag clusters, coupled with the low solubility of silver salts (e.g. K_{sp} of AgCl is 1.8×10^{-10}). Bare silver ions cannot survive in physiological conditions in which the chloride concentration reaches up to 100 mM.[269] Not only chloride, other biocompoments may also bind to silver strongly.[264, 270] With strong protection group, such as peptides, silver nanodots are still stable in such media.[21] However, the ssDNA-protected silver nanodots were less chemically stable than were the peptide-protected eithers. We urgently need to understand the interactions that facilitate stability and prepare chemically stable silver nanodots in physiological conditions, but still retain their excellent photophysical properties before further biological application for live cell imaging.

Moreover, the synthesis experience in our lab indicates that the chemical yields of silver nanodots in ssDNA scaffold are quite low, less than 1%, which means majority of

the ssDNA is left non-fluorescent, even though they bind silver ions. This is not only a waste of starting materials, but also leads to presence of a large amount of non-fluorescent ssDNA-silver complexes (fluorophore-inactive) which will in turn compete with the fluorophore-active ssDNA-silver nanodots to bind to targeting groups, and significantly decrease the labeling efficacy and increase non-specific staining. Therefore, we should also find the key factors which control the synthesis efficiency, and consequently increase the chemical synthesis yield of silver nanodots.

In this thesis, I am going to discuss the strategies to prepare highly concentrated, much more photophysically and chemically stable silver nanodots, and extend their biological applications.

1-8. References

1. Rao, J.H., Dragulescu-Andrasi, A. & Yao, H.Q. Fluorescence imaging in vivo: recent advances. *Curr. Opin. Biotechnol.* **18**, 17-25 (2007).

2. Ghoroghchian, P.P., Therien, M.J. & Hammer, D.A. In vivo fluorescence imaging: a personal perspective. *Wiley Interdisciplinary Reviews-Nanomedicine and Nanobiotechnology* **1**, 156-167 (2009).

3. Frangioni, J.V. In vivo near-infrared fluorescence imaging. *Curr. Opin. Chem. Biol.* **7**, 626-634 (2003).

4. Nuiachristos, V. Fluorescence molecular imaging. *Annu. Rev. Biomed. Eng.* **8**, 1-33 (2006).

5. Winkelman, J. & Rasmussen-Taxdal, D. Quantitative determination of porphyrin uptake by tumour tissue following parenteral administration. *Bull. Johns Hopkins Hosp.* **107**, 6 (1960).

6. Doiron, D., Profio, A., Vincent, R. & Dougherty, T. Florescence bronochoscopy for detection of lung cancer. *Chest* **76**, 6 (1979).

7. Profio, A.E., Doiron, D.R., Balchum, O.J. & Huth, G.C. Fluorescence bronchoscopy for localization of carcinoma in situ. *Medical Physics* **10**, 35-39 (1983).

8. Chance, B., Jobsis, F., Schoener, B. & Cohen, P. Intracellular oxidation-reduction states in vivo. *Science* **137**, 499-& (1962).

9. Hilderbrand, S.A. & Weissleder, R. Near-infrared fluorescence: application to in vivo molecular imaging. *Curr. Opin. Chem. Biol* **14**, 71-79 (2010).

10. Muller, P.J. & Wilson, B.C. An update on the penetration depth of 630 nm light in normal and malignant human-brain tissue in vivo. *Phys Med Biol* **31**, 1295-1297 (1986).

11. Bischoff, P.M. & Flower, R.W. 10 years experience with choroidal angiography using indocyanine green-dye - a new routine examination or an epilogue *Doc Ophthalmol* **60**, 235-291 (1985).

12. Desmettre, T., Devoisselle, J.M. & Mordon, S. Fluorescence properties and metabolic features of indocyanine green (ICG) as related to angiography. *Surv Ophthalmol* **45**, 15-27 (2000).

13. Kiesslich, R. et al. Methylene blue-aided chromoendoscopy for the detection of intraepithelial neoplasia and colon cancer in ulcerative colitis. *Gastroenterology* **124**, 880-888 (2003).

14. Tung, C.H., Lin, Y.H., Moon, W.K. & Weissleder, R. A receptor-targeted near-infrared fluorescence probe for in vivo tumor imaging. *ChemBioChem* **3**, 784-786 (2002).

15. Johnson, J.R. et al. Squaraine rotaxanes: Superior substitutes for Cy-5 in molecular probes for near-infrared fluorescence cell imaging. *Angew. Chem.-Int. Edit.* **46**, 5528-5531 (2007).

16. Licha, K. Contrast agents for optical imaging, *Top. Curr. Chem.* **222**, 1-29 (2002).

17. Choi, H.S. et al. Tissue- and Organ-Selective Biodistribution of NIR Fluorescent Quantum Dots. *Nano Lett.* **9**, 2354-2359 (2009).

18. Choi, H.S. et al. Renal clearance of quantum dots. *Nat. Biotechnol.* **25**, 1165-1170 (2007).

19. Connally, R.E. & Piper, J.A. in Fluorescence Methods and Applications: Spectroscopy, Imaging, and Probes, Vol. 1130. (ed. O.S. Wolfbeis) 106-116 (2008).

20. Cubeddu, R., Canti, G., Taroni, P. & Valentini, G. Time-gated fluorescence imaging for the diagnosis of tumors in a murine model. *Photochem Photobiol* **57**, 480-485 (1993).

21. Yu, J., Patel, S.A. & Dickson, R.M. In vitro and intracellular production of peptide-encapsulated fluorescent silver nanoclusters. *Angew. Chem.-Int. Edit.* **46**, 2028-2030 (2007).

22. Palsson, L.O., Pal, R., Murray, B.S., Parker, D. & Beeby, A. Two-photon absorption and photoluminescence of europium based emissive probes for bioactive systems. *Dalton Trans.*, 5726-5734 (2007).

23. Wu, J. et al. Luminescent europium nanoparticles with a wide excitation range from UV to visible light for biolabeling and time-gated luminescence bioimaging. *Chem. Commun.*, 365-367 (2008).

24. Richards, C.I. et al. Optically Modulated Fluorophores for Selective Fluorescence Signal Recovery. *J. Am. Chem. Soc.***131**, 4619-4621 (2009).

25. Moerner, W.E. & Kador, L. Optical Detection and Spectroscopy of Single Molecules in a Solid. *Phys. Rev. Lett.* **62**, 2535-2538 (1989).

26. Orrit, M. & Bernard, J. Single Pentacene Molecules Detected by Fluorescence Excitation in a p-Terphenyl Crystal. *Phys. Rev. Lett.* **65**, 2716-2719 (1990).

27. Betzig, E. & Chichester, R.J. Single Molecules Observed by Near-Field Scanning Optical Microscopy. *Science* **262**, 1422-1425 (1993).

28. Nie, S., Chiu, D.T. & Zare, R.N. Probing individual molecules with confocal fluorescence microscopy. *Science* **266**, 1018-1021 (1994).

29. Darzacq, X. et al. Imaging Transcription in Living Cells. *Annu. Rev. Biophys.* **38**, 173-196 (2009).

30. Forget, A.L. & Kowalczykowski, S.C. Single-molecule imaging brings Rad51 nucleoprotein filaments into focus. *Trends Cell Biol.* **20**, 269-276 (2010).

31. Gershenson, A. Single molecule enzymology: watching the reaction. *Curr. Opin. Chem. Biol* **13**, 436-442 (2009).

32. Moerner, W.E. & Orrit, M. Illuminating single molecules in condensed matter. *Science* **283**, 1670-1676 (1999).

33. Patterson, G., Davidson, M., Manley, S. & Lippincott-Schwartz, J. *Ann. Rev. Phys. chem.* Vol 61, 345-367 (2010).

34. Wang, Y.X., Shyy, J.Y.J. & Chien, S. Fluorescence proteins, live-cell imaging, and mechanobiology: Seeing is believing. *Annu. Rev. Biomed. Eng.* **10**, 1-38 (2008).

35. Joo, C., Balci, H., Ishitsuka, Y., Buranachai, C. & Ha, T. Advances in single-molecule fluorescence methods for molecular biology. *Annu. Rev. Biochem.* **77**, 51-76 (2008).

36. Haustein, E. & Schwille, P. Single-molecule spectroscopic methods. *Curr. Opin. Struct. Biol.* **14**, 531-540 (2004).

37. Hilario, J. & Kowalczykowski, S.C. Visualizing protein-DNA interactions at the single-molecule level. *Curr. Opin. Chem. Biol* **14**, 15-22 (2010).

38. Mehta, A.D., Rief, M., Spudich, J.A., Smith, D.A. & Simmons, R.M. Single-molecule biomechanics with optical methods. *Science* **283**, 1689-1695 (1999).

39. Okumoto, S. Imaging approach for monitoring cellular metabolites and ions using genetically encoded biosensors. *Curr. Opin. Biotechnol.* **21**, 45-54 (2010).

40. Wennmalm, S. & Simon, S.M. Studying individual events in biology. *Annu. Rev. Biochem.* **76**, 419-446 (2007).

41. Dickson, R.M., Cubitt, A.B., Tsien, R.Y. & Moerner, W.E. On/off blinking and switching behaviour of single molecules of green fluorescent protein. *Nature* **388**, 355-358 (1997).

42. Xie, X.S. & Dunn, R.C. Probing single-molecule dynamics. *Science* **265**, 361-364 (1994).

43. Tinnefeld, P. & Sauer, M. Branching out of single-molecule fluorescence spectroscopy: Challenges for chemistry and influence on biology. *Angew. Chem.-Int. Edit.* **44**, 2642-2671 (2005).

44. de Lange, F. et al. Cell biology beyond the diffraction limit: near-field scanning optical microscopy. *J. Cell Sci.* **114**, 4153-4160 (2001).

45. Schneckenburger, H. Total internal reflection fluorescence microscopy: technical innovations and novel applications. *Curr. Opin. Biotechnol.* **16**, 13-18 (2005).

46. Simon, S.M. Partial internal reflections on total internal reflection fluorescent microscopy. *Trends Cell Biol.* **19**, 661-668 (2009).

47. Funatsu, T., Harada, Y., Tokunaga, M., Saito, K. & Yanagida, T. Imaging of single fluorescent molecules and individual atp turnovers by single myosin molecules in aqueous-solution. *Nature* **374**, 555-559 (1995).

48. Zhuang, X.W. et al. A single-molecule study of RNA catalysis and folding. *Science* **288**, 2048-2051 (2000).

49. Ha, T. Single-molecule fluorescence resonance energy transfer. *Methods* **25**, 78-86 (2001).

50. Schutz, G.J., Kada, G., Pastushenko, V.P. & Schindler, H. Properties of lipid microdomains in a muscle cell membrane visualized by single molecule microscopy. *Embo Journal* **19**, 892-901 (2000).

51. Ueda, M., Sako, Y., Tanaka, T., Devreotes, P. & Yanagida, T. Single-molecule analysis of chemotactic signaling in Dictyostelium cells. *Science* **294**, 864-867 (2001).

52. Sako, Y., Minoghchi, S. & Yanagida, T. Single-molecule imaging of EGFR signalling on the surface of living cells. *Nat. Cell. Biol.* **2**, 168-172 (2000).

53. Ha, T. et al. Probing the interaction between two single molecules: Fluorescence resonance energy transfer between a single donor and a single acceptor. *Proc. Natl. Acad. Sci. U. S. A.* **93**, 6264-6268 (1996).

54. Forkey, J.N., Quinlan, M.E., Shaw, M.A., Corrie, J.E.T. & Goldman, Y.E. Three-dimensional structural dynamics of myosin V by single-molecule fluorescence polarization. *Nature* **422**, 399-404 (2003).

55. Xu, X.H. & Yeung, E.S. Direct measurement of single-molecule diffusion and photodecomposition in free solution. *Science* **275**, 1106-1109 (1997).

56. Sosa, H., Peterman, E.J.G., Moerner, W.E. & Goldstein, L.S.B. ADP-induced rocking of the kinesin motor domain revealed by single-molecule fluorescence polarization microscopy. *Nat. Struct. Biol.* **8**, 540-544 (2001).

57. Schmidt, T., Schutz, G.J., Baumgartner, W., Gruber, H.J. & Schindler, H. Imaging of single molecule diffusion. *Proc. Natl. Acad. Sci. U. S. A.* **93**, 2926-2929 (1996).

58. Dave, R., Terry, D.S., Munro, J.B. & Blanchard, S.C. Mitigating Unwanted Photophysical Processes for Improved Single-Molecule Fluorescence Imaging. *Biophys. J.* **96**, 2371-2381 (2009).

59. Fu, C.C. et al. Characterization and application of single fluorescent nanodiamonds as cellular biomarkers. *Proc. Natl. Acad. Sci. U. S. A.* **104**, 727-732 (2007).

60. Yu, J., Xiao, J., Ren, X.J., Lao, K.Q. & Xie, X.S. Probing gene expression in live cells, one protein molecule at a time. *Science* **311**, 1600-1603 (2006).

61. Golding, I., Paulsson, J., Zawilski, S.M. & Cox, E.C. Real-time kinetics of gene activity in individual bacteria. *Cell* **123**, 1025-1036 (2005).

62. Elf, J., Li, G.W. & Xie, X.S. Probing transcription factor dynamics at the single-molecule level in a living cell. *Science* **316**, 1191-1194 (2007).

63. Haggie, P.M. & Verkman, A.S. Monomeric CFTR in plasma membranes in live cells revealed by single molecule fluorescence imaging. *J. Biol. Chem.* **283**, 23510-23513 (2008).

64. Warshaw, D.M. et al. Differential Labeling of myosin V heads with quantum dots allows direct visualization of hand-over-hand processivity. *Biophys. J.* **88**, L30-L32 (2005).

65. Dahan, M. et al. Diffusion dynamics of glycine receptors revealed by single-quantum dot tracking. *Science* **302**, 442-445 (2003).

66. Howarth, M. et al. Monovalent, reduced-size quantum dots for imaging receptors on living cells. *Nat. Methods* **5**, 397-399 (2008).

67. Xiao, J. Single-Molecule Imaging in Live Cells. (Springer, Heidelberg; 2009).

68. Weiss, S. Fluorescence spectroscopy of single biomolecules. *Science* **283**, 1676-1683 (1999).

69. Schmidt, T., Kubitscheck, U., Rohler, D. & Nienhaus, U. Photostability Data for Fluorescent Dyes:An Update. *Single Molecules* **3**, 327 (2002).

70. Satsoura, D., Leber, B., Andrews, D.W. & Fradin, C. Circumvention of fluorophore photobleaching in fluorescence fluctuation experiments: A beam scanning approach. *ChemPhysChem* **8**, 834-848 (2007).

71. Lord, S.J. et al. DCDHF Fluorophores for Single-Molecule Imaging in Cells. *ChemPhysChem* **10**, 55-65 (2009).

72. Garcia-Parajo, M.F., Segers-Nolten, G.M.J., Veerman, J.A., Greve, J. & van Hulst, N.F. Real-time light-driven dynamics of the fluorescence emission in single green fluorescent protein molecules. *Proc. Natl. Acad. Sci. U. S. A.* **97**, 7237-7242 (2000).

73. Seefeldt, B. et al. Fluorescent proteins for single-molecule fluorescence applications. *J. Biophotonics* **1**, 74-82 (2008).

74. Mena, M.A., Treynor, T.P., Mayo, S.L. & Daugherty, P.S. Blue fluorescent proteins with enhanced brightness and photostability from a structurally targeted library. *Nat. Biotechnol.* **24**, 1569-1571 (2006).

75. Nikogosyan, D.N. Definition of photoreaction quantum yield at 2-quantum excitation of molecules in solution. *Laser Chemistry* **7**, 29-34 (1987).

76. Heikal, A.A., Hess, S.T., Baird, G.S., Tsien, R.Y. & Webb, W.W. Molecular spectroscopy and dynamics of intrinsically fluorescent proteins: Coral red (dsRed) and yellow (Citrine). *Proc. Natl. Acad. Sci. U. S. A.* **97**, 11996-12001 (2000).

77. Eggeling, C., Widengren, J., Rigler, R. & Seidel, C.A.M. Photobleaching of fluorescent dyes under conditions used for single-molecule detection: Evidence of two-step photolysis. *Anal. Chem.* **70**, 2651-2659 (1998).

78. Lord, S.J. et al. Photophysical properties of acene DCDHF fluorophores: Long-wavelength single-molecule emitters designed for cellular Imaging. *J. Phys. Chem. A* **111**, 8934-8941 (2007).

79. Delon, A. et al. Measuring, in Solution, Multiple-Fluorophore Labeling by Combining Fluorescence Correlation Spectroscopy and Photobleaching. *J. Phys. Chem. B* **114**, 2988-2996 (2010).

80. Soper, S.A., Nutter, H.L., Keller, R.A., Davis, L.M. & Shera, E.B. The photophysical constants of several fluorescent dyes pertaining to ultrasensitive fluorescence spectroscopy. *Photochem Photobiol* **57**, 972-977 (1993).

81. Lee, T.H., Gonzalez, J.I., Zheng, J. & Dickson, R.M. Single-molecule optoelectronics. *Acc. Chem. Res.* **38**, 534-541 (2005).

82. Mason, W.T. Biological Techniques Series: Fluorescent and luminescent probes for biological activity: A practical guide to technology for quantitative real-time analysis. *Biological Techniques Series; Fluorescent and luminescent probes for biological activity: A practical guide to technology for quantitative real-time analysis*, xxi+433p (1993).

83. Resch-Genger, U., Grabolle, M., Cavaliere-Jaricot, S., Nitschke, R. & Nann, T. Quantum dots versus organic dyes as fluorescent labels. *Nat. Methods* **5**, 763-775 (2008).

84. Willets, K.A., Ostroverkhova, O., He, M., Twieg, R.J. & Moerner, W.E. Novel fluorophores for single-molecule imaging. *J. Am. Chem. Soc.* **125**, 1174-1175 (2003).

85. Kulzer, F., Koberling, F., Christ, T., Mews, A. & Basche, T. Terrylene in p-terphenyl: single-molecule experiments at room temperature. *Chem. Phys.* **247**, 23-34 (1999).

86. Langhals, H., Jaschke, H., Ring, U. & von Unold, P. Peryleneimidazoloimides: Highly fluorescent and stable replacements of terrylene. *Angew. Chem.-Int. Edit.* **38**, 201-203 (1999).

87. Renikuntla, B.R., Rose, H.C., Eldo, J., Waggoner, A.S. & Armitage, B.A. Improved photostability and fluorescence properties through polyfluorination of a cyanine dye. *Org. Lett.* **6**, 909-912 (2004).

88. Widengren, J. & Rigler, R. Photobleaching investigations of dyes using fluorescence correlation spectroscopy (FCS). *Prog. Biophys. Mol. Bio.* **65**, PH109-PH109 (1996).

89. Leatherdale, C.A., Woo, W.K., Mikulec, F.V. & Bawendi, M.G. On the absorption cross section of CdSe nanocrystal quantum dots. *J. Phys. Chem. B* **106**, 7619-7622 (2002).

90. Chan, W.C.W. & Nie, S.M. Quantum dot bioconjugates for ultrasensitive nonisotopic detection. *Science* **281**, 2016-2018 (1998).

91. Bruchez, M., Moronne, M., Gin, P., Weiss, S. & Alivisatos, A.P. Semiconductor nanocrystals as fluorescent biological labels. *Science* **281**, 2013-2016 (1998).

92. Medintz, I.L., Uyeda, H.T., Goldman, E.R. & Mattoussi, H. Quantum dot bioconjugates for imaging, labelling and sensing. *Nat. Mater.* **4**, 435-446 (2005).

93. Lo, K.K.W., Lee, T.K.M., Lau, J.S.Y., Poon, W.L. & Cheng, S.H. Luminescent biological probes derived from ruthenium(II) estradiol polypyridine complexes. *Inorg. Chem.* **47**, 200-208 (2008).

94. Lo, K.K.W. et al. Non-covalent binding of luminescent transition metal polypyridine complexes to avidin, indole-binding proteins and estrogen receptors. *Coord. Chem. Rev.* **251**, 2292-2310 (2007).

95. Rajalakshmanan, E. & Alexander, V. Synthesis, luminescence, and electrochemical studies of tris(homoleptic) ruthenium(II) and osmium(II) complexes of 6 '-tolyl-2,2 ': 4 ',2 "-terpyridine. *Inorg. Chem.* **46**, 6252-6260 (2007).

96. Parker, D., Dickins, R.S., Puschmann, H., Crossland, C. & Howard, J.A.K. Being excited by lanthanide coordination complexes: Aqua species, chirality, excited-state chemistry, and exchange dynamics. *Chem. Rev.* **102**, 1977-2010 (2002).

97. Montgomery, C.P., Murray, B.S., New, E.J., Pal, R. & Parker, D. Cell-Penetrating Metal Complex Optical Probes: Targeted and Responsive Systems Based on Lanthanide Luminescence. *Acc. Chem. Res.* **42**, 925-937 (2009).

98. Parker, D. Luminescent lanthanide sensors for pH, pO(2) and selected anions. *Coord. Chem. Rev.* **205**, 109-130 (2000).

99. New, E.J., Parker, D., Smith, D.G. & Walton, J.W. Development of responsive lanthanide probes for cellular applications. *Curr. Opin. Chem. Biol* **14**, 238-246 (2010).

100. Yu, J.H., Parker, D., Pal, R., Poole, R.A. & Cann, M.J. A europium complex that selectively stains nucleoli of cells. *J. Am. Chem. Soc.* **128**, 2294-2299 (2006).

101. Pandya, S., Yu, J.H. & Parker, D. 2757-2766 (Royal Soc Chemistry, 2006).

102. Vinkenborg, J.L., Koay, M.S. & Merkx, M. Fluorescent imaging of transition metal homeostasis using genetically encoded sensors. *Curr. Opin. Chem. Biol* **14**, 231-237 (2010).

103. Gill, M.R. et al. A ruthenium(II) polypyridyl complex for direct imaging of DNA structure in living cells. *Nat. Chem.* **1**, 662-667 (2009).

104. Seybold, P.G., Gouterma.M & Callis, J. Calorimetric Photometric and Lifetime Determinations of Fluorescence Yields of Fluorescein Dyes. *Photochem Photobiol* **9**, 229-242 (1969).

105. Gruber, H.J. et al. Anomalous fluorescence enhancement of Cy3 and Cy3.5 versus anomalous fluorescence loss of Cy5 and Cy7 upon covalent linking to IgG and noncovalent binding to avidin. *Bioconjugate Chem.* **11**, 696-704 (2000).

106. Mujumdar, R.B., Ernst, L.A., Mujumdar, S.R., Lewis, C.J. & Waggoner, A.S. Cyanine dye labeling reagents - sulfoindocyanine succinimidyl esters. *Bioconjugate Chem.* **4**, 105-111 (1993).

107. Loudet, A. & Burgess, K. BODIPY dyes and their derivatives: Syntheses and spectroscopic properties. *Chem. Rev.* **107**, 4891-4932 (2007).

108. Panchuk-Voloshina, N. et al. Alexa dyes, a series of new fluorescent dyes that yield exceptionally bright, photostable conjugates. *J. Histochem. Cytochem.* **47**, 1179-1188 (1999).

109. Shimomura, O., Johnson, F.H. & Saiga, Y. Extraction, purification and properties of aequorin, a bioluminescent protein from luminous hydromedusan, aequorea. *Journal of Cellular and Comparative Physiology* **59**, 223-239 (1962).

110. Chalfie, M., Tu, Y., Euskirchen, G., Ward, W.W. & Prasher, D.C. Green fluorescent protein as a marker for gene-expression. *Science* **263**, 802-805 (1994).

111. Tsien, R.Y. The green fluorescent protein. *Annu. Rev. Biochem.* **67**, 509-544 (1998).

112. Heim, R., Cubitt, A.B. & Tsien, R.Y. Improved green fluorescence. *Nature* **373**, 663-664 (1995).

113. Chudakov, D.M., Lukyanov, S. & Lukyanov, K.A. Fluorescent proteins as a toolkit for in vivo imaging. *Trends in Biotechnology* **23**, 605-613 (2005).

114. Livet, J. et al. Transgenic strategies for combinatorial expression of fluorescent proteins in the nervous system. *Nature* **450**, 56-62 (2007).

115. Shaner, N.C., Steinbach, P.A. & Tsien, R.Y. A guide to choosing fluorescent proteins. *Nat. Methods* **2**, 905-909 (2005).

116. Shaner, N.C., Patterson, G.H. & Davidson, M.W. Advances in fluorescent protein technology. *J. Cell Sci.* **120**, 4247-4260 (2007).

117. Lukyanov, K.A., Chudakov, D.M., Lukyanov, S. & Verkhusha, V.V. Photoactivatable fluorescent proteins. *Nat. Rev. Mol. Cell Bio.* **6**, 885-891 (2005).

118. O'Hare, H.M., Johnsson, K. & Gautier, A. Chemical probes shed light on protein function. *Curr. Opin. Struc. Biol* **17**, 488-494 (2007).

119. Johnsson, N. & Johnsson, K. Chemical tools for biomolecular imaging. *ACS Chem Biol* **2**, 31-38 (2007).

120. Griffin, B.A., Adams, S.R. & Tsien, R.Y. Specific covalent labeling of recombinant protein molecules inside live cells. *Science* **281**, 269-272 (1998).

121. Guignet, E.G., Hovius, R. & Vogel, H. Reversible site-selective labeling of membrane proteins in live cells. *Nat. Biotechnol.* **22**, 440-444 (2004).

122. Keppler, A. et al. A general method for the covalent labeling of fusion proteins with small molecules in vivo. *Nat. Biotechnol.* **21**, 86-89 (2003).

123. Chen, I. & Ting, A.Y. Site-specific labeling of proteins with small molecules in live cells. *Curr. Opin. Biotechnol.* **16**, 35-40 (2005).

124. Howarth, M. & Ting, A.Y. Imaging proteins in live mammalian cells with biotin ligase and monovalent streptavidin. *Nat. Protoc.* **3**, 534-545 (2008).

125. Uttamapinant, C. et al. A fluorophore ligase for site-specific protein labeling inside living cells. *Proc. Natl. Acad. Sci. U. S. A.* **107**, 10914-10919 (2010).

126. Marks, K.M., Rosinov, M. & Nolan, G.P. In vivo targeting of organic calcium sensors via genetically selected peptides. *Chem Biol* **11**, 347-356 (2004).

127. Gao, X.H. et al. In vivo molecular and cellular imaging with quantum dots. *Curr. Opin. Biotechnol.* **16**, 63-72 (2005).

128. Nie, S.M., Xing, Y., Kim, G.J. & Simons, J.W. Nanotechnology applications in cancer. *Annu. Rev. Biomed. Eng.* **9**, 257-288 (2007).

129. Sutherland, A.J. Quantum dots as luminescent probes in biological systems. *Curr. Opin. Solid St. M.* **6**, 365-370 (2002).

130. Alivisatos, A.P. Semiconductor clusters, nanocrystals, and quantum dots. *Science* **271**, 933-937 (1996).

131. Giepmans, B.N.G., Adams, S.R., Ellisman, M.H. & Tsien, R.Y. The fluorescent toolbox for assessing protein location and function. *Science* **312**, 217-224 (2006).

132. Larson, D.R. et al. Water-soluble quantum dots for multiphoton fluorescence imaging in vivo. *Science* **300**, 1434-1436 (2003).

133. Michalet, X. et al. Quantum dots for live cells, in vivo imaging, and diagnostics. *Science* **307**, 538-544 (2005).

134. Chen, I., Howarth, M., Lin, W.Y. & Ting, A.Y. Site-specific labeling of cell surface proteins with biophysical probes using biotin ligase. *Nat. Methods* **2**, 99-104 (2005).

135. Delehanty, J.B., Mattoussi, H. & Medintz, I.L. Delivering quantum dots into cells: strategies, progress and remaining issues. *Anal. Bioanal. Chem.* **393**, 1091-1105 (2009).

136. Yang, R. et al. Tagging cells with quantum dots by electroporation. *Chem J Chinese U* **26**, 1043-1045 (2005).

137. Medintz, I.L. et al. Intracellular delivery of quantum dot-protein cargos mediated by cell penetrating peptides. *Bioconjugate Chem.* **19**, 1785-1795 (2008).

138. Zhang, Y. et al. Time-dependent photoluminescence blue shift of the quantum dots in living cells: Effect of oxidation by singlet oxygen. *J. Am. Chem. Soc.* **128**, 13396-13401 (2006).

139. Hoshino, A. et al. Physicochemical properties and cellular toxicity of nanocrystal quantum dots depend on their surface modification. *Nano Lett.* **4**, 2163-2169 (2004).

140. Ma, J. et al. Photostability of thiol-capped CdTe quantum dots in living cells: the effect of photo-oxidation. *Nanotechnology* **17**, 2083-2089 (2006).

141. Mancini, M.C., Kairdolf, B.A., Smith, A.M. & Nie, S.M. Oxidative quenching and degradation of polymer-encapsulated quantum dots: New insights into the long-term fate and toxicity of nanocrystals in vivo. *J. Am. Chem. Soc.* **130**, 10836-10837 (2008).

142. Hainfeld, J.F. & Powell, R.D. New frontiers in gold labeling. *J. Histochem. Cytochem.* **48**, 471-480 (2000).

143. Bishea, G.A. & Morse, M.D. Resonant 2-photon ionization spectroscopy of jet-cooled Au3. *J. Chem. Phys.* **95**, 8779-8792 (1991).

144. Bishea, G.A. & Morse, M.D. Spectroscopic studies of jet-cooled AgAu and Au2. *J. Chem. Phys.* **95**, 5646-5659 (1991).

145. Fedrigo, S., Harbich, W. & Buttet, J. Optical-response of Ag2, Ag3, Au2, and Au3 in argon matrices. *J. Chem. Phys.* **99**, 5712-5717 (1993).

146. Harbich, W., Fedrigo, S., Buttet, J. & Lindsay, D.M. Deposition of mass selected gold clusters in solid krypton. *J. Chem. Phys.* **96**, 8104-8108 (1992).

147. Klotzbucher, W.E. & Ozin, G.A. Optical Spectra of Hafnium, Tungsten, Rhenium, and Ruthenium Atoms and Other Heavy Transition-Metal Atoms and Small Clusters (Zrl,2, Pd1,2, A~1,2,3)in Noble Gas Matrices. *Inorg. Chem.* **19**, 3767-3776 (1980).

148. Link, S. et al. Visible to infrared luminescence from a 28-atom gold cluster. *J. Phys. Chem. B* **106**, 3410-3415 (2002).

149. Negishi, Y. & Tsukuda, T. One-pot preparation of subnanometer-sized gold clusters via reduction and stabilization by meso-2,3-dimercaptosuccinic acid. *J. Am. Chem. Soc.* **125**, 4046-4047 (2003).

150. Huang, C.C., Yang, Z., Lee, K.H. & Chang, H.T. Synthesis of highly fluorescent gold nanoparticles for sensing Mercury(II). *Angew. Chem.-Int. Edit.* **46**, 6824-6828 (2007).

151. Huang, C.C. et al. Synthesis of wavelength-tunable luminescent gold and gold/silver nanodots. *J. Mater. Chem* **19**, 755-759 (2009).

152. Lee, D., Donkers, R.L., Wang, G.L., Harper, A.S. & Murray, R.W. Electrochemistry and optical absorbance and luminescence of molecule-like Au-38 nanoparticles. *J. Am. Chem. Soc.***126**, 6193-6199 (2004).

153. Zheng, J., Nicovich, P.R. & Dickson, R.M. Highly fluorescent noble-metal quantum dots. *Annu. Rev. Phys. Chem.* **58**, 409-431 (2007).

154. Zheng, J., Petty, J.T. & Dickson, R.M. High quantum yield blue emission from water-soluble Au-8 nanodots. *J. Am. Chem. Soc.* **125**, 7780-7781 (2003).

155. Bao, Y.P. et al. Nanoparticle-free synthesis of fluorescent gold nanoclusters at physiological temperature. *J. Phys. Chem. C* **111**, 12194-12198 (2007).

156. Bigioni, T.P., Whetten, R.L. & Dag, O. Near-infrared luminescence from small gold nanocrystals. *J. Phys. Chem. B* **104**, 6983-6986 (2000).

157. Huang, T. & Murray, R.W. Visible luminescence of water-soluble monolayer-protected gold clusters. *J. Phys. Chem. B* **105**, 12498-12502 (2001).

158. Negishi, Y. et al. Magic-numbered Au-n clusters protected by glutathione monolayers (n=18, 21, 25, 28, 32, 39): Isolation and spectroscopic characterization. *J. Am. Chem. Soc.***126**, 6518-6519 (2004).

159. Xie, J.P., Zheng, Y.G. & Ying, J.Y. Protein-Directed Synthesis of Highly Fluorescent Gold Nanoclusters. *J. Am. Chem. Soc.* **131**, 888-889 (2009).

160. Huang, C.C., Chen, C.T., Shiang, Y.C., Lin, Z.H. & Chang, H.T. Synthesis of Fluorescent Carbohydrate-Protected Au Nanodots for Detection of Concanavalin A and Escherichia coli. *Anal. Chem.* **81**, 875-882 (2009).

161. Mooradia.A Photoluminescence of metals. *Phys. Rev. Lett.* **22**, 185-187 (1969).

162. Zheng, J. & Dickson, R.M. Individual water-soluble dendrimer-encapsulated silver nanodot fluorescence. *J. Am. Chem. Soc.* **124**, 13982-13983 (2002).

163. Diez, I. et al. Color Tunability and Electrochemiluminescence of Silver Nanoclusters. *Angew. Chem.-Int. Edit.* **48**, 2122-2125 (2009).

164. Guo, W.W., Yuan, J.P. & Wang, E.K. Oligonucleotide-stabilized Ag nanoclusters as novel fluorescence probes for the highly selective and sensitive detection of the $Hg2^{+}$ ion. *Chem. Commun.*, 3395-3397 (2009).

165. Lesniak, W. et al. Silver/dendrimer nanocomposites as biomarkers: Fabrication, characterization, in vitro toxicity, and intracellular detection. *Nano Lett.* **5**, 2123-2130 (2005).

166. Petty, J.T., Zheng, J., Hud, N.V. & Dickson, R.M. DNA-templated Ag nanocluster formation. *J. Am. Chem. Soc.* **126**, 5207-5212 (2004).

167. Richards, C.I. et al. Oligonucleotide-stabilized Ag nanocluster fluorophores. *J. Am. Chem. Soc.* **130**, 5038-5039 (2008).

168. Ritchie, C.M. et al. Ag nanocluster formation using a cytosine oligonucleotide template. *J. Phys. Chem. C* **111**, 175-181 (2007).

169. Shang, L. & Dong, S.J. Facile preparation of water-soluble fluorescent silver nanoclusters using a polyelectrolyte template. *Chem. Commun.*, 1088-1090 (2008).

170. Shen, Z., Duan, H.W. & Frey, H. Water-soluble fluorescent Ag nanoclusters obtained from multiarm star poly(acrylic acid) as "molecular hydrogel" templates. *Adv. Mater.* **19**, 349-352 (2007).

171. Vosch, T. et al. Strongly emissive individual DNA-encapsulated Ag nanoclusters as single-molecule fluorophores. *Proc. Natl. Acad. Sci. U. S. A.* **104**, 12616-12621 (2007).

172. Yu, J., Choi, S. & Dickson, R.M. Shuttle-based fluorogenic silver cluster biolabels. *Angew. Chem.-Int. Edit.*, **48**, 318–320 (2009).

173. Gwinn, E.G., O'Neill, P., Guerrero, A.J., Bouwmeester, D. & Fygenson, D.K. Sequence-dependent fluorescence of DNA-hosted silver nanoclusters. *Adv. Mater.* **20**, 279-283 (2008).

174. Patel, S.A., Richards, C.I., Hsiang, J.C. & Dickson, R.M. Water-soluble Ag nanoclusters exhibit strong two-photon-induced fluorescence. *J. Am. Chem. Soc.* **130**, 11602-11603 (2008).

175. Ferrari, M.B. et al. Synthesis, characterization, crystal structure and luminescence properties of phosphinic silver(I) complexes with thiourea derivatives. *Inorg Chim Acta* **360**, 3233-3240 (2007).

176. El Masloumi, M. et al. Structure and luminescence properties of silver-doped NaY(PO3)(4) crystal. *J Solid State Chem* **181**, 3078-3085 (2008).

177. Che, C.M. et al. Spectroscopic evidence for argentophilicity in structurally characterized luminescent binuclear silver(I) complexes. *J. Am. Chem. Soc.* **122**, 2464-2468 (2000).

178. Zhou, Y.B., Zhang, X.M., Chen, W.Z. & Qiu, H.Y. Synthesis, structural characterization, and luminescence properties of multinuclear silver complexes of pyrazole-functionalized NHC ligands containing Ag-Ag and Ag-pi interactions. *J. Organomet. Chem.***693**, 205-215 (2008).

179. Ren, T. et al. Bis(mu-N,N '-eta(2)-N,O-eta(2)-N ',O '-di(o-methoxyphenyl)formamidinato)disilver(I): an interesting coordination geometry for silver(I) and room temperature fluorescence. *Inorg. Chem. Commun.* **1**, 23-26 (1998).

180. Wei, Q.H. et al. Luminescent Ag-I-Cu-I heterometallic hexa-, octa-, and hexadecanuclear alkynyl complexes. *Inorg. Chem.* **43**, 3484-3491 (2004).

181. Wang, Q.M. et al. Intensely luminescent gold(I)-silver(I) cluster complexes with tunable structural features. *J. Am. Chem. Soc.* **126**, 9488-9489 (2004).

182. Kunkely, H. & Vogler, A. Optical properties of silver(I) hexafluoroantimonate(V): luminescence from a metal-to-metal charge transfer state involving a transition and a main group metal. *Inorg. Chem. Commun.* **7**, 400-401 (2004).

183. Kunkely, H. & Vogler, A. Optical properties of silver(I) perrhenate: luminescence from a metal-to-metal charge transfer state. *Inorg Chim Acta* **357**, 1317-1319 (2004).

184. Amoroso, A.J. et al. Crystal Structures of Silver(I) and Thallium(I) Complexes of Tris[3-(2-pyridyl)-pyrazol-l -yl]borate; Encapsulation of Either a Single Thallium(I) Ion or a Trinuclear Silver(I) Cluster by a Hexadentate Podand. *J Chem Soc Chem Comm*, 1175-1176 (1995).

185. Wang, J., Luo, Q.H., Shen, M.C., Huang, X.Y. & Wu, Q.J. Synthesis and X-ray crystal-structure of the first pentanuclear silver(II) cluster of the polyaza cryptands. *J Chem Soc Chem Comm*, 2373-2374 (1995).

186. Coyle, J.L., McKee, V. & Nelson, J. Response to steric constraint by d(10) cations: an 'A-frame' disilver cryptate. *Chem. Commun.*, 709-710 (1998).

187. Apperley, D.C. et al. Kinetically inert cryptate systems: solid state and solution NMR studies. *J. Chem. Soc.-Dalton Trans.*, 229-236 (1999).

188. McKee, V., Nelson, J., Speed, D.J. & Town, R.M. Conformational and coordination plasticity in silver(I) cryptates. *J. Chem. Soc.-Dalton Trans.*, 3641-3646 (2001).

189. Fei, B.L., Sun, W.Y., Okamura, T., Tang, W.X. & Ueyama, N. Synthesis and crystal structure of a luminescent infinite 2D brick-wall network with two- and three-coordinate silver(I) atoms and ligand-unsupported silver-silver interactions. *New J. Chem.* **25**, 210-212 (2001).

190. Lin, Y.Y., Lai, S.W., Che, C.M., Cheung, K.K. & Zhou, Z.Y. Luminescent tetranuclear silver(I) arylacetylide complexes bearing tricyclohexylphosphine ligands: Synthesis, molecular structures, and spectroscopic comparison with gold(I) and copper(I) arylacetylides. *Organometallics* **21**, 2275-2282 (2002).

191. Radak, S., Ni, Y.H., Xu, G.L., Shaffer, K.L. & Ren, T. Synthesis and crystallographic characterization of dinuclear silver complexes supported by N,N '-diarylformamidinates. *Inorg Chim Acta* **321**, 200-204 (2001).

192. Brooker, S., Ewing, J.D. & Nelson, J. A conformationally adaptable host capable of encapsulating single cations or homo and hetero dinuclear assemblies. *Inorg Chim Acta* **317**, 53-58 (2001).

193. Henglein, A. Small-Particle Research - Physicochemical Properties of Extremely Small Colloidal Metal and Semiconductor Particles. *Chem. Rev.* **89**, 1861-1873 (1989).

194. Eachus, R.S., Marchetti, A.P. & Muenter, A.A. The photophysics of silver halide imaging materials. *Annu. Rev. Phys. Chem.* **50**, 117-144 (1999).

195. Baetzold, R.C. Properties of silver clusters adsorbed to silver bromide. *J. Phys. Chem. B* **105**, 3577-3586 (2001).

196. Hovel, H., Grimm, B., Pollmann, M. & Reihl, B. Femtosecond dynamics of final-state effects in the valence band photoemission of silver clusters on a graphite substrate. *Eur Phys J D* **9**, 595-599 (1999).

197. Peyser, L.A., Lee, T.H. & Dickson, R.M. Mechanism of Ag-n nanocluster photoproduction from silver oxide films. *J. Phys. Chem. B* **106**, 7725-7728 (2002).

198. Peyser, L.A., Vinson, A.E., Bartko, A.P. & Dickson, R.M. Photoactivated fluorescence from individual silver nanoclusters. *Science* **291**, 103-106 (2001).

199. Gleitsmann, T., Bernhardt, T.M. & Woste, L. Luminescence properties of femtosecond-laser-activated silver oxide nanoparticles embedded in a biopolymer matrix. *Appl Phys A-Mater* **82**, 125-130 (2006).

200. Chen, W., Wang, Z.G., Lin, L.Y., Lin, J.H. & Su, M.Z. Photostimulated luminescence of silver clusters in zeolite-Y. *Phys. Lett. A* **232**, 391-394 (1997).

201. Chen, W. et al. Photostimulated luminescence of AgI clusters in zeolite-Y. *J. Appl. Phys.* **83**, 3811-3815 (1998).

202. Bruhwiler, D., Leiggener, C., Glaus, S. & Calzaferri, G. Luminescent silver sulfide clusters. *J. Phys. Chem. B* **106**, 3770-3777 (2002).

203. Leiggener, C. & Calzaferri, G. Monolayers of zeolite A containing luminescent silver sulfide clusters. *ChemPhysChem* **5**, 1593-1596 (2004).

204. Leiggener, C. & Calzaferri, G. Synthesis and luminescence properties of Ag2S and PbS clusters in zeolite A. *Chem.-Eur. J.* **11**, 7191-7198 (2005).

205. Sun, T. & Seff, K. Silver clusters and chemistry in zeolites. *Chem. Rev.* **94**, 857-870 (1994).

206. Kanan, M.C., Kanan, S.M. & Patterson, H.H. Luminescence properties of silver(I)-exchanged zeolite Y and its use as a catalyst to photodecompose carbaryl in the presence of natural organic matter. *Res Chem Intermediat* **29**, 691-704 (2003).

207. El-Sayed, M.A. Some interesting properties of metals confined in time and nanometer space of different shapes. *Acc. Chem. Res.* **34**, 257-264 (2001).

208. Whetten, R.L. et al. Crystal structures of molecular gold nanocrystal arrays. *Acc. Chem. Res.* **32**, 397-406 (1999).

209. Morse, M.D. Clusters of transition-metal atoms. *Chem. Rev.* **86**, 1049-1109 (1986).

210. Schmid, G. Large clusters and colloids - metals in the embryonic state. *Chem. Rev.* **92**, 1709-1727 (1992).

211. Wilcoxon, J.P. & Abrams, B.L. Synthesis, structure and properties of metal nanoclusters. *Chem. Soc. Rev.* **35**, 1162-1194 (2006).

212. Ozin, G.A. & Huber, H. Cryo-photo-clustering techniques for synthesizing very small, naked silver clusters agn of known size (where n=2-5) - molecular metal cluster bulk metal-particle interface. *Inorg. Chem.* **17**, 155-163 (1978).

213. Ozin, G.A. & Mitchell, S.A. Ligand-free metal-clusters. *Angew. Chem. Int. Ed.* **22**, 674-694 (1983).

214. Whittle, E., Dows, D.A. & Pimentel, G.C. Matrix isolation method for the experimental study of unstable species. *J. Chem. Phys.* **22**, 1943-1943 (1954).

215. Ievlev, D., Rabin, L., Schulze, W. & Ertl, G. Fluorescence spectroscopy of silver clusters formed in rare gas droplets. *Eur Phys J D* **16**, 157-160 (2001).

216. Apell, P., Monreal, R. & Lundqvist, S. Photoluminescence of Noble Metals. *Phys Scripta* **38**, 174-179 (1988).

217. Bechthold, P.S., Kettler, U. & Krasser, W. Trapping-site effects in resonance raman spectra of Ag2 molecules isolated in rare-gas matrices. *Surf. Sci* **156**, 875-882 (1985).

218. Boyd, G.T., Yu, Z.H. & Shen, Y.R. Photoinduced luminescence from the noble-metals and its enhancement on roughened surfaces. *Phys. Rev. B* **33**, 7923-7936 (1986).

219. Brucat, P.J., Zheng, L.S., Pettiette, C.L., Yang, S. & Smalley, R.E. Metal cluster ion photofragmentation. *J. Chem. Phys.* **84**, 3078-3088 (1986).

220. Busolt, U. et al. Two photon photoemission of deposited silver clusters. *Eur Phys J D* **9**, 523-527 (1999).

221. Fedrigo, S., Harbich, W. & Buttet, J. Collective dipole oscillations in small silver clusters embedded in rare-gas matrices. *Phys. Rev. B* **47**, 10706-10715 (1993).

222. Felix, C. et al. Fluorescence and excitation spectra of Ag-4 in an argon matrix. *Chem. Phys. Lett.* **313**, 105-109 (1999).

223. Felix, C. et al. Ag-8 fluorescence in argon. *Phys. Rev. Lett.* **86**, 2992-2995 (2001).

224. Harbich, W., Fedrigo, S. & Buttet, J. The optical-absorption spectra of small silver clusters (n=8-39) embedded in rare-gas matrices. *Z Phys D Atom Mol Cl* **26**, 138-140 (1993).

225. Harbich, W. et al. Deposition of mass selected silver clusters in rare-gas matrices. *J. Chem. Phys.* **93**, 8535-8543 (1990).

226. Haslett, T.L., Bosnick, K.A. & Moskovits, M. Ag-5 is a planar trapezoidal molecule. *J. Chem. Phys.* **108**, 3453-3457 (1998).

227. Henglein, A. Non-metallic silver clusters in aqueous-solution - stabilization and chemical-reactions. *Chem. Phys. Lett.* **154**, 473-476 (1989).

228. Henglein, A., Mulvaney, P. & Linnert, T. Chemistry of Agn aggregates in aqueous-solution - nonmetallic oligomeric clusters and metallic particles. *Faraday Discuss* **92**, 31-44 (1991).

229. Ievlev, D., Rabin, I., Schulze, W. & Ertl, G. Light emission in the agglomeration of silver clusters. *Chem. Phys. Lett.* **328**, 142-146 (2000).

230. Mostafavi, M., Marignier, J.L., Amblard, J. & Belloni, J. Nucleation dynamics of silver aggregates simulation of photographic development processes. *Radiat Phys Chem* **34**, 605-617 (1989).

231. Rabin, I., Schulze, W. & Ertl, G. Light emission during the agglomeration of silver clusters in noble gas matrices. *J. Chem. Phys.* **108**, 5137-5142 (1998).

232. Rabin, I., Schulze, W. & Ertl, G. Absorption spectra of small silver clusters Ag-n (n >= 3). *Chem. Phys. Lett.* **312**, 394-398 (1999).

233. Rabin, I. et al. Absorption and fluorescence spectra of Ar-matrix-isolated Ag-3 clusters. *Chem. Phys. Lett.* **320**, 59-64 (2000).

234. Radcliffe, P. et al. Excited-state relaxation of Ag8 clusters embedded in helium droplets. *Phys Rev Lett* **92**, 173403 (2004).

235. Schulze, W., Rabin, I. & Ertl, G. Formation of light-emitting Ag-2 and Ag-3 species in the course of condensation of Ag atoms with Ar. *ChemPhysChem* **5**, 403-407 (2004).

236. Yabana, K. & Bertsch, G.F. Optical response of small silver clusters. *Phys. Rev. A* **60**, 3809-3814 (1999).

237. Geddes, C.D., Parfenov, A., Gryczynski, I. & Lakowicz, J.R. Luminescent blinking from silver nanostructures. *J. Phys. Chem. B* **107**, 9989-9993 (2003).

238. Maurel, C. et al. Luminescence properties of silver zinc phosphate glasses following different irradiations. *J. Lumin.* **129**, 1514-1518 (2009).

239. Dey, G.R. & Kishore, K. Silver clusters in 2-propanol: a radiation chemical study. *Radiat Phys Chem* **72**, 565-573 (2005).

240. Linnert, T., Mulvaney, P., Henglein, A. & Weller, H. Long lived nonmetallic silver clusters in aqueous solution: preparation and photolysis. *J. Am. Chem. Soc.* **112**, 4657-4664 (1990).

241. Ershov, B.G., Janata, E., Henglein, A. & Fojtik, A. Silver atoms and clusters in aqueous-solution - absorption-spectra and the particle growth in the absence of stabilizing Ag+ ions. *J. Phys. Chem.* **97**, 4589-4594 (1993).

242. Janata, E., Henglein, A. & Ershov, B.G. First clusters of Ag+ ion reduction in aqueous-solution. *J. Phys. Chem.* **98**, 10888-10890 (1994).

243. Mostafavi, M., Dey, G.R., Francois, L. & Belloni, J. Transient and stable silver clusters induced by radiolysis in methanol. *J. Phys. Chem. A* **106**, 10184-10194 (2002).

244. Stevens, A.D. & Symons, M.C.R. Spectroscopic studies of silver (o) centers formed radiolytically in water-ethanol solvents at 4 and 77 K. *J. Chem. Soc. Farad T I* **85**, 1439-1450 (1989).

245. Dimitrijevic, N.M., Bartels, D.M., Jonah, C.D., Takahashi, K. & Rajh, T. Radiolytically induced formation and optical absorption spectra of colloidal silver nanoparticles in supercritical ethane. *J. Phys. Chem. B* **105**, 954-959 (2001).

246. Ershov, B.G., Abkhalimov, E.A. & Sukhov, N.L. Formation of long-lived clusters and silver nucleation in the gamma-irradiation of aqueous silver perchlorate solutions containing polyphosphate. *High Energ Chem* **39**, 55-59 (2005).

247. Mostafavi, M., Keghouche, N. & Delcourt, M.O. Complexation of silver clusters of a few atoms by a polyanion in aqueous-solution - pH effect correlated to structural-changes. *Chem. Phys. Lett.* **169**, 81-84 (1990).

248. Mostafavi, M., Keghouche, N., Delcourt, M.O. & Belloni, J. Ultra-slow aggregation process for silver clusters of a few atoms in solution. *Chem. Phys. Lett.* **167**, 193-197 (1990).

249. Ershov, B.G. & Henglein, A. Time-resolved investigation of early processes in the reduction of Ag+ on polyacrylate in aqueous solution. *J. Phys. Chem. B* **102**, 10667-10671 (1998).

250. Ershov, B.G. & Henglein, A. Reduction of Ag+ on polyacrylate chains in aqueous solution. *J. Phys. Chem. B* **102**, 10663-10666 (1998).

251. Crooks, R.M., Zhao, M.Q., Sun, L., Chechik, V. & Yeung, L.K. Dendrimer-encapsulated metal nanoparticles: Synthesis, characterization, and applications to catalysis. *Acc. Chem. Res.* **34**, 181-190 (2001).

252. Ottaviani, M.F., Valluzzi, R. & Balogh, L. Internal structure of silver-poly(amidoamine) dendrimer complexes and nanocomposites. *Macromolecules* **35**, 5105-5115 (2002).

253. Zhou, Y., Itoh, H., Uemura, T., Naka, K. & Chujo, Y. Preparation of pi-conjugated polymer-protected gold nanoparticles in stable colloidal form. *Chem. Commun.*, 613-614 (2001).

254. Kelly, T.L. & Wolf, M.O. Template approaches to conjugated polymer micro- and nanoparticles. *Chem. Soc. Rev.* **39**, 1526-1535 (2010).

255. Ofir, Y., Samanta, B. & Rotello, V.M. Polymer and biopolymer mediated self-assembly of gold nanoparticles. *Chem. Soc. Rev.* **37**, 1814-1823 (2008).

256. Shan, J. & Tenhu, H. Recent advances in polymer protected gold nanoparticles: synthesis, properties and applications. *Chem. Commun.*, 4580-4598 (2007).

257. Hao, E.C., Kelly, K.L., Hupp, J.T. & Schatz, G.C. Synthesis of silver nanodisks using polystyrene mesospheres as templates. *J. Am. Chem. Soc.* **124**, 15182-15183 (2002).

258. Treguer, M. et al. Fluorescent silver oligomeric clusters and colloidal particles. *Solid State Sci* **7**, 812-818 (2005).

259. Zhang, J.G., Xu, S.Q. & Kumacheva, E. Photogeneration of fluorescent silver nanoclusters in polymer microgels. *Adv. Mater.* **17**, 2336-2340 (2005).

260. Shang, L. & Dong, S.J. Sensitive detection of cysteine based on fluorescent silver clusters. *Biosens Bioelectron* **24**, 1569-1573 (2009).

261. Shchukin, D.G., Radtchenko, I.L. & Sukhorukov, G.B. Photoinduced reduction of silver inside microscale polyelectrolyte capsules. *ChemPhysChem* **4**, 1101-1103 (2003).

262. Scheer, U. & Hock, R. Structure and function of the nucleolus. *Curr. Opin. Cell Biol.* **11**, 385-390 (1999).

263. Goodpasture, C. & Bloom, S.E. Visualization of nucleolar organizer regions in mammalian chromosomes using silver staining. *Chromosoma* **53**, 37-50 (1975).

264. Roussel, P. & Hernandezverdun, D. Identification of ag-nor proteins, markers of proliferation-related to ribosomal gene activity. *Exp. Cell Res.* **214**, 465-472 (1994).

265. Narayanan, S.S. & Pal, S.K. Structural and functional characterization of luminescent silver-protein nanobioconjugates. *J. Phys. Chem. C* **112**, 4874-4879 (2008).

266. Cathcart, N. et al. Chiral Thiol-Stabilized Silver Nanoclusters with Well-Resolved Optical Transitions Synthesized by a Facile Etching Procedure in Aqueous Solutions. *Langmuir* **25**, 5840-5846 (2009).

267. O'Neill, P.R., Velazquez, L.R., Dunn, D.G., Gwinn, E.G. & Fygenson, D.K. Hairpins with Poly-C Loops Stabilize Four Types of Fluorescent Ag-n:DNA. *J. Phys. Chem. C* **113**, 4229-4233 (2009).

268. Sengupta, B. et al. Base-Directed Formation of Fluorescent Silver Clusters. *J. Phys. Chem. C* **112**, 18776-18782 (2008).

269. Walker, H.K., Hall, W.D.H. & Hurst, J.W. (eds.) Clinical Methods. (Butterworths, Boston; 1990).

270. Luk, K.F.S., Maki, A.H. & Hoover, R.J. Studies of heavy-metal binding with polynucleotides using optical detection of magnetic-resonance - silver(I) binding. *J. Am. Chem. Soc.* **97**, 1241-1242 (1975).

CHAPTER II

Engineering ssDNA to produce Ag nanodots

This Chapter describes the design of single stranded DNA (ssDNA) hairpins to encapsulate silver nanodots. The chemical and fluorescence quantum yield of silver nanodots are improved by four-fold and two-fold, respectively, compared to 12mer polycytosine-protected silver nanodots. The existence of such a hairpin design was confirmed by Förster resonance energy transfer (FRET), pH variation, and nanodot synthesis using mismatched stem pairs. Moreover, studies of photostability and brightness per molecule indicate that silver nanodots are more than 4-fold brighter and 15-fold more photostable, compared to the commercially available organic dyes tested.

2-1. Introduction

Recently, silver nanoclusters fluorophores have shown great promise due to their excellent photophysical properties and reasonably small size.[1, 2] Our lab developed the first methods to produce silver nanodots under the protection of ssDNA, with initial attempts relying heavily on poly cytosine scaffolds.[3] Initial studies were focused on synthesis of nanodots with bright fluorescence and good overall photophysical properties.[3, 4] However, the fluorescence from poly cytosine

based Ag nanodots has multiple peaks ranging from blue to near infrared, and these multiple peaks may interfere with other fluorophores when used for imaging..[3, 5-8] Thus, cellular imaging applications of these initial materials may be complicated by cross-talk among varied fluorescence signals. Although we, very recently, successfully produced spectrally pure Ag nanodots with fluorescence quantum yields of up to 40% and extinction coefficients exceeding 2×10^5 $M^{-1}cm^{-1}$by optimizing ssDNA sequences via DNA microarrays,[9] their poor chemical stability in biologically relevant media such as PBS and cell culture medium indicates that they are not yet ideal for biological applications. Meanwhile, the Fygenson group introduced DNA hairpin concept to produce Ag nanodots, but no improvement on species purity and photophysical properties were obtained.[7, 8]

Herein, we modified ssDNA in a hairpin structure to efficiently encapsulate Ag nanodots. The hairpin structure may form a rigid platform to stabilize silver nanodots. Based on previous reports,[3, 7] relatively high fluorescence intensity from Ag nanodots was produced when cytosine was highly abundant in the encapsulating ssDNA scaffold. Therefore, by keeping the loop base as cytosine and adjusting the loop base length and stem base pair, we generated a broad range of highly bright emitters with spectral purity as well as excellent photophysical properties.

2-2. Experimental section

Materials

All oligonucleotides were purchased from Integrated DNA Technologies (Coralville, IA) and purified with standard desalting by the manufacturer except for those tagged with a specific dye or a functional group which were purified with HPLC by the company. Basic chemical reagents were purchased from Sigma-Aldrich. Silver nitrate with 99.9999% purity and sodium borohydride with 98% purity were used. All syntheses were performed in deionized water (18 MΩ from Barnstead Thermolyne E-Pure system).

Synthesis

The designed oligonucleotide was first dissolved in deionized water to prepare a stock solution. Generally, silver nanodots were produced in sodium phosphate buffer, but cell culture medium, phosphate buffered saline (PBS), or 10% serum was also used instead of phosphate buffer. All DNA-encapsulated Ag nanodots were prepared by mixing 53 μM of designed oligonucleotide with $AgNO_3$ at 1.33 ~ 2 : 1 ratio of loop base : silver. This mixture was kept in the dark at room temperature overnight, followed by reduction with one equivalent of aqueous $NaBH_4$ solution (versus silver) with vigorous stirring. Then, the solution was stored at 4^oC overnight for stability. The resulting solutions show very bright emission under 365 nm excitation. The emissive Ag nanodot solution was used directly for photophysical characterization.

Bulk photophysical characterization

Measuring fluorescence and absorption are a basic but essential steps to characterize Ag nanodots' photophysical properties. A Photon Technology International (PTI) Quanta Master 40 fluorometer was used for fluorescence measurement with a Xenon arc lamp as an excitation source and a photomultiplier tube sensitive out to 900 nm as a detector. A Shimadzu UV 2401 PC spectrophotometer was used for absorption measurements. All samples were transferred to either a quartz or glass cuvette for collecting data. Fluorescence lifetime measurements were performed with an Edinburgh Instruments Lifespec-ps system with a Hamamatsu multi-channel plate photomultiplier tube detector. Picoquant laser diode heads were used for lifetime measurement as excitation sources controlled by either a PDL 800-B or Sepia II laser driver system.

Fluorescence microscopy

All fluorescence samples used in microscope experiments were performed on Olympus IX-70 or IX-71 microscopes and followed the standard setup; light from excitation source by a laser or a Hg lamp was reflected by dichroic mirror into objective and excited the sample. The emission then passed through the objective and then the dichroic mirror to reach photon detection system, such as a CCD camera (MicroMax, Princeton Instruments). A water immersion objective (60×, NA 1.20) was used for aqueous samples, but an oil immersion objective (60×, NA 1.45) was used for immobilized samples including films. All samples for microscopy were prepared on 22.5 mm × 22.5 mm glass cover slips with a thickness of 0.15 ± 0.02

mm (Fisher, Fisherfinest). Before using the glass cover slips, they were cleaned with a three step process. First, glass cover slips were immersed in 0.1 M NaOH solution and sonicated for one hour. The cover slips were rinsed with deionized water 3 times and then sonicated in deionized water again for one hour. After being washed with acetone 3 times, they were sonicated in acetone for one hour, and then quickly dried in flowing nitrogen gas. Finally, the glass cover slips were further dried in a vacuum oven overnight.

Fluorescence correlation spectroscopy

Fluorescence correlation spectroscopy (FCS) is a typical technique to characterize the dynamics of fluorescent materials in solution, for example, diffusion constants and hydrodynamic radii.[10] The FCS setup is quite similar to the typical microscopy set up as described earlier. A laser beam is used and focused into a very dilute solution having the fluorophore of interest such that the fluorescence fluctuations of emitted photons which diffuse in and out of the laser focus are collected and recorded. The detection volume of about 10^{-15} L (1 femtoliter) is defined by the tightly focused laser beam and only emission from a small fixed focal volume is detected using a pinhole to reject out of focus emission. The diffusion of molecules through the focal volume of the laser generates a decay in the autocorrelation curve. The autocorrelation of a time function F(t) is written as,[11]

$$G(\tau) = \frac{< \delta F(t) \delta F(t+\tau) >}{< F(t) >^2}$$

Where $\delta F(t)$ is the deviation from the temporal average, in $\delta F(t) = F(t) - \langle F(t) \rangle$. For a fluorescent molecule diffusing through a 3-dimensional Gaussian-shaped laser beam, the autocorrelation can be represented as[11, 12]

$$G(\tau) = \frac{1}{n}\left(\frac{1}{1+\frac{\tau}{\tau_D}}\right)\left(\frac{1}{1+\left(\frac{\varpi_o}{\varpi_Z}\right)^2\left(\frac{\tau}{\tau_D}\right)}\right)^{1/2}$$

in which n is the average number of molecules in the focal volume, τ_D is the diffusion time, ω_0 is the waist size defined by the boundary where the Gaussian excitation profile decays to $1/e^2$ in the x and y directions, and ω_z is the distance in the z direction. At $\tau = 0$ the autocorrelation becomes $G(t)= 1 + 1/n$, thus the amplitude of the autocorrelation at zero lag time is the inverse of the number of molecules. The diffusion constant D can be determined by the relationship $\tau_D = \omega_0^2/4D$.

The focal volume can be determined by measuring the highly diluted standard dye. The effective volume can then be calculated from the known diluted concentration and the average number of molecules in the solution. The local concentration of a diluted fluorophore sample is calculated based on the focal volume and the average number of molecules in this focal volume, and then the sample concentration can be known according to the dilution number. The extinction coefficient (ε) is calculated based on Beer's law ($A=\varepsilon lc$), where A is the absorbance of the fluorophore sample, l is the path length (1 cm), and c is the concentration.

2-3. Results and discussion

Hairpin scaffold does show better efficiency in creation of silver nanodots compared to simple polycytosine. 5′-CGCGCCCCCCCCCCCCCGCG-3′ (CGCGC12) was investigated first, in which the flanking CGCG parts form a hairpin stem, and the 12 cytosine bases configure the loop section. Figure 2-1 shows the comparison of emission intensity of silver nanodots produced in the presence of either a regular ssDNA (5′-CCCCCCCCCCCC-3′; C12) or a hairpin structure (CGCGC12). To check the chemical yield of silver nanodots, the DNA concentration in each solution is kept at 53 μM and Ag^+ at 318 μM. The nanodots protected with CGCGC12 exhibit a single emission band at 615 nm and its emission intensity is 8-fold higher than that with a simple polycytosine single strand 12mer DNA. By FCS measurement, the final concentration of silver nanodots is determined to be 800 nM, about 4-fold higher than that of C12 silver nanodots. The fluorescence quantum yield also shows a two-fold improvement over C12 silver nanodots. Similarly, by changing the hairpin structure, several spectrally-pure emitters were also generated, such as 5′-GGGGCCCCCCCCCCCC-3′ (GGGGC8) yielding 670 nm emission. The stem part of the hairpin sequence actually influences the emitter's properties. For instance, when the stem part of CGCGC12 is changed to CGAA (5′-CGAACCCCCCCCCCCCTTCG-3′, CGAAC12), the emission of silver nanodots shifts to 590 nm. Interestingly, the replacement of the stem part with AATT results in 635 nm emission. However, this emission gradually shifts to 562 nm (5′-AATTCCCCCCCCCCCCAATT-3′, AATTC12). Another sequence, 5′-ATATCCCCCCCCCCCCATAT-3′ (ATATC12) also shows a similar trend, shifting

from 635 nm to 560 nm shown in Figure 2-2A. Moreover, by changing the cytosine loop length, different emitters can be produced as well. Figure 2-2B shows the emission and absorption spectra of 5′-ATATCCCCCCCCATAT-3′ (ATATC8), four bases shorter in the loop part compared to ATAT12, forming a stable 635 nm emitter. These differences suggest that shorter loop may actually configure a tighter envelope around silver nanodots, and consequently the resulting silver nanodots are more stable. All nanodots within a hairpin structure show much higher emission than that in a non-hairpin ssDNA. The normalized emission spectra of Ag nanodots produced in different designed DNA sequences are shown in Figure 2-2. It seems that most of the polycytosine derivatives lead to the formation of red emitter at the very beginning. However, a weak hairpin could not maintain the silver nanodot structure, resulting in spectral shift. It is not clear from which factors such shifts are derived: the change in oxidation state of silver, the coordination structure of silver-DNA complexes, or the number silver atoms in the nanodots.

Those hairpins with a CGCG stem create more stable emission, i.e. their emission peak will not drift once emission is observed. It is possible that a longer loop with more binding sites may easily enclose more Ag ions and consequently has higher probability to form Ag nanodots after reduction. However, it is not the longer the loop, the more intense the emission. Each particular emitter needs to be optimized by adjusting the length of cytosine to produce higher emission intensity. For example, all of 5′-CGCGC$_x$CGCG-3′ (CGCGCx; x = 8, 12, 15) sequence are able to protect silver nanodots. However, only 12 mer cytosine (x = 12) as a loop

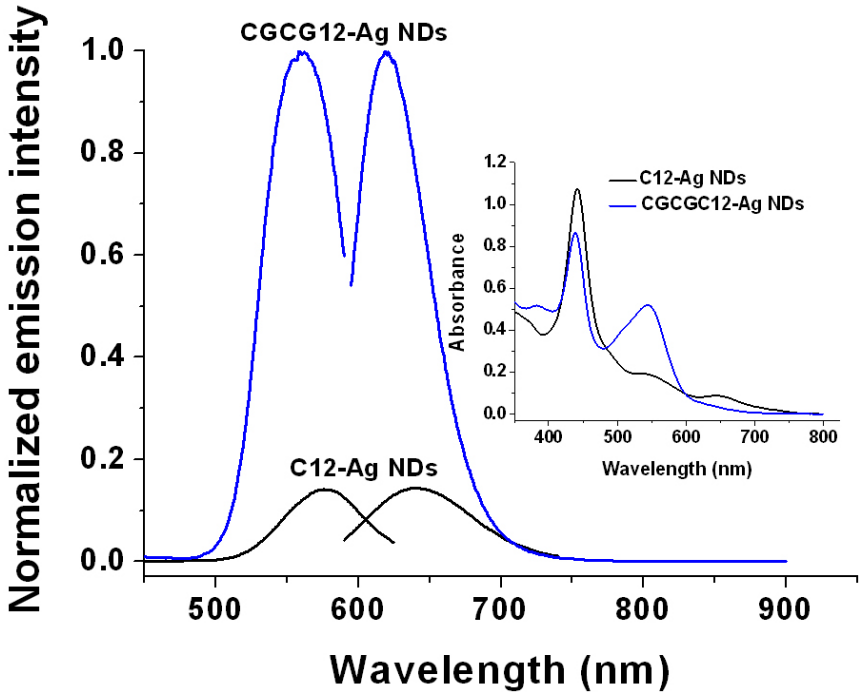

Figure 2-1. Emission intensity and absorption comparison of Ag nanodots between protection sequence with a hairpin structure (blue, CGCGC12: 5′-CGCGCCCC CCCCCCCCCGCG-3′) and that with a simple polycytosine structure (black, C12: 5′-CCCCCCCCCCCC-3′). In the emission figure, the curves on the left are excitation spectra and on the right are emission spectra. For emission spectrum, the emitter was excited at 560 nm, and excitation spectrum was monitored at 615 nm. C12 (ε = 195,000 $M^{-1}cm^{-1}$, Φ= 23%)[13] and CGCGC12 (ε = 950,000 $M^{-1}cm^{-1}$, Φ= 42%).

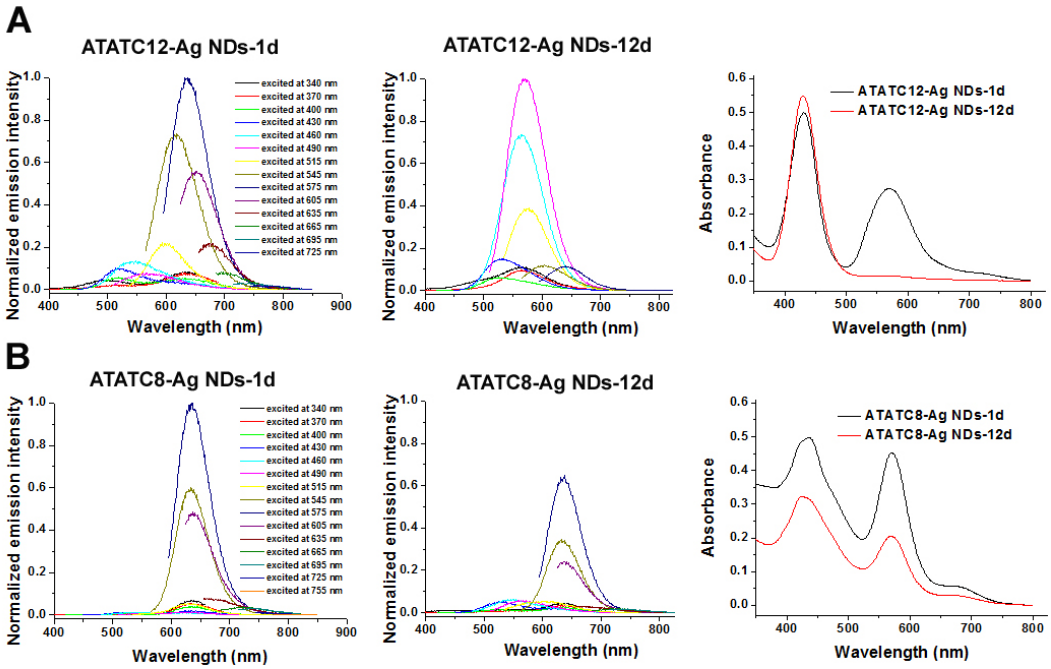

Figure 2-2. Emission and absorption spectra of Ag nanodots after reduction. A. Ag NDs protected by ATATC12 sequence (5′-ATATCCCCCCCCCCCCATAT-3′) and B. Ag NDs protected by ATATC8 sequence (5′-ATATCCCCCCCCATAT-3′). Full emission spectra were scanned at the first day (left) and the 12th day (middle) after reduction, and absorption spectra (right) were checked at the first day (black) and the 12th day (red) after reduction. All samples were stored at 4^{o}C.

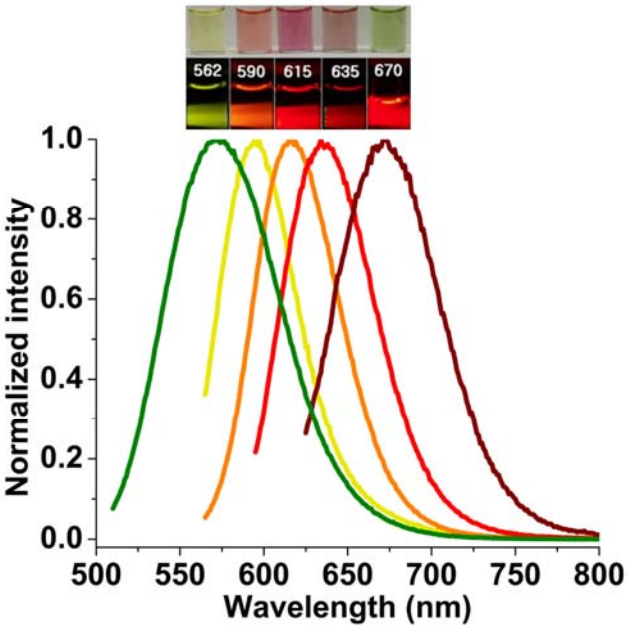

Figure 2-3. Normalized emission spectra of various emitters, from left to right: 562 nm emitter (AATTC12, 5′-AATTCCCCCCCCCCCCAATT-3′), 590 nm emitter (CGAAC12, 5′-CGAACCCCCCCCCCCCCCGAA-3′), 615 nm emitter (CGCGC12, 5′-CGCGCCCCCC CCCCCCCGCG-3′), 635 nm emitter (ATATC8, 5′-ATAT CCCCCCCCATAT-3′), 670 nm emitter (GGGGC8, 5′-GGGGCCCCCCCCCCCC-3′). (Inset) different color Ag emitters: Their visible color (top) and their fluorescence (bottom) excited at their near excitation maximum.

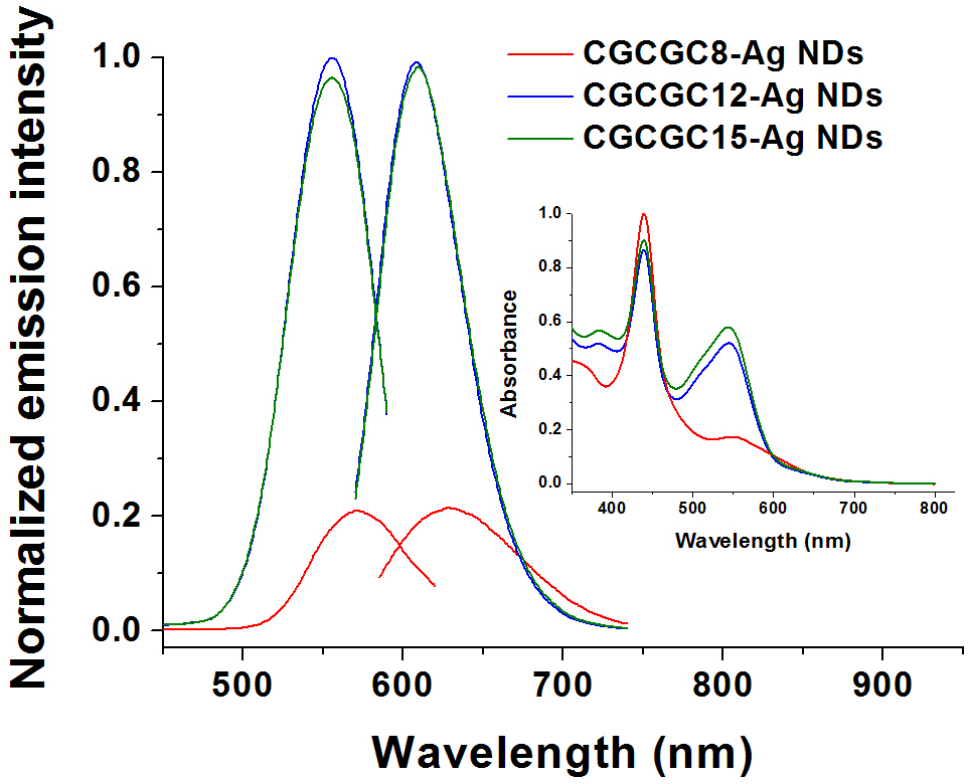

Figure 2-4. Emission and absorption spectra of Ag nanodots created in modifying different loop length of CGCGC12 sequence: CGCGC8 (5′-CGCGCCCCCCCCCGCG-3′, red), CGCGC12 (5′-CGCGCCCCCCCCCCCCCGCG-3′, blue), CGCGC15 (5′-CGCGCCCC CCCCCCCCCCCCGCG-3′, green). In the emission figure, the curves on the left are excitation spectra and on the right are emission spectra. For emission spectrum, the emitter was excited at 560 nm, and excitation spectrum was monitored at 615 nm.

exhibits the highest emission intensity, as shown in Figure 2-3. The calculated melting temperatures of these hairpins have little difference, with CGCGC8 having the highest of 59^{o}C, CGCGC15 the lowest of 54^{o}C and 57^{o}C for CGCGC12. The nanodot creation yield might be a balance between the binding efficiency of silver to DNA base and the capability of DNA to stabilize the silver nanodots. The CGCGC8 has a tighter stem and therefore silver ions might not be easy to coordinate into the loop. Contrarily, the loop of CGCGC15 is not fastened, and silver nanodots could not be stabilized well. Since denaturation of hairpin before being mixed with silver ions does not increase the nanodot creation efficiency, the binding of silver to DNA might be always at their thermal equilibrium, which is partially in line with that report that silver ions could stabilize C-C base pair by forming C-Ag-C coordination due to their strong affinity.[14] In order to probe the degree of hairpin formation, Förster resonance energy transfer (FRET) was used. In general, some of energy initiated from excitation at a certain wavelength in a donor molecule may be transferred to an acceptor molecule, resulting in excited acceptor. This process depends on the spectral match between the emission of donor and the absorption of acceptor, the conformation of the FRET pair and, strongly on the distance between the donor and acceptor ($E_{fret} \propto 1/r^6$, where E_{fret} is the energy transfer efficiency, and r is the distance between donor and acceptor)[15, 16].

In the absence of silver, we used Cy3 and Cy5 pair to check the FRET efficiency, which are attached to the 5′ and 3′ ends of the hairpin DNA sequence, respectively. Cy3 has emission near 570 nm when excited at 550 nm and Cy5 near 670 nm when excited at 650 nm. Thus, the emission ratio between Cy5 and Cy3 was

monitored while the Cy3/Cy5 pair was excited at 550 nm in varied temperature. In this case, FRET efficiency depends on the transition melting temperature (T_m) of a hairpin structure. The FRET efficiency will be high when the temperature is much below T_m and get lower when the temperature is increased gradually above T_m. There are two possibilities for designed DNA sequence to interact with each other (scheme 2-1.); one is from intermolecular interaction (the 5′ edge part from one of the ssDNA molecule may bind to the 3′ edge part of another molecule which are complementary to each other), and the other from intramolecular interaction (hairpin structure). Therefore, we modified DNA with Cy3 and Cy5, respectively: 5′-Cy5-AATTCCCCCCCCCCCCAATT-3′ (sequence 1) and 5′-AATTCCCCCCCCCCCC AATT-Cy3-3′ (sequence 2) and 5′-Cy5-AATTCCCCCCCCCCCCAATT-Cy3-3′ (sequence 3). If it is intermolecular interaction, we would be able to observe FRET between sequence 1 and sequence 2. Otherwise, FRET in sequence 3 would suggest the formation of hairpin (intramolecular interaction). As shown in Figure 2-7, we observed the change in emission intensity ratio of (Cy5)/570 nm (Cy3) at 550 nm excitation measured at various temperatures from sequence 3 (Figure 2-7C), but no change between sequence 1 and 2 (Figure 2-7B). Although T_m of AATTC12 (5′-AATTCCCCCCCCCCCCAATT-3′) is calculated as 4^{o}C, the FRET efficiency indicates a T_m of about 25^{o}C. The higher T_m might be ascribed to the contribution from Cy3 and Cy5 modification, or the procedure we applied to measure the FRET. The dye-tagged ssDNA samples were first stored at 2^{o}C and slowly warmed up for FRET measurements. For measurement at each temperature point, samples were equilibrated for 5 minutes. The hairpin may melt much more slowly than what we

have expected. However, no FRET was observed between sequence 1 and 2 in the same conditions, as shown in Figure 2-5, indicating that there was no strong intermolecular interaction, but intramolecular interaction does happen, at least at low temperature. A control to examine the emission intensity changes at different temperature of Cy3 or Cy5 suggests that the Cy3 emission changes little after temperature jump, as shown in Figure 2-6.

The hairpin melting point was also determined by monitoring the absorption of hairpin CGCGC12 (5'-CGCGCCCCCCCCCCCCCGCG-3') at 260 nm, as shown in Figure 2-8. The absorbance of hairpin DNA at 260 nm will increase as it undergo from a tight to a loose structure.[17] The melting temperature is 42^{o}C, close to the calculated hairpin melting point 57^{o}C. Transition temperature was calculated based on Integrated DNA Technologies web source. Available at: http://www.idtdna.com/analyzer/ Applications/OligoAnalyzer/. The single strand DNA CGCGC12 indeed forms hairpin structure. It is quite likely that the particular hairpin structure contribute the highly bright silver nanodots under such hairpin DNA protection.

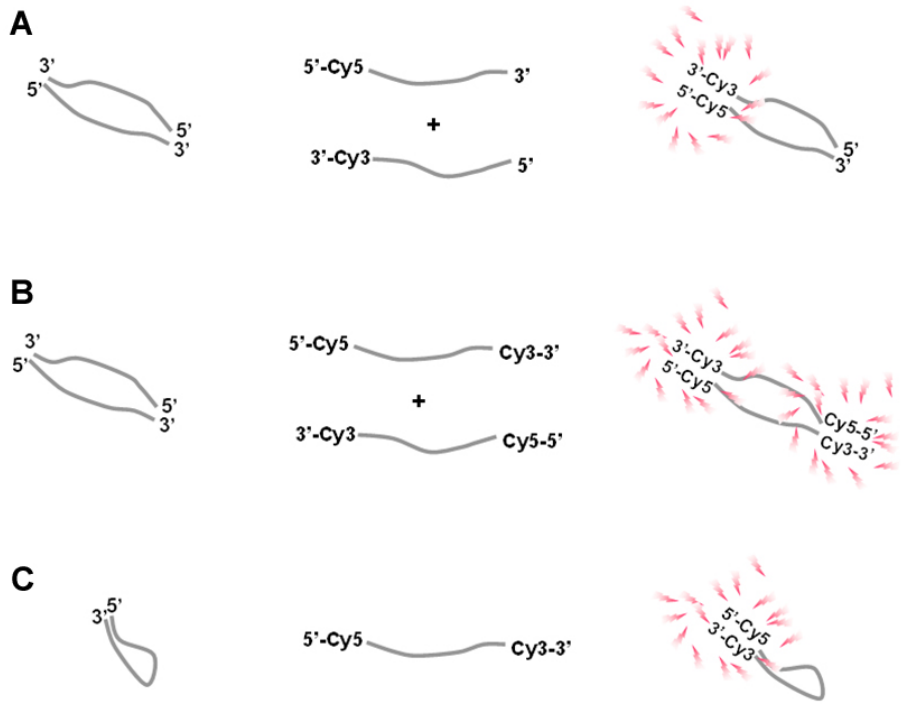

Scheme 2-1. FRET between Cy3 and Cy5 in designed single strand DNA. The single strand DNA was modified with 5'-Cy5-DNA, DNA-Cy3-3', and 5'Cy5-DNA-Cy3-3' respectively. There are three possibilities for DNA sequences to form intermolecular or intramolecular interactions as shown in A, B and C. For 5'Cy5-DNA-Cy3-3' sequence, both intermolecular interaction, as shown in B, and intramolecular interaction, as shown in C, are possible. However, the FRET possibility between 5'-Cy5-DNA, DNA-Cy3-3' tells if there is intermolecular interaction, as shown in A. If there is no FRET in case A, there is no FRET in case B as well. However, if FRET is observed in case C, but not in case A, this will suggest that there is intramolecular interaction, *i.e.*, it forms hairpin structure.

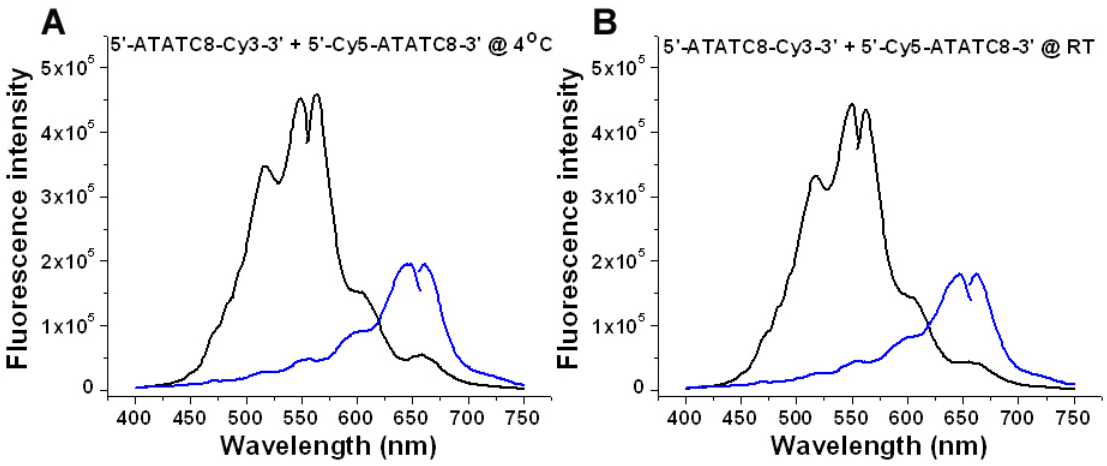

Figure 2-5. Emission and excitation spectra of 5'-ATATC8-Cy3-3' and 5'-Cy5-ATATC8-3' mixture at 1:1 ratio at different temperature. Each sequence was first mixed and then characterized at different temperature. A. the mixture solution of 5'-ATATC8-Cy3-3' (black) and 5'-Cy5-ATATC8-3' (blue) was checked at 4°C. B. the mixture solution of 5'-ATATC8-Cy3-3' (black) and 5'-Cy5-ATATC8-3' (blue) was checked at room temperature. Each dye showed its excitation spectrum (left part) and emission spectrum (right part). For emission spectrum, the emitter was excited at 550 nm and 650 nm, respectively for Cy3 and Cy5, and excitation spectrum was monitored at 570nm and 670 nm, respectively for Cy3 and Cy5. ATATC8, 5'-ATATCCCCCCCCATAT -3'.

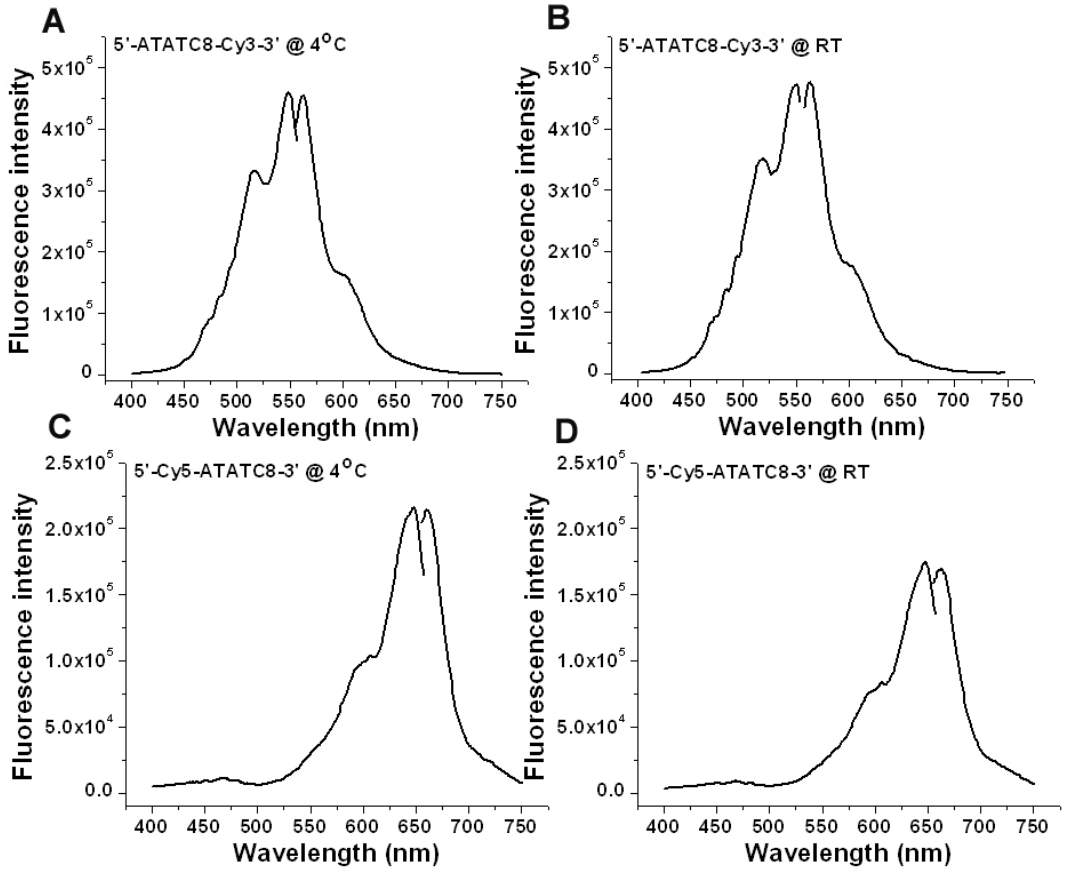

Figure 2-6. Emission and excitation spectra of 5'-ATATC8-Cy3-3' and 5'-Cy5-ATATC8-3' at different temperature. Each sequence was measured at different temperature. The solution of 5'-ATATC8-Cy3-3' was checked at 4°C (A) and room temperature (B). The solution of 5'-Cy5-ATATC8-3' was checked at 4°C (C) and room temperature (D) as well. Each dye showed its excitation spectrum (left part) and emission spectrum (right part). For emission spectrum, the emitter was excited at 550 nm and 650 nm, respectively for Cy3 and Cy5, and excitation spectrum was monitored at 570 nm and 670 nm, respectively for Cy3 and Cy5. ATATC8, 5'-ATATCCCCCCCCATAT -3'.

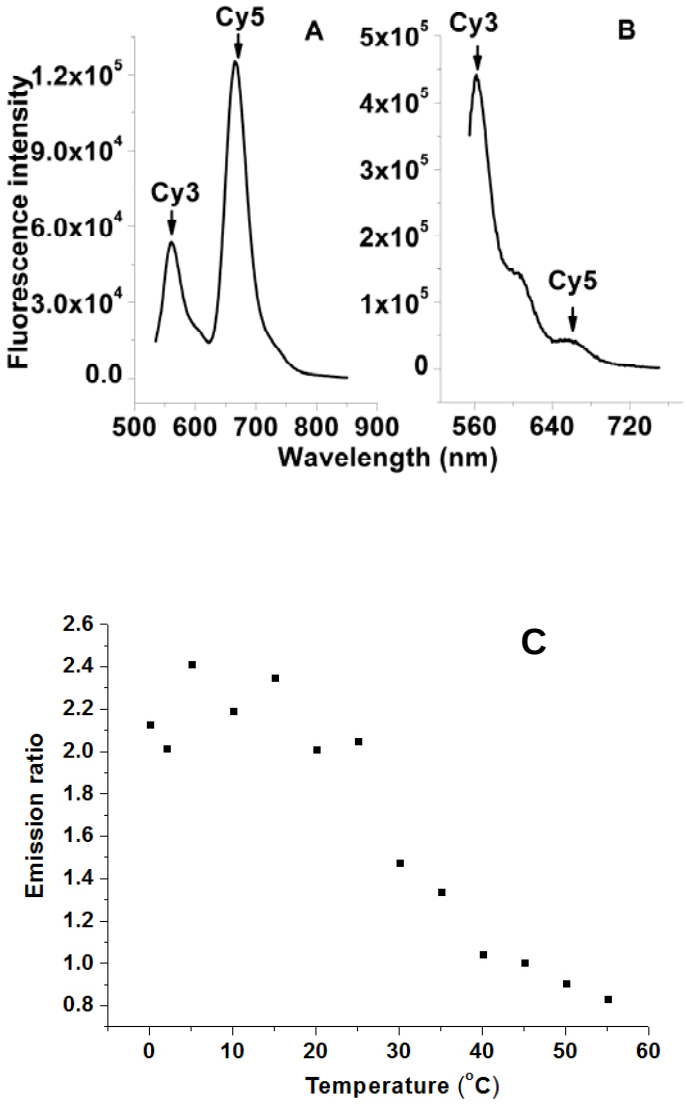

Figure 2-7. Emission ratio of 670 nm (Cy5)/570 nm (Cy3) at 550 nm excitation measured at various temperatures. A. The emission spectrum of 5'-Cy3-ATATC8ATAT-Cy5-3' at 4°C with excitation at 550 nm. B. The emission spectrum of the mixture of 5'-Cy3-ATATC8ATAT-3' and 5'-ATATC8ATAT-Cy5-3' at 1:1 ratio at 4°C with excitation at 550 nm. C. The emission ratio of 670 nm (Cy5)/570 nm (Cy3) for 5'-Cy3-ATATC8ATAT-Cy5-3' at 550 nm excitation measured at various temperatures.

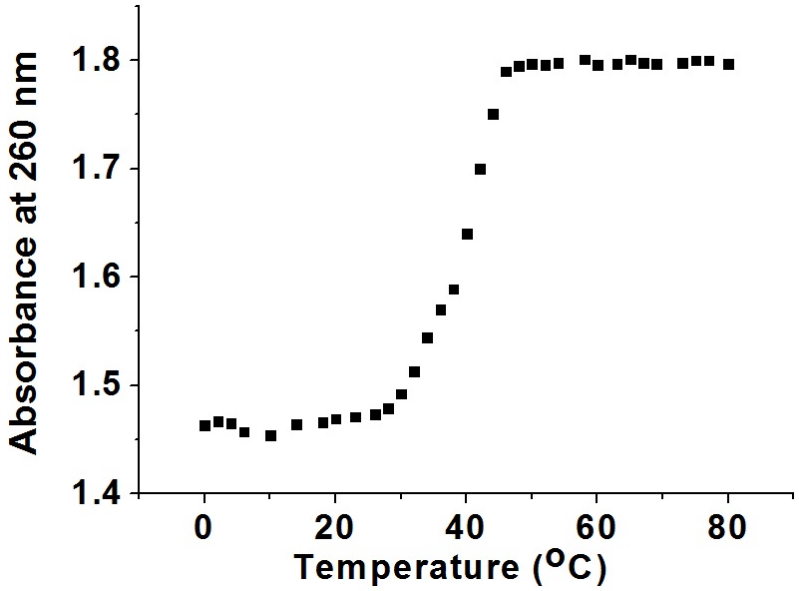

Figure 2-8. Absorption of single strand DNA CGCGC12 at 260 nm in 50 mM sodium phosohate buffer, measured at various temperatures. CGCGC12, 5'-CGCGCCCCCC CCCCCCCGCG -3'.

In addition, we tested the importance of a strong hairpin structure for the efficient creation of silver nanodots. Ag nanodots are created from a hairpin sequence (5′-CGCGCCCCCCCCCCCCCGCG-3′) and that with mismatched stem part (5′-CGGCCCCCCCCCCCCCCGCG-3′), respectively. Figure 2-9 shows the comparison of emission intensity between these two sequences, in which the mismatched one exhibits much lower emission than does the matched sequence. It is likely that the mismatched stem could not efficiently form a hairpin structure in order to encapsulate Ag nanodots firmly. In general, forming a hairpin structure is also influenced by other factors such as ionic strength. Higher ionic strength facilitates the formation of hairpin structure.[18] The emission intensity of hairpin-protected silver nanodots is 4-fold higher when nanodots are created in 50 mM phosphate buffer, compared to those in deionized water, suggesting that a strong hairpin stabilizes the silver nanodots better. However, there is no big difference in nanodots prepared in 50 mM or 100 mM of sodium phosphate (data not shown here).

The ssDNA protected silver nanodots are pH sensitive. As shown in Figure 2-10, the emission intensity of Ag nanodots (CGCGC12 Ag nanodots) is even higher at pH 7 than those at pH 6 or pH 9. It was reported that silver ions bound nitrogen primarily on cytosine base. For free cytidine, it has a pKa of 4.2. However, the pKa varies in polycytosine chain, as reported from 4.5 to 6.2.[19-21] As the pH of the solution moves close to polycytosine's pKa from 7, more nitrogen atoms will be protonated, which inhibits the binding of silver atom to the nitrogen and consequently destabilizes the silver nanodots. On the other hand, the decrease in emission intensity at pH 9 might be ascribed to destabilization of silver nanodots by

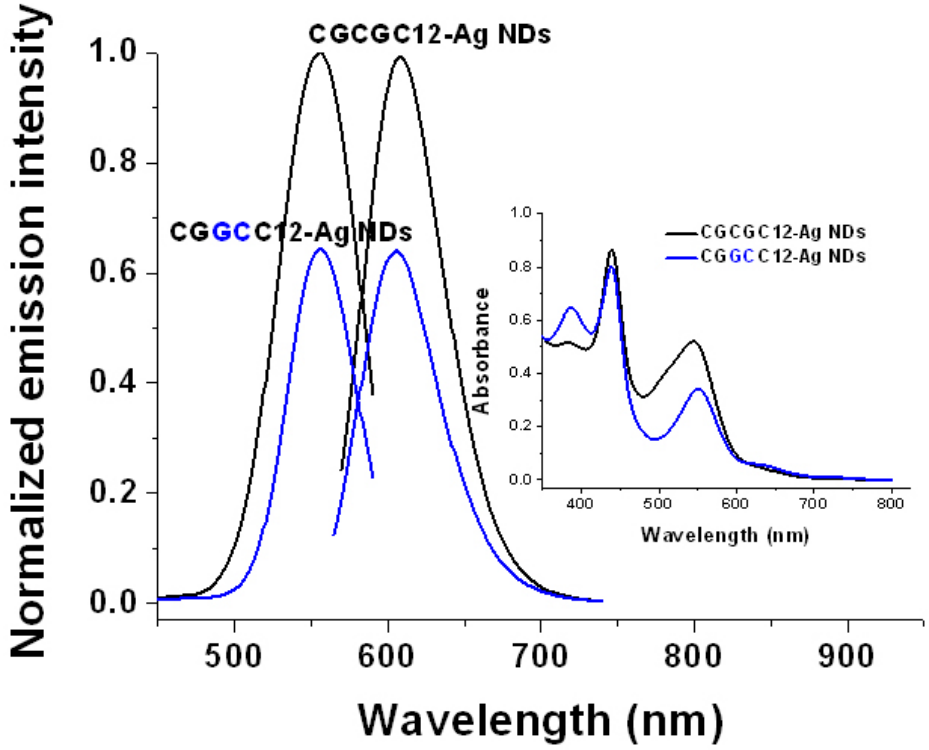

Figure 2-9. Emission and absorption comparison of Ag nanodots protected by a hairpin structure with matched stem pair (black) or mismatched stem pair (blue). Matched stem pair is 5′-CGCGCCCCCCCCCCCCCGCG-3′ and mismatched stem pair 5′-CGGCCCCCCCCCCCCCGCG-3′. In the emission figure, the curves on the left are excitation spectra and on the right are emission spectra. For emission spectrum, the emitter was excited at 560 nm, and excitation spectrum was monitored at 615 nm.

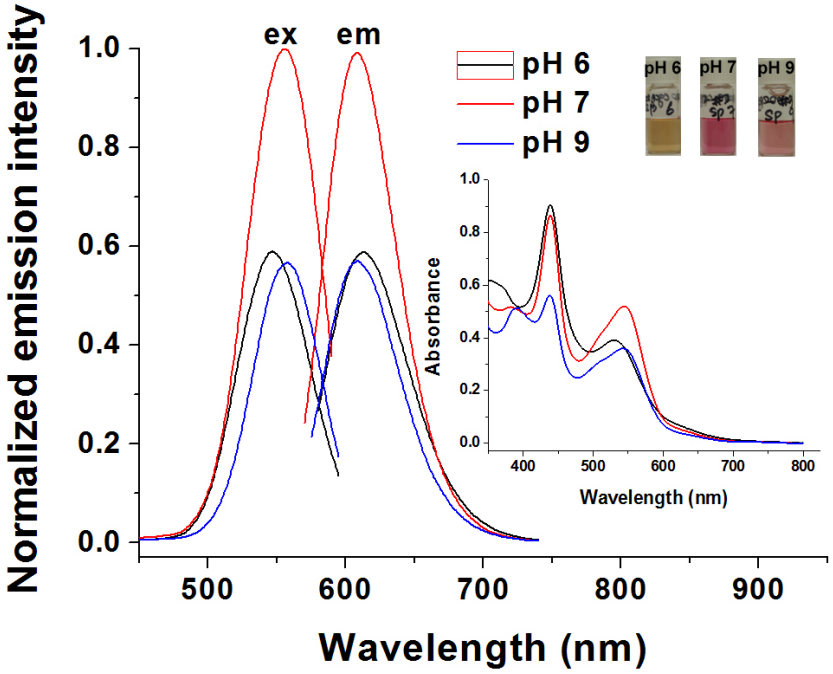

Figure 2-10. Emission and absorption comparison of Ag nanodots protected by a hairpin structure, CGCGC12 (5′-CGCGCCCCCCCCCCCCCGCG-3′), at different pH condition. (Inset) color pictures of Ag nanodot solutions. In the emission figure, the curves on the left are excitation spectra and on the right are emission spectra. For emission spectrum, the emitter was excited at 560 nm, and excitation spectrum was monitored at 615 nm.

forming silver oxide in basic solution. However, it was also reported that some silver nanodot emitters have to be produced in pH 5.[9] Therefore, it is likely that pH influences not only the binding of silver atoms to the nitrogen on the cytosine base, but also the ssDNA secondary structure. In terms of hairpin-protected silver nanodots, pH 7 yields better emission intensity and this pH is applied to other emitters' syntheses.

Under the protection of the hairpin, silver nanodots display dramatic improvement in their photophysical properties. As shown in Table 1, all emitters have a few nanosecond lifetimes, and high quantum yields which almost double those produced in regular C12. The loop structure of hairpin might bring silver atoms closer and there is high probability to form silver nanodots. Moreover, the rigid hairpin feature also stabilizes the newly formed nanodots better, resulting higher concentration solutions. The nanodot extinction coefficients were measured by FCS. One of the emitters (CGCGC12 Ag silver nanodots) has an extinction coefficient as high as 950,000 $M^{-1}cm^{-1}$. However, most of emitters range between 200,000 ~ 350,000 $M^{-1}cm^{-1}$. As we discussed FCS earlier in this Chapter, the diffusion constant D can be determined by the relationship $\tau_D = \omega_0^2/4D$. Based on this equation, the diffusion constant of Ag nanodots can be calculated. Consequently, the hydrodynamic radius (R_h) will be determined by the Einstein-Stokes equation ($D = k_B T/ 6\pi\eta R_h$).[22] The diffusion constant of 615 nm emitter (CGCGC12, 5′-CGCGCCCC CCCCCCCCCGCG-3′) and 635 nm emitter (ATATC8, 5′-ATATCCCCCCCCATAT-3′) is calculated at 8.9×10^{-11} m^2/s and 7.5×10^{-11} m^2/s, respectively, which corresponds to the R_h of 2.4 nm (for 615 nm emitter) and 2.8 nm (for 635 nm emitter).

Table 1. Photophysical Parameters of Ag Nanodots

(sodium phosphate buffer, pH 7, room temperature)

Species	Hairpin T_m (^oC)	Exc/Em (nm)	Lifetime (ns)	Φ (%)	ε ($M^{-1}cm^{-1}$)
Yellow (AATTC12)	9	480/562	4.3	38	200,000
Orange 1 (CGAAC12)	32	543/590	2.0	36	350,000
Orange 2 (CGCGC12)	57	560/615	2.5	42	950,000
Orange 3 (CGAACGCGC12)	72	560/618	2.3	16	280,000
Red1 (ATATC8)	3	570/635	2.7	26	320,000
Red2 (GGGGC8)	64	600/670	3.5	34	250,000

Silver nanodots protected with hairpin DNA also show excellent photophysics not only in bulk solution, but also at the single molecule level. We compared their brightness and photostability with a commercially available organic dye, Texas Red, in PVA film at the single molecule level. As shown in Figure 2-11, Ag nanodots are at least 4 times brighter and 15-fold more photostable. Texas Red quickly disappeared with a surviving lifetime of 15 +/- 5 s, but Ag nanodots exhibit a survival lifetime of 220 +/- 10 s. With these decent photophysical properties and different color emission regions, it is quite promising that silver nanodots can be a strong candidate for single molecule imaging as well as *in vivo* imaging when conjugated to delivery vehicles.

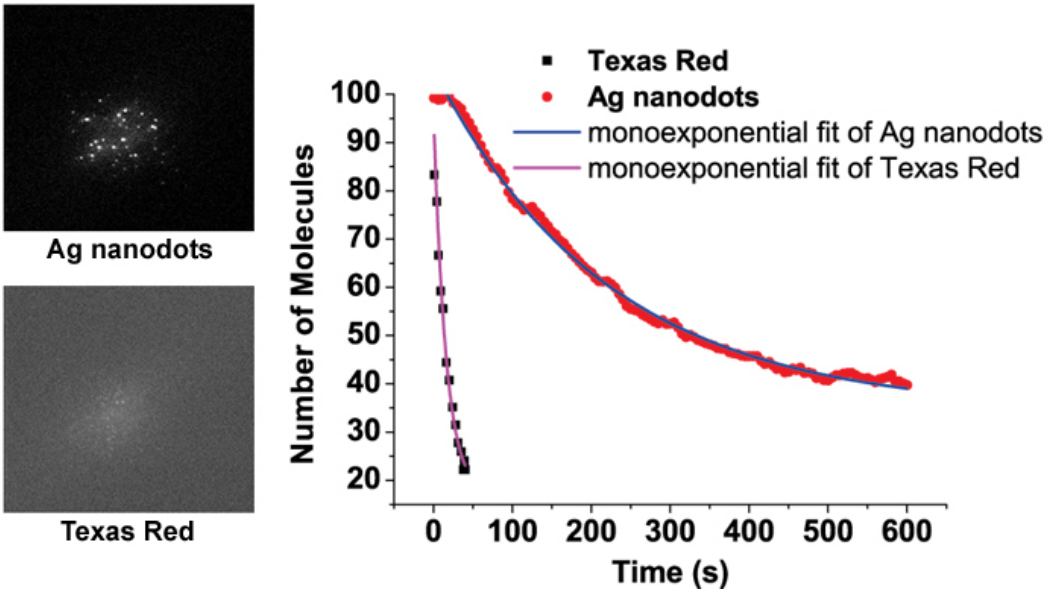

Figure 2-11. Comparison of brightness and photostability between Ag nanodots (red) and Texas Red (black). 568 nm excitation at 0.5 kW/cm^2, 635 nm emitter; decay time: 220 +/- 10 sec., brightness : 17,000 counts/molecule/sec. Texas Red; decay time: 15 +/- 5 sec., brightness: 4,000 counts/molecule/sec. The curves were fitted monoexponentially. The left panel shows typical fluorescent images of silver nanodots and Texas Red at single molecule level.

2-4. Conclusions

In this Chapter, DNA hairpin structures were introduced to protect Ag nanodots. Compared to regular ssDNA, silver nanodots were produced more efficiently. These silver nanodots exhibit spectrally pure emissions, higher quantum yields as well as excellent extinction coefficients. Given the 4-fold higher brightness and 15-fold high photostability compared to commercially available organic dyes, silver nanodots may hold promise for cellular staining.

2-5. References

1. Xu, H.X. & Suslick, K.S. Water-Soluble Fluorescent Silver Nanoclusters. *Adv. Mater.* **22**, 1078-1082 (2010).

2. Lin, C.-A. et al. Synthesis of Fluorescent Metallic Nanoclusters toward Biomedical Application: Recent Progress and Present Challenges. *J. Med. Biol. Eng.* **29**, 8 (2009).

3. Petty, J.T., Zheng, J., Hud, N.V. & Dickson, R.M. DNA-templated Ag nanocluster formation. *J. Am. Chem. Soc.* **126**, 5207-5212 (2004).

4. Vosch, T. et al. Strongly emissive individual DNA-encapsulated Ag nanoclusters as single-molecule fluorophores. *Proc. Natl. Acad. Sci. U. S. A.* **104**, 12616-12621 (2007).

5. Ritchie, C.M. et al. Ag nanocluster formation using a cytosine oligonucleotide template. *J. Phys. Chem. C* **111**, 175-181 (2007).

6. Sengupta, B. et al. Base-Directed Formation of Fluorescent Silver Clusters. *J. Phys. Chem. C* **112**, 18776-18782 (2008).

7. Gwinn, E.G., O'Neill, P., Guerrero, A.J., Bouwmeester, D. & Fygenson, D.K. Sequence-dependent fluorescence of DNA-hosted silver nanoclusters. *Adv. Mater.* **20**, 279-283 (2008).

8. O'Neill, P.R., Velazquez, L.R., Dunn, D.G., Gwinn, E.G. & Fygenson, D.K. Hairpins with Poly-C Loops Stabilize Four Types of Fluorescent Ag-n:DNA. *J. Phys. Chem. C* **113**, 4229-4233 (2009).

9. Richards, C.I. et al. Oligonucleotide-stabilized Ag nanocluster fluorophores. *J. Am. Chem. Soc.* **130**, 5038-5039 (2008).

10. Elson, E.L. & Magde, D. Fluorescence correlation spectroscopy .1. conceptual basis and theory. *Biopolymers* **13**, 1-27 (1974).

11. Widengren, J., Mets, U. & Rigler, R. Fluorescence correlation spectroscopy of triplet-states in solution - a theoretical and experimental-study. *J. Phys. Chem.* **99**, 13368-13379 (1995).

12. Ringemann, C. et al. Enhancing fluorescence brightness: Effect of reverse intersystem crossing studied by fluorescence fluctuation spectroscopy. *ChemPhysChem* **9**, 612-624 (2008).

13. Antoku, Y. Fuorescent Polycytosine-Encapsulated Silver Nanoclusters *Ph. D thesis. Georgia Institute of Technology* (2007).

14. Ono, A. & Miyake, Y. Highly selective binding of metal ions to thymine-thymine and cytosine-cytosine base pairs in DNA duplexes. *Nucleic Acids Res.*, 227-228 (2003).

15. Jares-Erijman, E.A. & Jovin, T.M. FRET imaging. *Nat. Biotechnol.* **21**, 1387-1395 (2003).

16. Truong, K. & Ikura, M. The use of FRET imaging microscopy to detect protein-protein interactions and protein conformational changes in vivo. *Curr. Opin. Struct. Biol.* **11**, 573-578 (2001).

17. Xodo, L.E., Manzini, G., Quadrifoglio, F., Vandermarel, G.A. & Vanboom, J.H. Oligodeoxynucleotide Folding in Solution: Loop Size and Stability of B-Hairpins. *Biochemistry* **27**, 6321-6326 (1988).

18. Schildkr.C & Lifson, S. Dependence of melting temperature of DNA on salt concentration. *Biopolymers* **3**, 195-208 (1965).

19. Mei, B.C., Susumu, K., Medintz, I.L. & Mattoussi, H. Polyethylene glycol-based bidentate ligands to enhance quantum dot and gold nanoparticle stability in biological media. *Nat. Protoc.* **4**, 412-423 (2009).

20. Lu, Y. & Liu, J.W. Functional DNA nanotechnology: emerging applications of DNAzymes and aptamers. *Curr. Opin. Biotechnol.* **17**, 580-588 (2006).

21. Dubertret, B., Calame, M. & Libchaber, A.J. Single-mismatch detection using gold-quenched fluorescent oligonucleotides. *Nat. Biotechnol.* **19**, 365-370 (2001).

22. Zeiss, C. *Advanced Imaging Microscopy- Confocor 2 Applications Handbook. Zeiss, Jena, Germany; 2001.*

CHAPTER III

Intracellular staining with Ag nanodots

In this Chapter, I describe the improvement of chemical and thermal stability of Ag nanodots based on modifying the hairpin structure, and the protocol for preparation of highly concentrated Ag nanodots. The applications of these improved Ag nanodots were demonstrated by conjugation to antibodies for multi-color specific staining in fixed cells. In addition, nanodots' reliability in biological environments was also examined by microinjection of silver nanodots directly into live cells.

3-1. Introduction

Fluorophores, especially for bio-imaging, should not only exhibit outstanding photophysics, but also show good biocompatibility. Not like organic dyes, silver nanodots are built up based on coordination bonds between silver atoms and their protection groups. This means that competition coordination will always happen, leading to destabilization of nanodots. Consequently, a large and tight protection is fundamental to keep those competing reactions away from silver nanodots. Otherwise, the protection group itself should have very high affinity to silver nanodots so that other ligands could not compete with this group, such as peptide-protected silver nanodots reported earlier from our lab.[1] Likely due to its high affinity to silver ions and relatively large size,[2]

ssDNA, particularly polycytosine, affords strong protection for nanodots, resulting in the creation of Ag nanodots with outstanding photophysics, e.g., high quantum yield, high molar extinction coefficient and excellent photostability.[3-6] However, the major silver binding position of cytosine is reported to be **N3** atom of cytidine, indicating that multi-bases are involved in the protection of nanodots.[2, 7, 8] Therefore, the conformation of DNA may influence nanodot stability. In other words, the DNA-protected silver nanodots might be more vulnerable in physiological medium. Understanding the critical factors for highly stable silver nanodot creation is essential for bio-related applications.

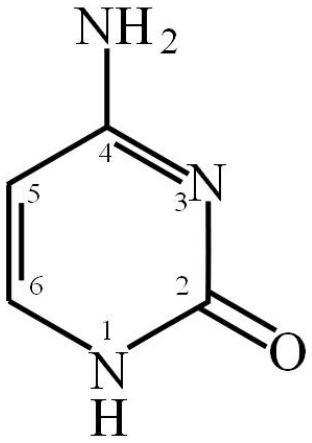

Scheme 3-1. Cytosine structure and N3 position

Although silver nanodots are still under improvement as new fluorophores, there have been reports on their applications as sensors. By detecting the fluorescence intensity change, partially ascribed to their vulnerabilities, oligonucleotide-stabilized Ag nanodots were found to be sensitive to the presence of Hg(II).[9] Similarly, poly(methacrylic acid) protected silver nanodots were used for the detection of Cu^{2+}.[10] Moreover, it was noticed that the latter silver nanodots also show strong solvatochromic and solvato-fluorochromic properties.[11] Our lab has started some tentative research on the biological application of silver nanodots, but mainly focused on fixed cells.[1, 12, 13] However, live cell imaging is one of the biggest challenges for silver nanodots because Ag ions easily react with chloride as well as other anions in physiological conditions, leading to instability.[14-16] Notwithstanding, Ag nanodots optimized via DNA microarrays were improved with spectral purity and photophysical properties, they still need improvement on their chemical stability in biological environments such as PBS and cell culture medium.

As discussed in Chapter 2, we utilized ssDNA hairpin structures to encapsulate Ag nanodots and demonstrated improved spectral purity and photophysical properties. Herein, we tried to modify DNA hairpins to increase silver nanodots' chemical stability, and describe methods to prepare concentrated silver nanodots. The compatibility of silver nanodots for multicolor staining is also examined by conjugating DNA protected silver nanodots to various antibodies before proceeding to specific staining. Moreover, other synthesis strategies, such as direct synthesis of Ag nanodots in biologically relevant conditions including PBS and cell culture medium, alcohol precipitation, and re-reduction, were also applied to improve their chemical stability, resulting in promising advances in live cell intracellular staining by microinjection.

3-2. Experimental section

Materials

All oligonucleotides and chemical reagents were purchased and prepared as previously described in the Chapter 2 unless otherwise specified. Phosphate buffered saline (PBS), ethylenediaminetetraacetic acid (EDTA), trypsin (0.25%), Dulbecco's Modified Eagle's Medium (DMEM), sodium borohydride, 4-(N-Maleimidomethyl) cyclohexane-1-carboxylic acid 3-sulfo-N-hydroxysuccinimide ester sodium salt (sulfo-SMCC), tris(2-carboxyethyl)phosphine (TCEP), penicillin-streptomycin solution, and Sephadex G50 were purchased from Sigma-Aldrich and used as received. 3,000 MWCO centrifugal ultrafiltration vials were obtained from Vivascience, Stonehouse, UK. Anti-heparin/heparan sulfate mouse IgG1 (anti-HS) was obtained from Millipore, MA, USA, and anti-OxPhos complex IV subunit Va mouse IgG2a (anti-OP) from Invitrogen, CA, USA.

Synthesis

DNA-Ag nanodots were synthesized following procedures described earlier in Chapter 2. For direct synthesis of Ag nanodots, PBS and cell culture medium were used instead of sodium phosphate buffer. For cellular experiments using micro-injection, samples should be concentrated by the following method. The emitter was prepared in sodium phosphate buffer or deionized water and concentrated 10 to 20 times, respectively, by a Savant DNA SpeedVac® Concentrator. The concentrated samples were then re-

reduced with an additional 30% of original reduction agents, and stored at 4^{o}C overnight for stabilization. Emitters synthesized in DMEM were concentrated by alcohol precipitation. Emitter solution was added with two volumes of pre-cooled ethanol, stored at -20^{o}C for 30 minutes. The solution was then spun down at 5,000 rcf for 3 minutes. The precipitates were collected and re-dissolved in DMEM to meet a desired concentration (10-20 times concentrated).

Conjugation of antibody-DNA. The disulfide protected ssDNA (5′- ThioMC6-D-DNA-3′, 500 μM) was mixed with TCEP (1 mM) at room temperature in phosphate buffered EDTA (PBE, phosphate 100 mM, sodium chloride 137 mM, potassium chloride 2.5 mM, EDTA 5 mM) in a 1000 MWCO dialysis tube (Spectrum Laboratories). The dialysis tube was then suspended in PBE overnight at 4^{o}C. Antibodies (anti-heparin/heparan sulfate mouse IgG1 (anti-HS, Millipore) or anti-OxPhos complex IV subunit Va mouse IgG2a (anti-OP, Invitrogen)) (50 μg) were mixed with sulfo-SMCC (150 μg) in PBS for 4 hours at room temperature. The mixture was then purified over Sephadex G100 column with PBS as eluant. The purified antibody was mixed with the de-protected ssDNA and kept at 4^{o}C for another 8 hrs and the protein was purified over Sephadex G100 column with PBS as eluant.

Cell culture

NIH 3T3 cells were provided by Dr. D. F. Doyle. (Georgia Institute of Technology). Cells were incubated under 5% carbon dioxide/air at 37°C, in DMEM with

4.5 g/L glucose, L-glutamine and pyruvate, supplemented with 10% natal bovine serum and 1% penicillin/ 100 units streptomycin mixture.

Cellular staining

NIH 3T3 cells were washed with PBS and then fixed with pre-cooled MeOH/acetone at -20^{o}C for 10 minutes, rinsed with deionized water (5 min × 3), and then loaded with anti-mitochondria (ANTI-OXPHOS COMPLEX IV SU) ATATC8 (5′-ATATCCCCCCCCATAT-3′) silver nanodots (5 μM, based on DNA) in 300 μL of DI water for one hour at room temperature. The cells were then washed and incubated with anti-heparan sulfate AATTC12 (5′-ATATCCCCCCCCCCCCATAT-3′)silver nanodots (5 μM, based on DNA) in 300 μL of DI water for 1.2 hours. Cells were washed with deionized water and then mounted on a slide for imaging.

3-3. Results and discussion

We first tested the compatibility of silver nanodots for multicolor staining. As reported earlier, DNA silver nanodot-tagged antibodies stained fixed cells well.[13] Occasionally, emission from some silver nanodots will diminish in the presence of different DNA sequence protected silver nanodots. This is due to silver nanodot transfer from a weak DNA-Ag binding sequence to a strong DNA-Ag binding one. Interestingly, these hairpin-DNA protected silver nanodots are very stable when several emitters are mixed, keeping their characteristic emission. As shown in Figure 3-1, a green C20 emitter was mixed with 670 nm emitter at 1:2 and 1:1 fluorescence intensity ratio. The spectra and intensity of individual emitters did not shift. We then tagged several antibodies with each one of the above emitters. Scheme 3-1 shows the reaction scheme for conjugating antibody with Ag nanodots. For cell membrane staining, we conjugated the 562 nm emitter (AATTC12, 5′-AATTCCCCCCCCCCCCAATT-3′) and anti-heparin/heparan sulfate mouse IgG1 (anti-HS, Millipore).[17, 18] Figure 3-2 shows the emission and excitation spectra of antibody-silver nanodot conjugate. The emission of Ag nanodots blue-shifted to 522 nm, which might be ascribed to the weak encapsulation from AATTC12. As we discussed in Chapter 2, longer length of cytosine base inside A and T matched hairpin structure may not hold Ag nanodots tightly compared to shorter length of cytosine base inside the hairpin structure. Thus, emission spectra were blue-shifted. Here, this sequence conjugated with antibody may also have similar pattern, resulting in the blue-shifted emission. Moreover, to avoid overdose of silver ions, silver ions were added 10% less. It was found the less Ag^{+}/base ratio facilitate the formation of green emitter.[19] The lower local silver concentration leads to the formation of green emitter.

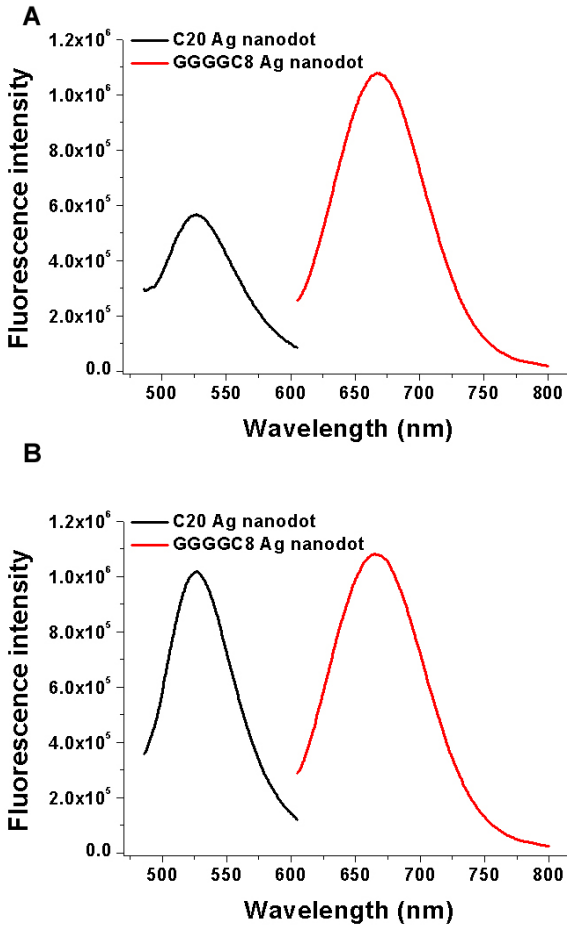

Figure 3-1. Emission spectra after mixing green C20 emitter (5′-CCCCCCCCCCCCCCCC CCCC-3′) and 615 nm emitter (5′-CGCGCCCCCCCCCCCCCGCG -3′) at 1:2 (A) and 1:1 (B) fluorescence intensity ratio. The spectra and intensity did not shift in the mixture, indicating that several silver nanodots emitters are relatively stable in the emitter mixture.

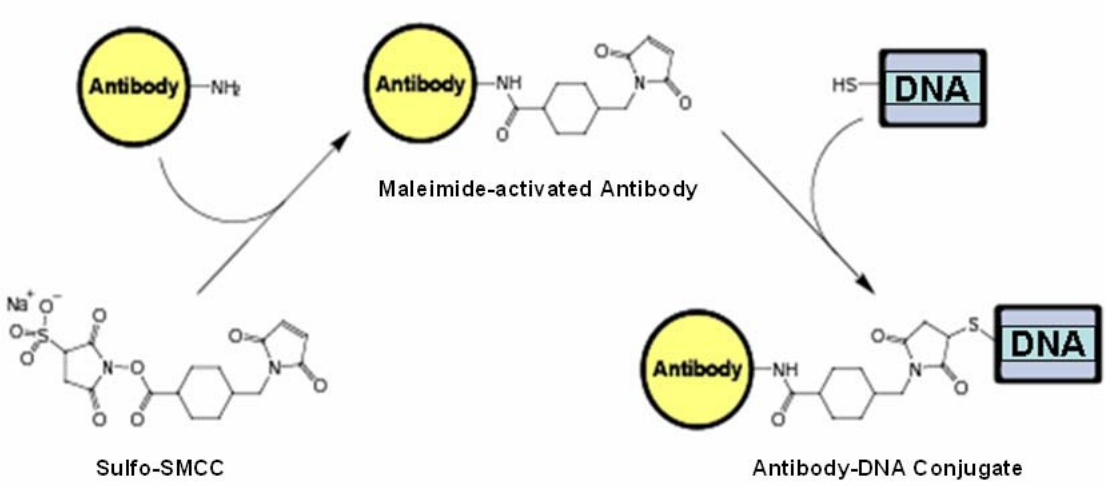

Scheme 3-2. Antibody-DNA conjugation. Antibody (anti-heparin/heparan sulfate mouse IgG1 or anti-OxPhos complex IV subunit Va mouse IgG2a) and thiolated single strand DNA were cross-linked with sulfo-SMCC.

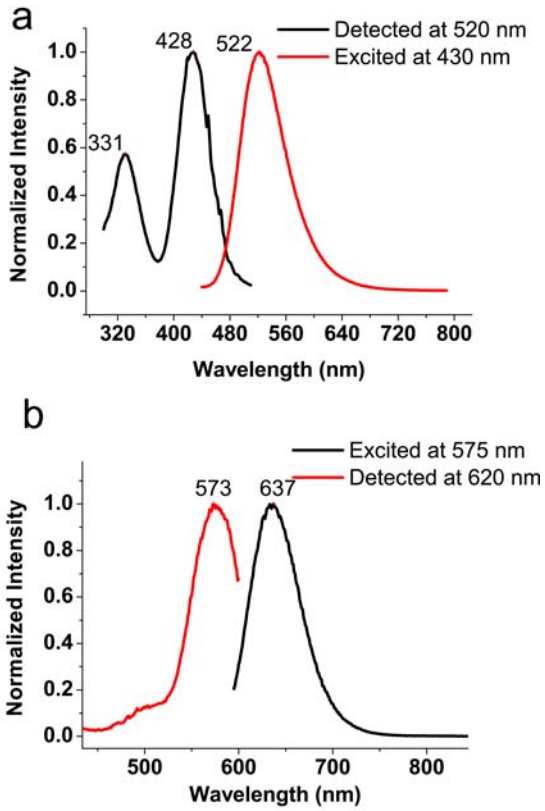

Figure 3-2. Emission and excitation spectra of Ag nanodot conjugated with antibody. (a) 562 nm emitter (AATTC12, 5′-AATTCCCCCCCCCCCCAATT-3′) and anti-heparin/heparan sulfate mouse IgG1 (anti-HS, Millipore). For emission spectrum, the emitter was excited at 430 nm, and excitation spectrum was obtained at 520 nm. (b) 635 nm emitter (ATATC8, 5′-ATATCCCCCCCCATAT-3′) and anti-OxPhos complex IV subunit Va mouse IgG2a (anti-OP, Invitrogen). For emission spectrum, the emitter was excited at 575 nm, and excitation spectrum was obtained at 620 nm.

For mitochondria staining, 635 emitter (ATATC8, 5′-ATATCCCCCCCCATAT-3′) and anti-OxPhos complex IV subunit Va mouse IgG2a (anti-OP, Invitrogen) which marked for mitochondria were used.[20, 21] This emission from the conjugated 635 nm emitter was not shifted from original spectrum. The anti-mitochondria ATATC8 silver nanodot conjugates were first applied to fixed NIH 3T3 cells, followed by the anti-HS AATTC12 conjugate. As shown in Figure 3-3, cell membrane (green) and mitochondria (red) were successfully stained by different color Ag nanodots. There was no obvious interference from silver nanodot transfer between the two antibody-nanodot conjugates. However, we observed non-specific staining, which needs to be minimized in future work.

We improved the stability of Ag nanodots dramatically even in different harsh conditions. Stability of Ag nanodots in different environments such as PBS, cell culture medium, and 10% serum was poor in our previous report, with quick decay of fluorescence. Adding Ag nanodots prepared in deionized water into PBS or DMEM, their emissions were quickly quenched by salts inside standard buffer, especially those containing Cl^-. Therefore improving stability of Ag nanodots in biological media is most challenging. Now, what we introduce here is synthesizing Ag nanodots directly in biological media. Instead of deionized water, PBS and DMEM were used as medium for silver nanodots. Not all the DNA sequences listed in Chapter 2 can produce highly intense emission in such harsh media. An example is 5′-ATATCCCCCCCCCCCCATAT-3′ (ATATC12) sequence, which yields bright 607 nm emission in DMEM (Figure 3-4), with a fluorescence quantum yield of 34% and an extinction coefficient of 360,000 L cm^{-1} mol^{-1}.

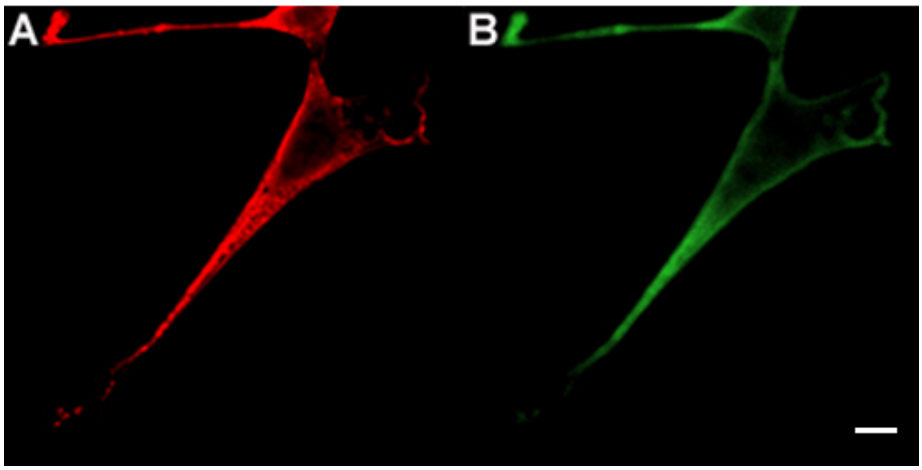

Figure 3-3. Multi-color staining fixed NIH3T3 cells with anti-OxoPhos/ATATC8 Ag nanodots for mitochondria (red) and anti-Heparin Sulfate/AATTC12 Ag nanodots for cell membrane (green). Images were taken on Zeiss laser confocal scanning miscrisope NLS-510. For ATATC8, 543 nm laser was used as excitation light source and 560 LP filter as emission filter. For AATTC12, 452 nm laser line was used for excitation and 505-550 BP as emission filter.ATATC8, 5′-ATATCCCCCCCCATAT-3′ and AATTC12, 5′-AATTCCCCCCCCCCCCAATT-3′. Scale bar, 30 μm.

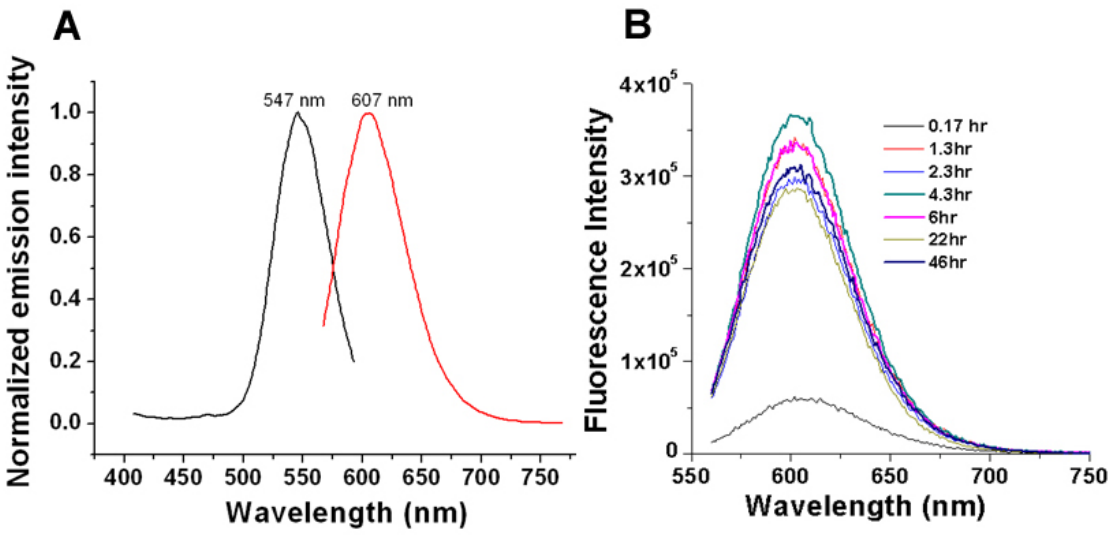

Figure 3-4. (A) Emission and excitation spectra of 607 nm emitter (ATATC12, 5′-ATATCCCCCCCCCCCCATAT-3′) directly synthesized in DMEM. (B) Stability of the 607 nm emitter at 4 ^{o}C was checked after reduction. Its emission spectra were at 547 nm excitation.

We assume that only stable configurations of the mixture from Ag ion and DNA in PBS or DMEM, can survive and proceed to silver nanodot formation. It seems that changing environmental conditions from deionized water to PBS (or others such as 10% serum and a cell culture medium) may influence the microenvironments of silver nanodots in DNA configuration. Since ATATC12 silver nanodots synthesized in deionized water have similar emission wavelength as those prepared in phosphate buffer, the DNA conformation change resulting from ionic strength shift may not alter the spectrum of silver nanodots much. However, the ion components in the buffer, as suggested by the synthesis in PBS/DMEM, may influence the nanodot stability.

In addition, we studied nanodot stability with varying temperature. Lower temperature is better for storing Ag nanodots, but Ag nanodots should also be stable at temperatures for further biological applications, for example, 37^{o}C. Most Ag nanodots in PBS at 4^{o}C are quite stable even one day after reduction, but decay slowly at room temperature. However, at 37^{o}C it decays much faster, likely due to more loose structures of Ag-DNA complexes.[22-24] Stable Ag nanodots at body temperature are requisite. As we discussed a hairpin concept in Chapter 2, we can change the complimentary base pairs of the stem to give a higher melting temperature such as CGAACGCGC12, 5′-CGAACGCGCCCCCCCCCCCCCGCGTTCG-3′, (T_m = 72^{o}C), instead of ATATC12 (T_m = 0.3^{o}C).[24] It is likely that the hairpin DNA composed of higher melting temperature sequences will hold the Ag nanodots more firmly at higher temperature to delay the decay of emitters. As we expected, the thermal stability of Ag nanodots directly synthesized in PBS or cell culture medium is successfully improved at 37^{o}C, with a half chemical lifetime of 6 hours, as shown in Figure 3-5.

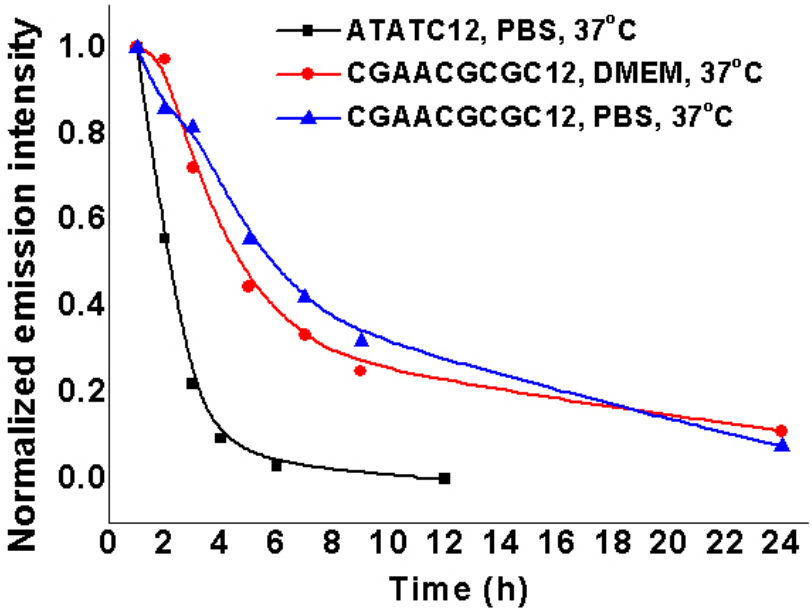

Figure 3-5. Improved thermal stability of CGAACGCGC$_{12}$CGCGTTCG-protected Ag nanodots in PBS and DMEM compared to ATATC12-protected Ag nanodots in PBS. The emission intensities of the above nanodots at 618 were monitored at 560 nm excitation. CGAACGCG C$_{12}$CGCGTTCG, 5′-CGAACGCGCCCCCCCCCCCCCGCGTTCG-3′ and ATATC12, 5′-AT ATCCCCCCCCCCCCATAT-3′.

With this improved thermally stable emitter, it could be applied for the biological applications in the near future.

Live cell staining is more difficult than fixed cell staining due to much more complicated components in live cells. Due to the highly-charged surface, DNA-protected silver nanodots could not pass through cell membrane freely. Intracellular delivery, however, can be affected by microinjection, by which nanodots are physically injected into cells. Although we can successfully synthesize Ag nanodots directly in biological media, the concentration of Ag nanodots is quickly diluted inside live cells. Thus, more concentrated Ag nanodots might be necessary for successful live cell staining.

We tried to concentrate Ag nanodots by three different methods depending on buffer systems. In deionized water, Ag nanodot solution is concentrated about 20 times by DNA SpeedVac® Concentrator. However, in buffer system including sodium phosphate, the concentration increases 10-12 fold, causing problems for Ag nanodot stability. For direct synthesis in PBS or cell culture medium, it is not ideal to concentrate the solution by DNA SpeedVac® Concentrator because salts, amino acids, and more in the medium, are concentrated as well. Therefore, we have to use a fast way to concentrate Ag nanodots, but it should not damage Ag nanodots. In general, alcohol precipitation is widely used to purify biomacromolecules.[25] Fortunately, DNA hairpin structure encapsulates Ag nanodots so well that the Ag particles can still be soluble.

The collected Ag nanodots are re-dissolved in DMEM at the desired concentration, according to its absorption from silver nanodots. Then, we can apply the concentrated emitter for live NIH 3T3 cell staining by microinjection. In Figure 3-6, Ag

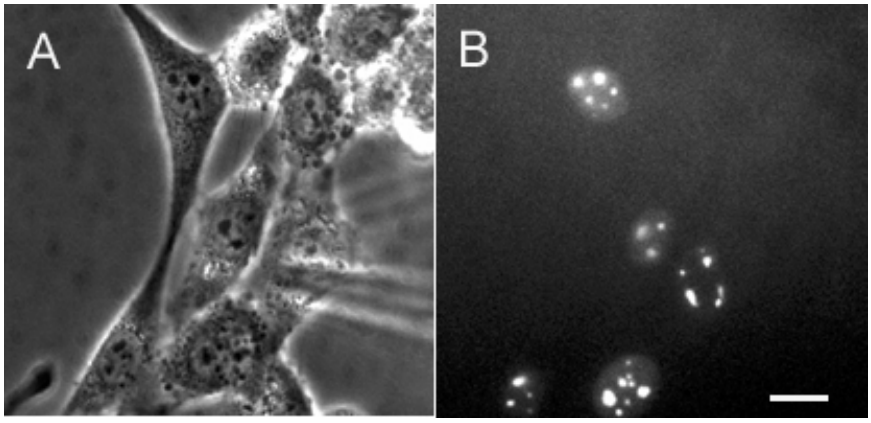

Figure 3-6. Live NIH 3T3 cells were microinjected with Ag nanodots (607 nm emitter). (A) Phase contrast image of cells (used 40x phase contrast objective). (B) Fluorescence image of Ag nanodots under Hg lamp excitation, 535/50x, 580LP, Exposure time 0.5 sec for bright image and 1 sec for fluorescence image, Scale bar 40 μm.

nanodots clearly stained cells, especially with higher intensity at nucleoli. Even though it shows that Ag nanodots homogenously distribute in the cell right after microinjection, they quickly diffuse to the nucleus and finally stain what looks like the nucleoli.

As mentioned earlier, silver nanodots prepared in regular deionized water or phosphate buffer are not stable in physiological conditions. We discovered that an extra procedure could strengthen the stability of such silver nanodots dramatically, and therefore it is not always necessary to prepare nanodots in cell media. The DNA SpeedVac® concentrated 615 nm emitter or 670 nm emitter is reduced with sodium borohydride for a second time, and the resulting silver nanodots show much better stability in physiological conditions as shown in Figure 3-7. Silver nanodots (670 nm emitter) without secondary reduction were not as chemically stable; the emission disappeared right after microinjection. However, silver nanodots with secondary reduction showed longer chemical stability, as shown in Figure 3-7. We do not know why secondary reduction yields better chemical stability inside cells, even though they exhibit similar absorption and fluorescence intensity with or without this procedure.

It seems that the cellular localization of silver nanodots depends on DNA sequence for nanodot protection. When CGCGC12 protected silver nanodots (615 emitter) were injected into live cells, most of them (12 cells) stayed in the cytoplasm right after injection, and then gradually diffused into nucleus, resulting in homogeneous stain in about 2 to 6 minutes (Figure 3-8 (a)), depending on individual cells. Interestingly, fluorescein labeled CGCGC12 (CGCGC12-fl, 5′-fluorescein-CGCGCCCCCCCC CCCCCGCG-3′) also showed similar pattern to the 615 emitter (Figure 3-8 (b)), as

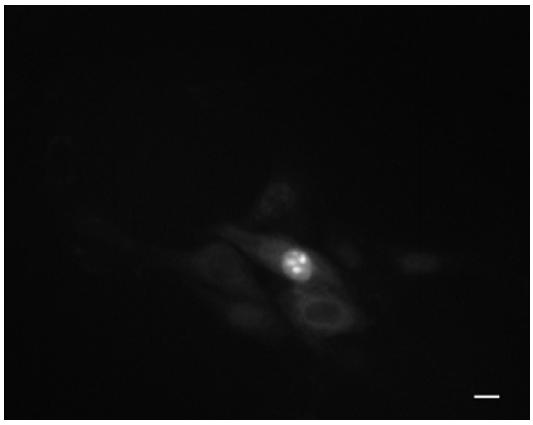

Figure 3-7. Live NIH 3T3 cells were microinjected with 670 nm emitter ($GGGGC_8CCCC$) under Hg lamp excitation, 575/30x, 650LP. Fluorescence images were taken 14 minutes after microinjection, exposure time 1 sec. Scale bar: 25 μm.

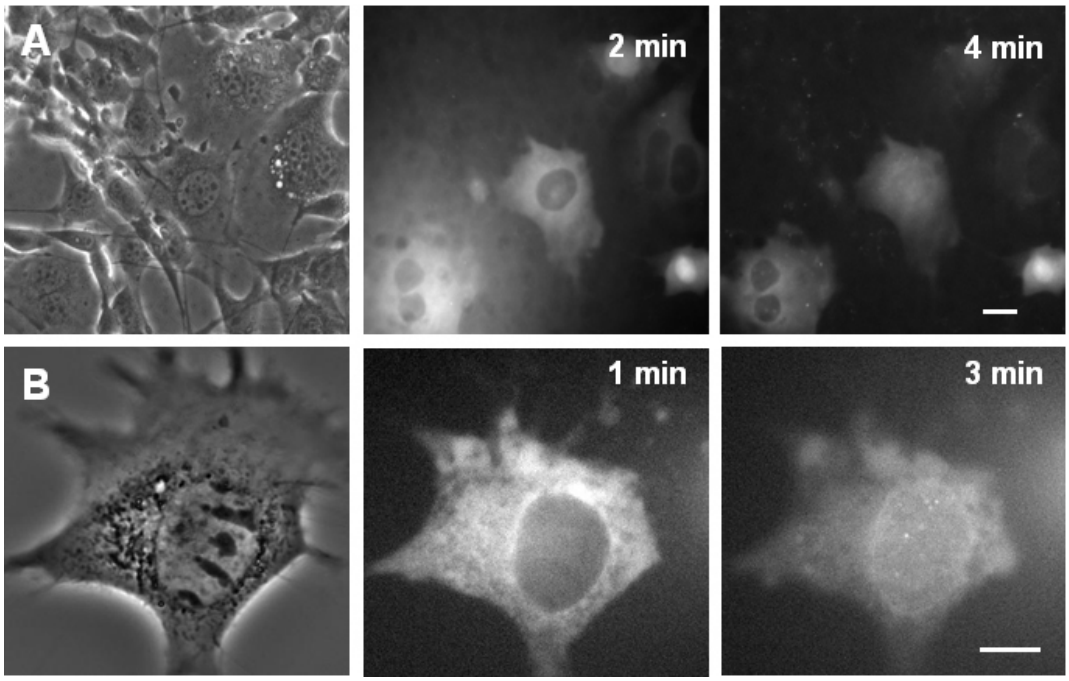

Figure 3-8. Cell staining pattern depends on DNA sequence. Live NIH 3T3 cells were microinjected with 615 nm emitter (5′-CGCGCCCCCCCCCCCCCGCG-3′, A) and with CGCGC12-fl (5′-fluorescein-CGCGCCCCCCCCCCCCCGCG-3′, B) under Hg lamp excitation. 535/50x and 610LP for 615 nm emitter, 460-490BP and 514LP for CGCGC12-fl, Exposure time 1 sec, Scale bar: 20 μm.

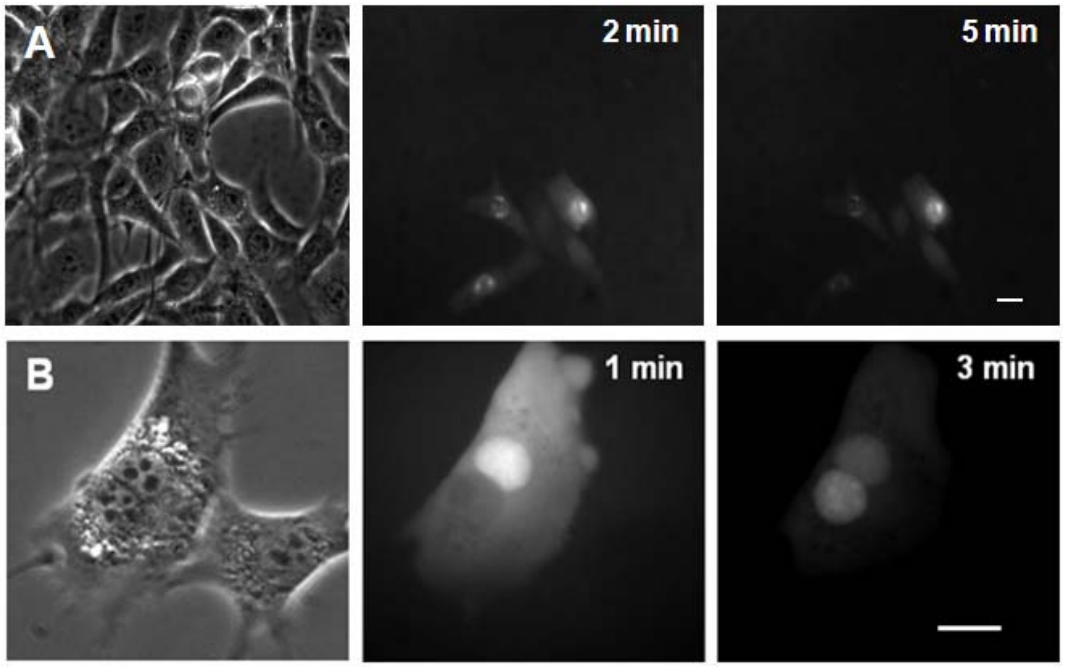

Figure 3-9. Cell staining pattern depends on DNA sequence. Live NIH 3T3 cells were microinjected with 670 nm emitter (5′-GGGGCCCCCCCCCCCC-3′, A) and with GGGGC8-fl (5′-fluorescein-GGGGCCCCCCCCCCCC-3′, B) under Hg lamp excitation. 575/30x and 650LP for 670 nm emitter, 460-490BP and 514LP for GGGGC8-fl, Exposure time 1 sec, Scale bar: 25 μm.

observed in 15 injected cells. The other sequence, GGGGC8, either with tagged fluorescein (GGGGC8-fl, 5′-fluorescein-GGGGCCCCCCCCCCCC-3′), or with coordinated silver nanodots (670 emitter), stayed in cytoplasm at the very beginning, but then quickly diffused into the nucleus in less than 1 minute, resulting in bright nucleus stain (Figure 3-9). Compared to CGCGC12-fl, diffusion of GGGGC8-fl into nucleus is faster, as we observed strong nucleus stain from GGGGC8-fl within 1 minute after microinjection (Figure 3-9), but CGCGC12-fl still stayed in cytoplasm in 2-4 mintues (Figure 3-8). We further tried to examine the influence of silver ions (not reduced) on the diffusion of DNA sequence inside cells by adding silver nitrate to GGGGC8-fl solution, but found that there was little difference in the diffusion pattern of the DNA sequence either in the presence or absence of silver ions. Reduction of the above mixture with $NaBH_4$ did not change the diffusion pattern either. At this moment, we do not know exactly what fact more strongly affects the localization of DNA-silver nanodot conjugate. It was reported that diffusion of macromolecule-sized solutes in cytoplasm and nucleus was relatively free. However, the DNA fragments in nucleoplasm were nearly immobile.[26-28] The strong nuclear staining of GGGGC8 might be ascribed to the binding of DNA to immobile obstacles in nucleus.[29, 30] However, the distinct diffusion patterns between GGGGC8 and CGCGC12 may not be explained by the DNA size difference of only 4-base. There might be other factors determining such difference, such as secondary structure.

3-4. Conclusions

Through tailored oligonucleotide scaffolds, silver nanodot syntheses have yielded thermally and cell culture stable silver cluster-based emitters. Optimizing ssDNA stability has enabled creation of highly concentrated and spectrally pure nanodot emitters with strong intracellular emission. Both fixed and live-cell staining becomes possible, as demonstrated by antibody targeting and microinjection, respectively.

3-5. References

1. Yu, J., Patel, S.A. & Dickson, R.M. In vitro and intracellular production of peptide-encapsulated fluorescent silver nanoclusters. *Angew. Chem.-Int. Edit.* **46**, 2028-2030 (2007).

2. Ono, A. & Miyake, Y. Highly selective binding of metal ions to thymine-thymine and cytosine-cytosine base pairs in DNA duplexes. *Nucleic Acids Res.* **supplement 3**, 2 (2003).

3. Patel, S.A., Richards, C.I., Hsiang, J.C. & Dickson, R.M. Water-soluble Ag nanoclusters exhibit strong two-photon-induced fluorescence. *J. Am. Chem. Soc.* **130**, 11602-11603 (2008).

4. Petty, J.T., Zheng, J., Hud, N.V. & Dickson, R.M. DNA-templated Ag nanocluster formation. *J. Am. Chem. Soc.* **126**, 5207-5212 (2004).

5. Richards, C.I. et al. Oligonucleotide-stabilized Ag nanocluster fluorophores. *J. Am. Chem. Soc.* **130**, 5038-5039 (2008).

6. Vosch, T. et al. Strongly emissive individual DNA-encapsulated Ag nanoclusters as single-molecule fluorophores. *Proc. Natl. Acad. Sci. U. S. A.* **104**, 12616-12621 (2007).

7. Ritchie, C.M. et al. Ag nanocluster formation using a cytosine oligonucleotide template. *J. Phys. Chem. C* **111**, 175-181 (2007).

8. Antoku, Y. Fuorescent Polycytosine-Encapsulated Silver Nanoclusters *Ph. D thesis. Georgia Institute of Technology* (2007).

9. Guo, W.W., Yuan, J.P. & Wang, E.K. Oligonucleotide-stabilized Ag nanoclusters as novel fluorescence probes for the highly selective and sensitive detection of the Hg^{2+} ion. *Chem. Commun.*, 3395-3397 (2009).

10. Shang, L. & Dong, S.J. Silver nanocluster-based fluorescent sensors for sensitive detection of Cu(II). *J. Mater. Chem* **18**, 4636-4640 (2008).

11. Diez, I. et al. Color Tunability and Electrochemiluminescence of Silver Nanoclusters. *Angew. Chem.-Int. Edit.* **48**, 2122-2125 (2009).

12. Yu, J., Choi, S. & Dickson, R.M. Shuttle-based fluorogenic silver cluster biolabels. *Angew. Chem.-Int. Edit.*, in press (2008).

13. Yu, J.H., Choi, S.M., Richards, C.I., Antoku, Y. & Dickson, R.M. Live Cell Surface Labeling with Fluorescent Ag Nanocluster Conjugates. *Photochem Photobiol* **84**, 1435-1439 (2008).

14. Roussel, P. & Hernandezverdun, D. Identification of ag-nor proteins, markers of proliferation-related to ribosomal gene activity. *Exp. Cell Res.* **214**, 465-472 (1994).

15. Walker, H.K., Hall, W.D.H. & Hurst, J.W. (eds.) Clinical Methods. (Butterworths, Boston; 1990).

16. Luk, K.F.S., Maki, A.H. & Hoover, R.J. Studies of heavy-metal binding with polynucleotides using optical detection of magnetic-resonance - silver(I) binding. *J. Am. Chem. Soc.* **97**, 1241-1242 (1975).

17. Belting, M. Heparan sulfate proteoglycan as a plasma membrane carrier. *Trends Biochem.Sci.* **28**, 145-151 (2003).

18. van Kuppevelt, T.H., Dennissen, M., van Venrooij, W.J., Hoet, R.M.A. & Veerkamp, J.H. Generation and application of type-specific anti-heparan sulfate antibodies using phage display technology - Further evidence for heparan sulfate heterogeneity in the kidney. *J. Biol. Chem.* **273**, 12960-12966 (1998).

19. Choi, S., Yu, J., Patel, A., Tzeng, Y.L. & Dickson, R.M. Tailoring silver nanodots for intracellular staining. *Photochem. Photobiol. Sci.* (submitted).

20. Smeitink, J., van den Heuvel, L. & DiMauro, S. The genetics and pathology of oxidative phosphorylation. *Nat. Rev. Genet.* **2**, 342-352 (2001).

21. Triepels, R.H. et al. Human complex I defects can be resolved by monoclonal antibody analysis into distinct subunit assembly patterns. *J. Biol. Chem.* **276**, 8892-8897 (2001).

22. Van Orden, A. & Jung, J. Fluorescence correlation spectroscopy for probing the kinetics and mechanisms of DNA hairpin formation. *Biopolymers* **89**, 1-16 (2008).

23. Hernandez, B., Baumruk, V., Gouyette, C. & Ghomi, M. Thermal stability, structural features and B-to-Z transition in DNA tetraloop hairpins as

determined by optical spectroscopy in d(CG)(3)T-4(CG)(3)and d(CG)(3)A(4)(CG)(3) oligodeoxynucleotides. *Biopolymers* **78**, 21-34 (2005).

24. Vallone, P.M. et al. Melting studies of short DNA hairpins: Influence of loop sequence and adjoining base pair identity on hairpin thermodynamic stability. *Biopolymers* **50**, 425-442 (1999).

25. Kang, T.J. & Yang, M.S. Rapid and reliable extraction of genomic DNA from various wild-type and transgenic plants. *BMC Biotechnology* **4** (2004).

26. Seksek, O., Biwersi, J. & Verkman, A.S. Translational diffusion of macromolecule-sized solutes in cytoplasm and nucleus. *J. Cell. Biol.* **138**, 131-142 (1997).

27. Allen, T.D., Cronshaw, J.M., Bagley, S., Kiseleva, E. & Goldberg, M.W. The nuclear pore complex: mediator of translocation between nucleus and cytoplasm. *J. Cell Sci.* **113**, 1651-1659 (2000).

28. Guigas, G., Kalla, C. & Weiss, M. The degree of macromolecular crowding in the cytoplasm and nucleoplasm of mammalian cells is conserved. *FEBS Lett.* **581**, 5094-5098 (2007).

29. Lukacs, G.L. et al. Size-dependent DNA mobility in cytoplasm and nucleus. *J. Biol. Chem.* **275**, 1625-1629 (2000).

30. Dauty, E. & Verkman, A.S. Actin cytoskeleton as the principal determinant of size-dependent DNA mobility in cytoplasm. *J. Biol. Chem.* **280**, 7823-7828 (2005).

CHAPTER IV

Encapsulation of silver nanodots in delivery vehicles

Here we tried to extend the scope of silver nanodots for *in vivo* application. Nanogel and PLGA particle were chosen as delivery vehicles. Silver nanodots were either kinetically trapped inside nanogel as dry nanogel was dissolved in nanodot solution, or encapsulated in PLGA particle by emulsion-based synthesis. The encapsulation efficacy of silver nanodots in nanogel is higher compared to that in PLGA system, with about 14 silver nanodots/nanogel particle. Preservation of the photophysics of silver nanodots in such new environments suggests nanodots as imaging agents for *in vivo* applications.

4-1. Introduction

High quality fluorophores are essential for imaging studies, especially in the fields of single molecule and *in vivo* imaging.[1] Strong scattering occurs inside tissues in addition to high backgrounds, causing challenges for *in vivo* applications. Brighter and photostable fluorophores enable less loading dose, and better absorption of photons in low light systems.[2] The excellent photophysics of silver nanodots prompt us to extend their application to *in vivo* imaging. In addition to direct labeling of bioactive molecules with fluorophores, many delivery vehicles are also used as a platform for imaging

fluorophores.[3-10] Liposomes are one of the most well investigated drug delivery vehicle, with uses ranging from basic cosmetic formulations to the treatment of various infectious diseases.[11, 12] Mesoporous silica nanoparticles, with defined structures and surface properties, are known to be biocompatible, and newly developed as drug delivery vehicles due to their capability to store and gradually release therapeutically relevant drugs.[13] Several drugs and large molecules, such as antibodies,[14] have been successfully encapsulated in these nanoparticles. Compared to silica nanoparticles, gold nanoparticles are solid, and can only carry cargoes at their surface. However, its low toxicity and other properties, such as near IR absorption for thermotherapy, enable their wide applications in drug delivery studies and *in vivo* imaging.[15-17] Polymer-based nanoparticles can controllably release pharmaceutical drugs in aqueous solution upon being triggered by various chemical factors, such as pH, under physiological conditions, introducing extra functionality.[18, 19]

Hybrid nano-sized hydrogels have been attractive in pharmaceutical applications due to their swelling and permeability characteristics influenced by a various range of external factors including temperature, pH, ionic strength, and sensitivity of light.[20-26] It is used for hydrophilic drug encapsulation. However, for hydrophobic drugs, another type of polymeric nanoparticles made of Poly(D,L-lactic-co-glycolic acid) (PLGA), is applied frequently due to their FDA-proved, biodegradable, biocompatible characteristics.[27-29] In general, those stimuli-responsive vehicles for *in vivo* applications should endure longer circulation in blood stream and be biodegradable.[30] Additionally, drug delivery systems require that the designed particles should appropriately release drugs on the targeted areas of interest to reduce inefficacy and toxic side effects, leading to designing the hybrid gels

including organic dye or quantum dots (QDs) to track or monitor the carriers.[5, 31-33] Therefore, developing new fluorophores and new measuring technologies are necessary. Recently, optically modulated silver nanodots were reported, which demonstrated an increase in signal to noise ratio resulting from reduction of noise in high backgrounds.[34] These new fluorophores and modulation technique definitely afford new ways to recover signal and information toward *in vivo* application. Herein, we examined encapsulation of our silver nanodots in such drug delivery vehicles and the photophysics of resulting silver nanodot-nanoparticle complexes, and evaluated the possibility of current silver nanodots towards *in vivo* imaging application.

4-2. Experimental section

Materials

All materials were purchased from Sigma-Aldrich unless otherwise specified. Nanogels were made by and obtained from Mike Smith through a collaboration with Dr. L. A. Lyon's lab (School of Chemistry and Biochemistry, Georgia Institute of Technology). All oligonucleotides were purchased from Integrated DNA Technologies and purified with standard desalting by the manufacturer. 1,2-Dioleoyl-3-Trimethylammonium Propane (Chloride Salt) (DOTAP) was purchased from Avanti Polar Lipids, Inc. (Alabaster, AL). Poly(D,L-lactic-co-glycolic acid), PLGA (RG 503H, 35.4 kDa (polydispersity index: 2.5), Boehringer Ingelheim), was obtained from Dr. N. Murthy lab. (Department of Biomedical Engineering, Georgia Institute of Technology). Silver nitrate was used with 99.9999% purity and sodium borohydride with 98% purity. All syntheses used deionized water (18M Ω, Barnstead Thermolyne E-Pure system).

Synthesis

DNA-Ag nanodots were synthesized by the same method discussed in Chapter 3, and concentrated by lyophilization.

Nanogels were synthesized by Dr. Lyon's lab following previous report except that the amount of acrylamidofluorescein (AFA) was 10 times less.[35] The freeze-dried nanogels were suspended in 250 μL of concentrated DNA-Ag nanodot solution and

incubated overnight at 4°C. The solution was then centrifuged at 100,000 rpm for 30 minutes at 4°C, and the precipitates were collected for the characterization and further applications.

Double emulsion

A mixture of PLGA (40 mg) in 1 mL of methylene chloride and DNA-Ag nanodot solution (50 μM of DNA concentration, 150 μL) was homogenized at 21,500 rpm for 30 seconds by a mechanical stirrer, followed by the addition of 8 mL of 5% (w/v) aqueous polyvinyl alcohol (PVA) solution The solution was quickly emulsified by homogenization at 9,400 rpm for one minute. The resulting emulsion was added into 12 mL of 0.5% PVA solution and then methylene chloride was removed by rotary evaporator. The particles were collected after centrifugation at 10,000 rpm for 10 minutes, washed twice, and freeze-dried.

Ion-pairing step for single emulsion

DOTAP (74.8 μL of 20 μg/μL) was diluted with methylene chloride (775.2 μL) and DNA-Ag nanodot solution (50 μL of DNA concentration, 850 μL). Methanol (1.785 mL) was gently dropped to the top of the mixture, which formed two separated phases. After a 5 minute incubation, the above solution was added into a mixture of methylene:water at 1:1 ratio (v/v), vortexed for 30 seconds, and then centrifuged at 600 g for 5 minutes. The organic phase was immediately collected.

Single emulsion

PLGA (40 mg) in 1mL of methylene chloride was added into the ion-paired DOTAP and DNA-Ag complex solution. The mixture was emulsified by homogenization at 21,500 rpm for one minute, and then was poured into 8 mL of 5% (w/v) aqueous PVA solution, followed by homogenization at 9,400 rpm for one minute. The resulting emulsion was added into 12 mL of 0.5% PVA solution and methylene chloride was removed by rotary evaporator. The particles were collected after centrifugation at 10,000 rpm for 10 minutes, washed twice, and freeze-dried overnight.

Thermal stability study

The precipitates of DNA-Ag nanodot-nanogel nanoparticles were re-dissolved in the solution of interest, divided into aliquots, and then incubated at 37^{o}C. At the desired time point, an aliquot was centrifuged at 100,000 rpm for 30 minutes at 4^{o}C. The resulting precipitates were collected. The emissions and absorptions from both supernatant and precipitates were examined. As a control, DNA-Ag nanodots without nanogels were also checked following the same procedure.

Cell culture

Hey cells (obtained from Gordon B. Mills, Department of Systems Biology, the University of Texas, M. D. Anderson Cancer Center) were prepared by Dr. Dickerson,

Department of Biology and Ovarian Cancer Institute, Georgia Institute of Technology. The Hey cells were cultured in RPMI 1640 (Mediatech, Manassas, VA) supplemented with 10% v/v fetal calf serum (Invitrogen), 2 mM L-glutamine (Mediatech), 10 mM HEPES buffer (Mediatech), penicillin (100 U/mL), and streptomycin (100 µg/mL).

Toxicity study

The toxicity study was investigated with the help of Dr. Erin Dickerson. Briefly, Hey cell viability was checked after treatment with Nanodots (670 emitter), Nanogel/Nanodots/ or $AgNO_3$, respectively, at 37^oC and 5% CO_2 for 24 hrs. Then, the cells were washed with PBS followed by replacement of medium. Tox 8 reagent (Sigma) was added to the cells following the manufacturer's instructions, and then the cell viability was checked. Note that the concentration is for DNA, and the corresponding $AgNO_3$ concentration should be 6× that of DNA.

4-3. Results and discussion

4-3-1. DNA-Ag nanodot/PLGA system

Since PLGA is hydrophobic and DNA protected silver nanodots are highly hydrophilic, they are not miscible. However, double emulsion technique is able to entrap the DNA-Ag nanodots inside PLGA particles. In this case, DNA-Ag nanodot solution was used as a water phase (W_1) and was emulsified in PLGA solution dissolved in methylene chloride, an organic phase (O), to form W_1/O emulsion. Then, the emulsion is emulsified in a second water phase (W_2) to make $W_1/O/W_2$ emulsion, i.e., double emulsion. In order to increase entrapment efficiency, we adjusted the ratio between DNA-Ag nanodots (here 615 nm emitter) and PLGA starting material. However, the encapsulated DNA-Ag nanodots were not proportionally increased even though their concentrations were increased at constant PLGA concentration. Some DNA-Ag nanodots were still in water phase, so it may not be easy to drastically improve the efficiency. As shown in Figure 4-1A, the nanodot-encapsulated PLGA particles are not well dispersed with obvious aggregates. Moreover, only some of particles display emission. It was reported that double emulsion showed low encapsulation efficacy to small molecular weight hydrophilic materials.[36] While removing organic phase in this technique by a rotary evaporator, some of DNA-Ag nanodot solution may be already released from PLGA particles, and might be easily washed off during washing step.

Another approach to increase the encapsulation of silver nanodots in PLGA is via single emulsion. In this case, hydrophilic DNA silver nanodots have to be transferred

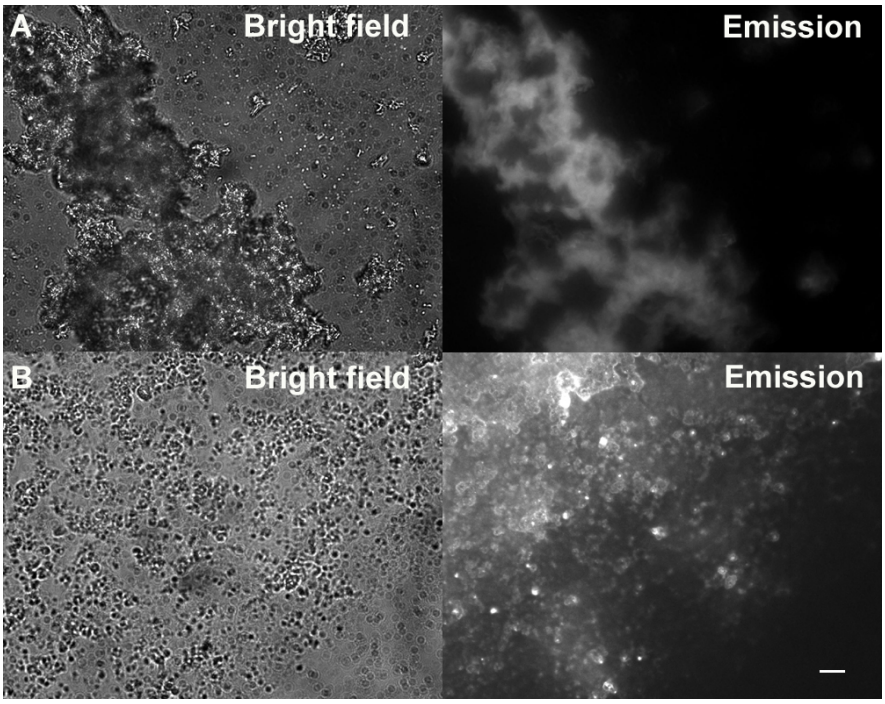

Figure 4-1. The bright field and emission images of 615 nm emitter-PLGA particle solution on glass cover slip were taken by Ixon camera under excitation from Hg lamp excitation (535/50x for excitation and 610LP for emission). Compared to particles prepared by double emulsion method (A), 615 nm emitter-PLGA particles disperse much better when prepared by single emulsion methods (B). Scale bar: 5 μm. 615 nm emitter produced within 5′-CGCGCCCC CCCCCCCCCGCG-3′.

from the aqueous phase to the organic phase via ion pairing between the negatively charged DNA and the positively-charged DOTAP, a lipid with a single positive charge. We first optimized the ratio between DOTAP and DNA-Ag nanodots. Too low DOTAP/DNA ratio could not induce the phase transfer of DNA-Ag nanodots from the aqueous phase to the organic phase until the ratio reached 2.5 DOTAP per DNA base shows. However, some of DNA-Ag nanodots still remained in the water phase in spite of more DOTAP added into the DNA-Ag nanodot solution. Then, these ion paired DNA-Ag nanodots were encapsulated with PLGA by single emulsion. The resulting DNA-Ag nanodot-PLGA particles were characterized by a microscope, as shown in Figure 4-1B. The encapsulated DNA-Ag nanodot-PLGA particles were well dispersed without aggregation. Most of the PLGA particles encapsulate multicopies of silver nanodots as we see the bright emission from each PLGA particle. However, some PLGA particles show fluorescent blinking behavior,[37-40] indicating that in some of the PLGA particles, the encapsulation efficacy is still low.

Due to the large two photon absorption cross section of DNA-Ag nanodots,[41] it would be useful to observe strong emission from these nanodot-PLGA particles by a commercial confocal microscope under two-photon excitation. As shown in Figure 4-2, 615 nm emitter has large two photon absorption at 780 nm. As expected, the entrapped DNA Ag nanodots (615 nm emitter) show bright, stable emission by either one photon excitation (Figure 4-3A, 543 nm excitation, pseudocolor as green) or two photon excitation (Figure 4-3B, 780 nm excitation, pseudocolor as red) at its lowest power output. Their emissions colocalize well as shown in Figure 4-3C, but with much less background noise from two photon excitation. DNA-Ag nanodot-PLGA particles are also

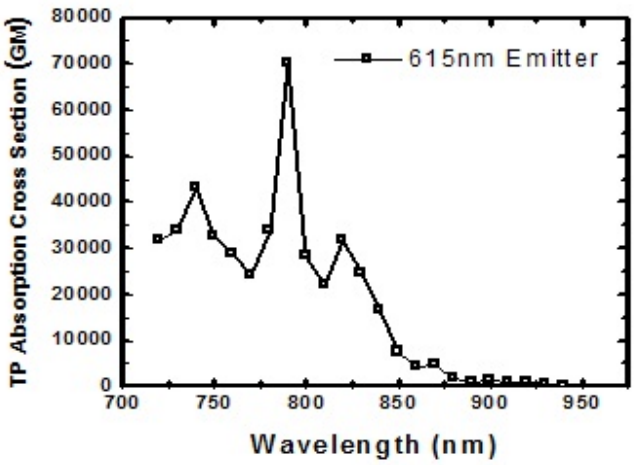

Figure 4-2. Two-photon excitation spectrum of 615 nm emitter. The spectra is calibrated to the absorption cross section of 615 nm emitter for those species whose quantum yields are known (shown in Table 1 in Chapter 2). All of the curves were generated by recording the emission as a function of excitation wavelength by a 8kHz femtosecond Ti-sapphire laser. The cross sections were measured by ratiometric comparison to dye standards with known cross sections at the excitation wavelengths used. 615 nm emitter produced within 5′-CGCGCCCC CCCCCCCCCGCG-3′. Reproduced with permission from Ph. D. thesis (Sandeep A. Patel, Georgia Institute of Technology). Copyright 2009, Georgia Institute of Technology.

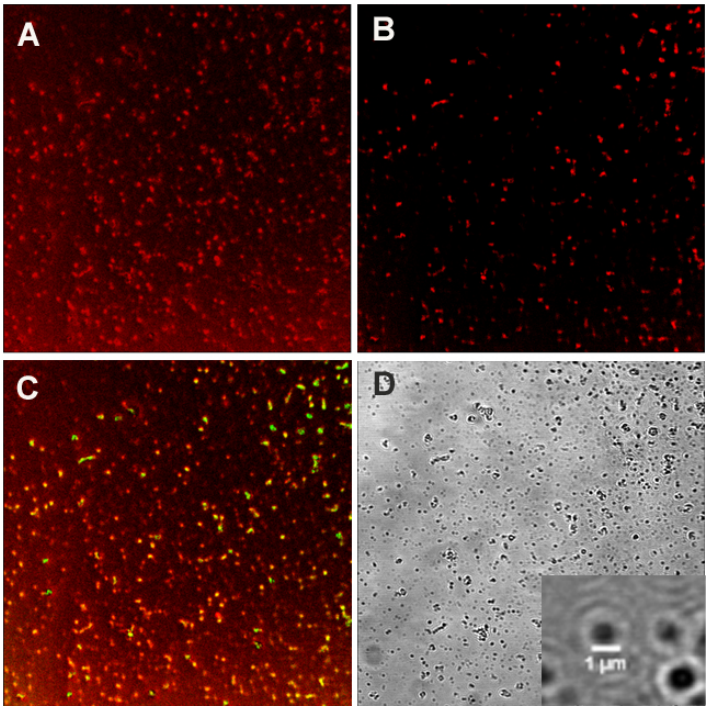

Figure 4-3. The entrapped DNA Ag nanodots (615 nm emitter) in PLGA show bright, stable emission. A, by one photon excitation at 543 nm and detected with 590 LP filter; B, two photon excitation at 780 nm at its lowest power output (2 mW) with 590-695 BP as emission filter; C, their colocalization; D, bright field image of the PLGA particles. Inset, a closeup image of PLGA particles. Scale bar 1 µm. 615 nm emitter produced within 5′-CGCGCCCC CCCCCCCCCGCG-3′.

quite photostable under two photon excitation: very little emission intensity change after 15 min two photon excitation. Although we especially used quite low excitation power and detection gain on a commercial confocal scanning microscope, we can still see bright emission from Ag nanodots. This might be useful for further biological application such as trafficking particles inside cells or *in vivo* imaging under two photon excitation.

Besides excellent emission under two photon excitation, silver nanodots can also be applied for *in vivo* imaging by taking advantage of fluorescence modulation to increase S/N ratio.[34, 42] Fluorescence emission rate can be enhanced when the dark state of the emission process is depopulated. The maximum enhancement is defined as

$$Max\ enhancement = \frac{\tau_{on} + \tau_{off}}{\tau_{on}}$$

For silver nanodots, the emission intensity under the primary laser excitation, for example, 561 nm laser, can be greatly increased by an additional, lower energy secondary laser excitation, e.g. 805 nm, which can increase dark state depopulation resulting in increased fluorescence, but without inducing additional background. Moreover, by modulating the lower energy secondary laser by a variable mechanical chopper which is placed in the secondary laser excitation path, a waveform is encoded onto the fluorescent signal resulting in a regular modulation of the emission, for example at 10 Hz. Series images are taken by CCD camera at a frame rate 10-fold higher than the frequency of modulation. A time trace for each pixel is then constructed from the above images. A Fourier transform ($F(\upsilon) = \int_{-\infty}^{\infty} f(t)e^{2\pi i \upsilon t} dt$) of the resulting time trace is used to extract the frequency component matching the modulated laser. Plotting the amplitude at modulated

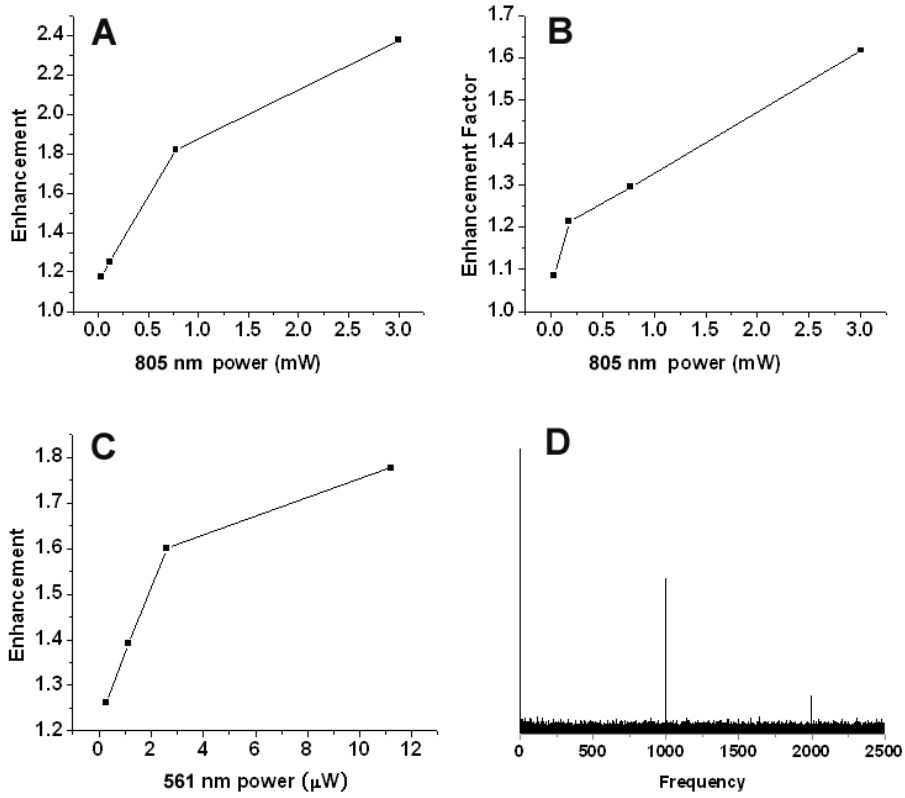

Figure 4-4. Fluorescence enhancement of 615 nm emitter-PLGA particles. A, keeping the primary laser higher power (561 nm laser, 11.2 μW) and changing secondary laser power (805 nm laser, 0~3 mW); B, similar to A except for lower power of primary laser (561 nm laser, 0.3 μW); C, keeping the lower power (775 μW) of secondary laser (805 nm) and changing the primary laser power; D, Fourier transform of the emission in A. 615 nm emitter produced within 5′-CGCGCCCC CCCCCCCCCGCG-3′.

laser frequency, for example, 10 Hz, for each pixel resulted in the demodulated image. This indicates that only the modulable emission from silver nanodots is recovered, meanwhile, those pixels, such as high background, containing no modulated laser frequency component will be removed, resulting in greatly improved S/N ratio.

The silver nanodots in PLGA still exhibit modulation. With relatively higher primary laser intensity (568 nm laser, 11.2 μW), the 615 nm emitter inside PLGA particles shows good enhancement at varied secondary laser intensities (805 nm laser, 0~3 mW), as shown in Figure 4-4A. The entrapped 615 nm emitter also shows enhancement with even lower intensity of primary laser (568 nm laser, 0.3 μW) (Figure 4-4B). Conversely, fixing the lower intensity (775 μW) of secondary laser (805 nm) and changing the primary laser intensities also shows enhancement inside PLGA particles (Figure 4-4C). Clearly, higher primary laser intensity increases the emission rate of nanodots and the possibility of dark state depopulation so that more photons can be emitted. Nevertheless, such a lower secondary laser intensity is also enough to make photons depopulate in dark state as we observed here.

Similar to our previous approach, we tested this enhancement with artificially large background, by adding commercial organic dye. DNA-Ag nanodot-PLGA was immobilized in PVA film and Texas Red solution was added on the top of the PVA sample. Applying a primary laser (594 nm, 350 W/cm^2) to excite the film and Texas Red solution and detecting with a CCD camera yield an image showing a large fluorescent area as shown in Figure 4-5A. Afterward, secondary laser (805 nm, 16kW/cm^2) was applied, focused on the sample and modulated at 2 Hz. With Fourier analysis, a time trace was rebuilt to monitor for the frequency component corresponding to the modulated laser.

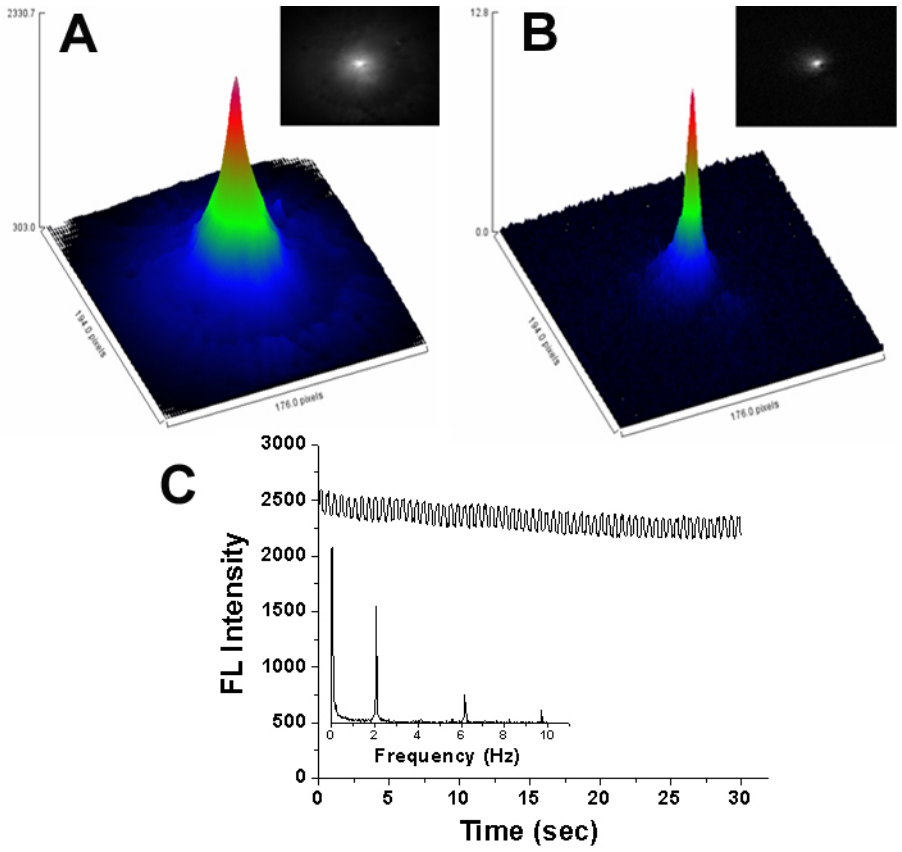

Figure 4-5. A. Raw image of a PVA immobilized sample of 615 nm emitter-PLGA particles after adding Texas red solution on the top of the PVA sample, excited with constant 594 nm (350 W/cm^2) and modulated 805 nm (16 kW/cm^2) laser at 2 Hz; B; Demodulated image of (A) showing sharp spikes at the secondary laser focus point. C. Fourier transforms of the emission in A. 615 nm emitter produced within 5´-CGCGCCCC CCCCCCCCCGCG-3´.

Recombination of signal for each pixel offers the demodulated image completely removing Texas Red fluorescence as shown in Figure 4-5B. With these preliminary results, the DNA-Ag nanodot-PLGA system might be great for biological application, especially in high background environments.

4-3-2. DNA-Ag nanodot/nanogel system

Noncovalent encapsulation of DNA-Ag nanodots within nanogels not only avoids any complicated surface modification, but also retains the characteristic emissions of silver nanodots as shown in Figure 4-6, which illustrates different Ag nanodot emitters encapsulated within nanogels. Several emitters were successfully encapsulated in the nanogel, such as a green C20 emitter (λ_{max}, 523 nm), yellow 562 nm emitter, orange 590 nm emitter, red 615 nm emitter, 635 nm emitter, and 670 nm emitter. These emitters were concentrated before being loaded into nanogel, However, several emitters, such as CCCATATTCCCC (660 em @594 ex), CCTCCTTCCTCC (620 em@540 ex) and CCCTAACTCCCC (700 em @ 620 ex), show very low loading efficiency. For clarity, we just show the result of 670 nm emitter as an example. After encapsulation, Ag nanodot-nanogels are still well-dispersed in solution with 67% encapsulation efficiency (Encapsulation efficiency = [1- (fluorescence of loading solution supernatant / fluorescence of Ag nanodot stock)]*100). The 670 nm emitter in nanogel still exhibits intense emission with no spectral shift (Figure 4-6C, red line). Since there is fluorescein conjugated as an indicator during the synthesis of nanogels (Figure 4-6C, black line), the molecular weight of nanogel and the average number of fluorescein molecules per nanogel particle were determined to be ~50,000,000 Da 18 fluorescein molecules/nanogel particle, respectively, by FCS. Consequently, by measuring the absorption intensity of fluorescein the concentration of nanogel particles was obtained. Similarly, the concentration of 670 nm emitter was also determined, given that it has an extinction coefficient of 250,000 $M^{-1}cm^{-1}$. By comparing these two concentrations, the loading of

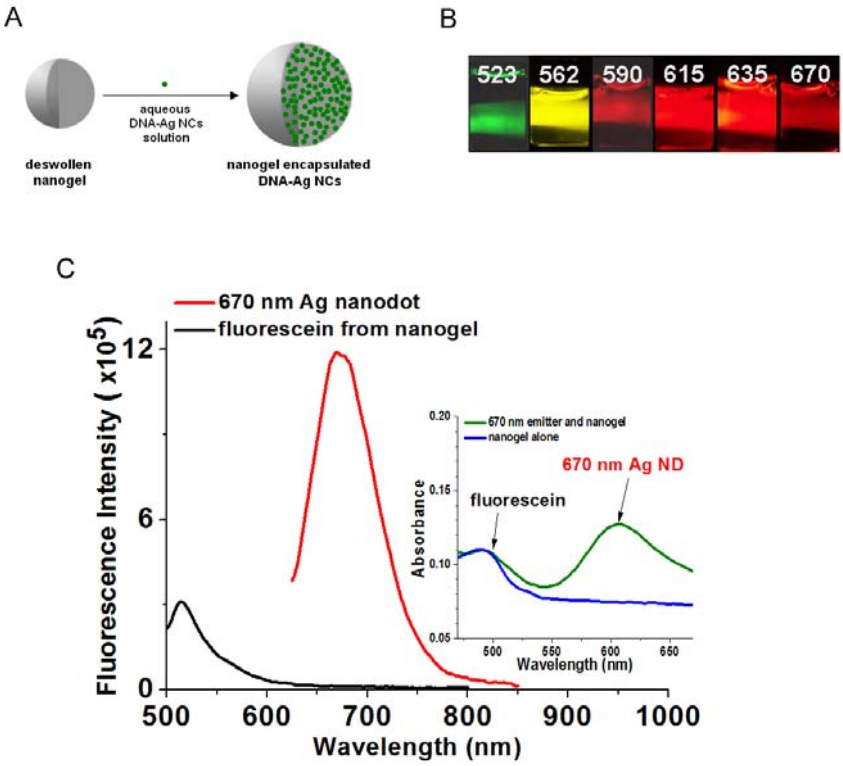

Figure 4-6. Noncovalent encapsulation of DNA-Ag nanodots within nanogels. (a) A scheme illustrates this process. (b) Emission image of different emitters of Ag nanodot encapsulated within nanogels under individual best excitation wavelength. (c) Emission spectrum of 670 nm emitter in nanogel (red line) and fluorescein (black line) which was conjugated as an indicator during the synthesis of nanogels. They were excited at 600 nm and 480 nm, respectively. Inset, the absorption spectra of nanogel alone (blue in inset) and 670 nm emitter in nanogel (green in inset). 670 nm emitter produced within 5′-GGGGCCCCCCCCCCC-3′.

silver nanodots was also determined to be 14 fluorescent silver nanodots in each nanogel particle. Given the 1% synthetic yield of 670 emitter, there are about 1,400 DNA molecules/nanogel particle assuming that DNA and DNA-silver nanodots have similar loading efficiencies.

In addition, we investigated the brightness of nanodots in nanogels by microscopy. The 670 nm emitter still exhibits bright emission inside nanogels as shown in Figure 4-7. As the solution was diluted continuously, fewer and fewer bright single nanogel particles appear on cover slips until well-separated single nanogel particles are achieved (Figure 4-7A). The photon count rate reaches up to 180,000 photons/sec/nanogel particle, corresponding to 13,000 photons/sec/nanodot at 670 nm under Hg lamp excitation with 575/30x for excitation and 650LP for emission as shown in Figure 4-7B and C. Moreover, these gels are stable in different chemical environments. Figure 4-8 presents that the 670 emitter-nanogel has a half life time of more than 10 hours in 10% serum or sodium phosphate buffer at 37^{o}C, showing similar stability as DNA-Ag nanodots alone in such media.

Although the hybrid gel system meets the requirement such as bright emission and thermal stability, biocompatibility is one of the greatest challenges for *in vivo* study. With Dr. Erin Dickerson's help, we checked the cell viability with Hey cells. Cells were incubated in three different conditions: DNA-Ag nanodot-nanogels, DNA-Ag nanodots, and $AgNO_3$ at 37^{o}C for 24 hrs, followed by treatment with Tox 8 reagent. Figure 4-9 shows that cell viability is good with lower concentration (less than 5 μM of DNA-nanodot complex). Note that the concentration is for DNA, and the corresponding $AgNO_3$

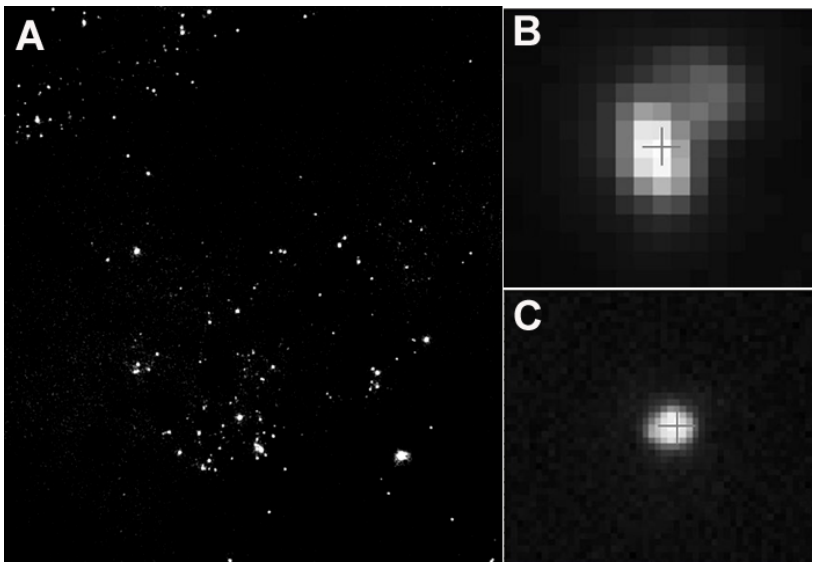

Figure 4-7. Emission images from 670 nm Ag nanodot-nanogel solution on glass cover slip were taken by Ixon camera under excitation from mercury lamp excitation (575/30x for excitation and 650LP for emission). images B and C were close-up images of single particles of Ag ND-ngs from image A. 670 nm Ag nanodot produced within 5′-GGGGCCCCCCCCCCCC-3′.

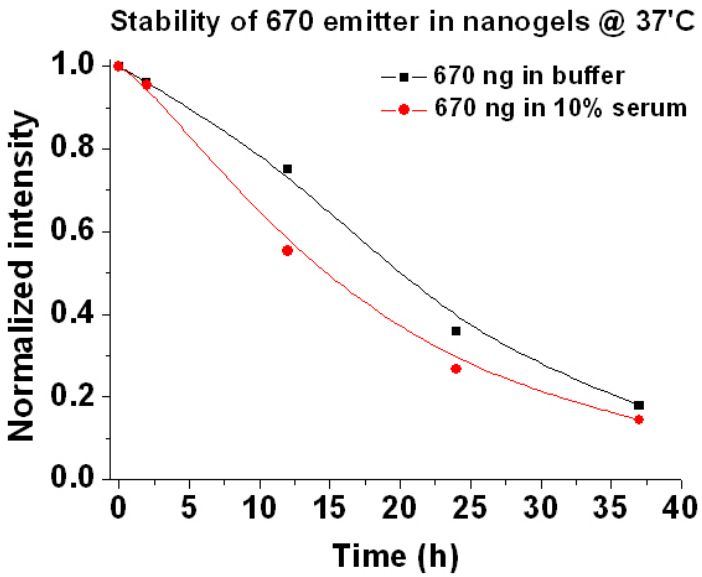

Figure 4-8. Stability of 670 emitter-nanogel in 10% serum and sodium phosphate buffer at 37^{o}C. The emission intensities of the above nanodots at 670 were monitored at 600 nm excitation. 670 nm Ag nanodot produced within 5′-GGGGCCCCCCCCCCCC-3′

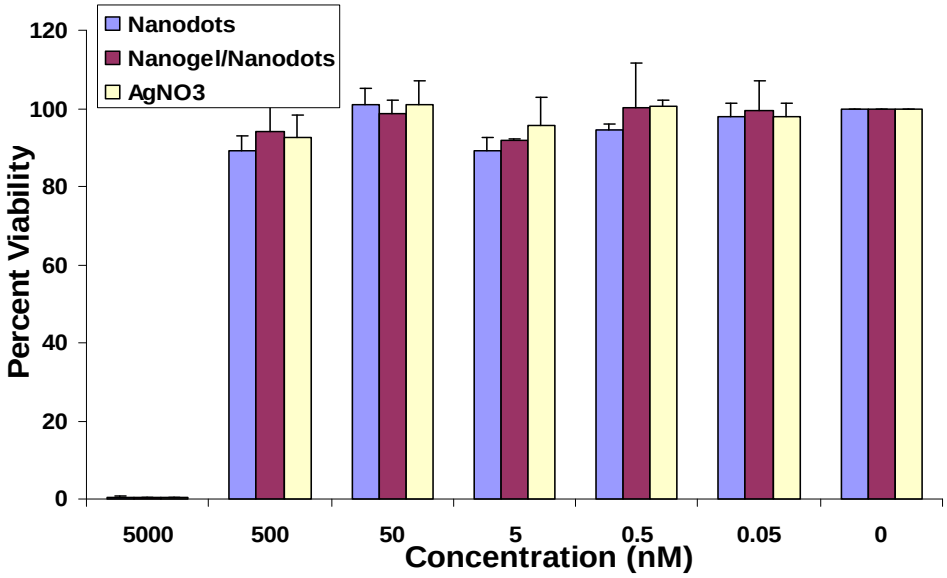

Figure 4-9. Hey cell viability checked with Tox8 (Sigma) after treatment with Nanodots (670 emitter), Nanogel/Nanodots/ and $AgNO_3$ for 24 hrs. Note that the concentration is for DNA, and the corresponding $AgNO_3$ concentration should be 6× that of DNA. 670 nm Ag nanodot produced within 5′-GGGGCCCCCCCCCCC-3′. Test performed by Dr. Erin Dickerson.

concentration should be 6× that of DNA. However, cells could not survive well at higher silver concentration in individual condition (more than 5 μM). In any case, the toxicity results are similar, likely originating from the presence of silver ions. Though silver ions were regarded being toxic to bacteria but safe to mammalian cells, and accordingly it was used as wound healing drug, there were also reports on it concentration-dependent toxicity on mammalian cells.[43, 44] It was shown some neurotoxicity after high dose contact with silver ions.[45-47] For the biological application of silver nanodots, it might be necessary to ensure effective encapsulation of silver ions. However, nanogel affords some protection of silver nanodots due to a delay of releasing silver nanodots. The bare 670 nm emitter would quickly stain nucleoli strongly after microinjection. Contrarily, in 8 out 10 cells injected with 670 nm emitter-nanogel system, nanodots did not diffuse into nucleus right after microinjection as the large size of nanogels may prevent their translocation freely into nucleus, as shown in Figure 4-10. This also suggests that silver nanodots can be applied easily without disturbing the delivery vehicle characteristics. Nanogel is porous network. Some small molecules can easily diffuse into it. The stability of silver nanodots was not improved because the amino acids, short peptides, anions, especially Cl^-, will deteriorate the emission of nanodots.

As mentioned earlier, Ag nanodot itself has good enhancement as well as modulation characteristics. Thus, it is quite interesting whether the Ag nanodots keep those kinds of nanodots' properties after entrapment in nanogel. Figure 4-11A shows the fluorescence enhancement of Ag nanodots depending on primary laser power and Figure 4-11B depending on the secondary laser power. It clearly shows that Ag nanodots inside nanogels exhibit similar enhancement as nanodots alone. To apply this system for

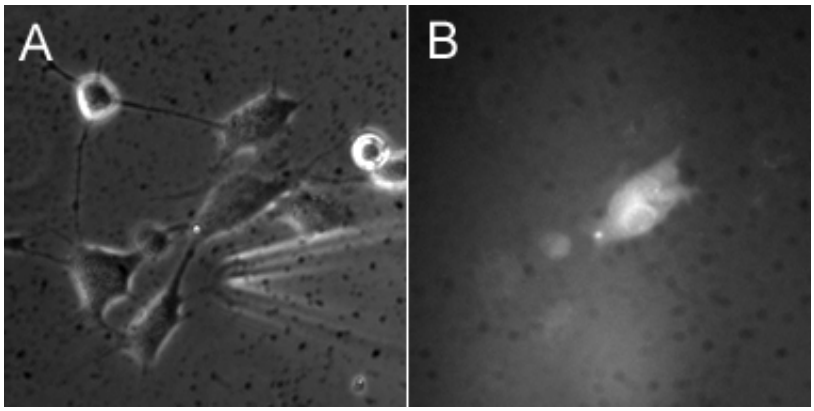

Figure 4-10. Live NIH 3T3 cells were micro-injected with 670 nm emitter-nanogels. (A) Phase contrast image of cells. (B) Fluorescence image of Ag nanodots under Hg lamp excitation (575/30x, 650LP). 670 nm Ag nanodot produced within 5′-GGGGCCCCCCCCCCCC-3′

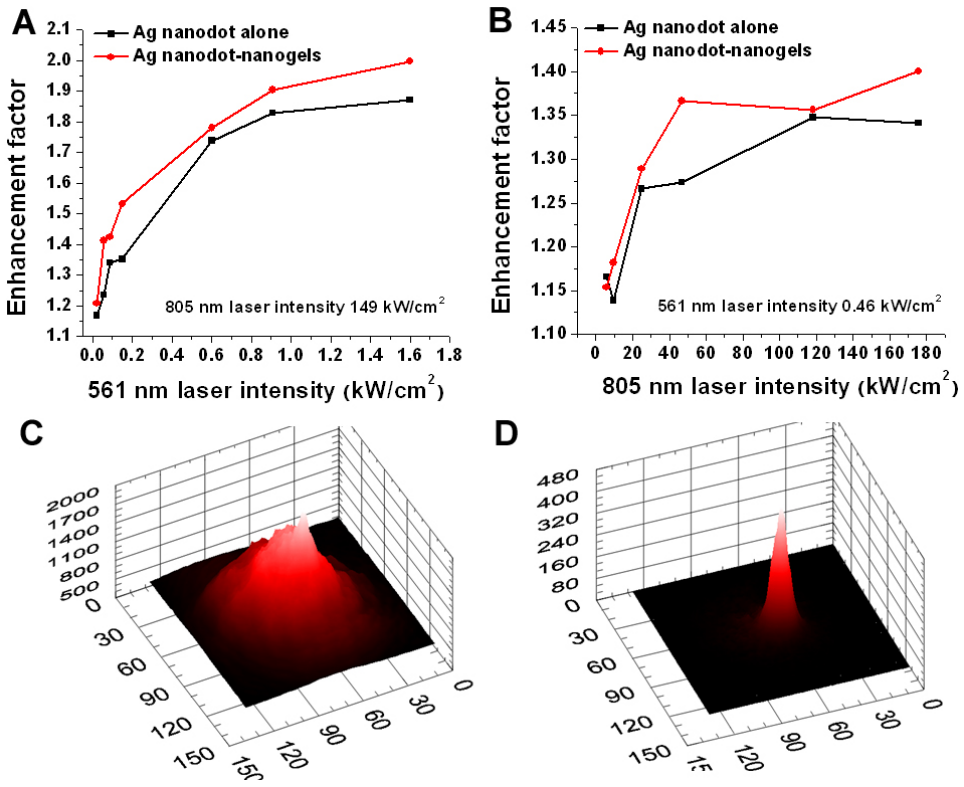

Figure 4-11. Comparison of enhancement between 615 nm Ag nanodot itself and 615 nm Ag nanodot-nanogel depending on varied primary laser intensity (561 nm laser) at fixed secondary laser intensity (805 nm laser, 64.9 kW/cm^2) (A), or varied secondary laser intensity (805 nm laser) at fixed 561 nm laser intensity (4.89 kW/cm^2) (B). Samples were prepared by spin coating of Ag nanodot-nanogel solution. C and D, Images of Ag nanodot-nanogel solution on glass cover slip with constant defocused 561 nm laser and optically chopped 805 nm laser excitation, before (C) and after demodulation (D). 615 nm Ag nanodot produced within 5′-CGCGCCCC CCCCCCCCCGCG-3′.

monitoring and tracking target *in vivo*, the gel system should be demodulated even in solution. This is demonstrated in Figure 4-11C and 4-11D in which the strong, universal emission from bulk solution of Ag nanodots-nanogels, representing more scattering in liquid and thus high background and weak signals inside cells or tissues, was demodulated, resulting in dramatically decreased background. This result is promising to show that gel system incorporating with Ag nanodots may be useful for *in vivo* studies, e.g., drug delivery.

4-4. Conclusions

Silver nanodots can be encapsulated into hydrophobic PLGA particles and hydrophilic nanogels. After encapsulation, they still retain their characteristic photophysics in such new environments, such as excellent brightness under either one photon excitation or two photon excitation. Moreover, the resulting silver nanodot-nanogel/PLGA systems still show strong fluorescence enhancement when the fluorophores are irradiated with an extra lower energy secondary laser, which is useful to obtain higher signal to noise ratio in high background environments. These primary data indicate that it may be possible to apply these nanodots for *in vivo* imaging.

4-5. References

1. Rao, J.H., Dragulescu-Andrasi, A. & Yao, H.Q. Fluorescence imaging in vivo: recent advances. *Curr. Opin. Biotechnol.* **18**, 17-25 (2007).

2. Chan, W.C.W. & Nie, S.M. Quantum dot bioconjugates for ultrasensitive nonisotopic detection. *Science* **281**, 2016-2018 (1998).

3. Kim, J. et al. Designed fabrication of a multifunctional polymer nanomedical platform for simultaneous cancer-targeted imaging and magnetically guided drug delivery. *Adv. Mater.* **20**, 478- 483 (2008).

4. Chowdhury, E.H. & Akaike, T. Bio-functional inorganic materials: An attractive branch of gene-based nano-medicine delivery for 21st century. *Curr. Gene Ther.* **5**, 669-676 (2005).

5. Evgenov, N.V., Medarova, Z., Dai, G.P., Bonner-Weir, S. & Moore, A. In vivo imaging of islet transplantation. *Nat. Med.* **12**, 144-148 (2006).

6. Janes, K.A., Calvo, P. & Alonso, M.J. Polysaccharide colloidal particles as delivery systems for macromolecules. *Adv. Drug Deliv. Rev.* **47**, 83-97 (2001).

7. Otsuka, H., Nagasaki, Y. & Kataoka, K. PEGylated nanoparticles for biological and pharmaceutical applications. *Adv. Drug Deliv. Rev.* **55**, 403-419 (2003).

8. Phillips, W.T. Delivery of gamma-imaging agents by liposomes. *Adv. Drug Deliv. Rev.* **37**, 13-32 (1999).

9. Torchilin, V.P. Targeting of drugs and drug carriers within the cardiovascular-system. *Adv. Drug Deliv. Rev.* **17**, 75-101 (1995).

10. Sofou, S. & Sgouros, G. Anti body-targeted liposomes in cancer therapy and imaging. *Expert Opin. Drug Del.* **5**, 189-204 (2008).

11. Ikehara, Y. & Kojima, N. Development of a novel oligomannose-coated liposome-based anticancer drug-delivery system for intraperitoneal cancer. *Curr.Opin. Mol. Ther.* **9**, 53-61 (2007).

12. Khuller, G.K., Kapur, M. & Sharma, S. Liposome technology for drug delivery against mycobacterial infections. *Curr. Pharm. Design* **10**, 3263-3274 (2004).

13. Slowing, II, Vivero-Escoto, J.L., Wu, C.W. & Lin, V.S.Y. Mesoporous silica nanoparticles as controlled release drug delivery and gene transfection carriers. *Adv. Drug Deliv. Rev.* **60**, 1278-1288 (2008).

14. Radin, S., El-Bassyouni, G., Vresilovic, E.J., Schepers, E. & Ducheyne, P. In vivo tissue response to resorbable silica xerogels as controlled-release materials. *Biomaterials* **26**, 1043-1052 (2005).

15. Arvizo, R., Bhattacharya, R. & Mukherjee, P. Gold nanoparticles: opportunities and challenges in nanomedicine. *Expert Opin. Drug Del.* **7**, 753-763 (2010).

16. Boisselier, E. & Astruc, D. Gold nanoparticles in nanomedicine: preparations, imaging, diagnostics, therapies and toxicity. *Chem. Soc. Rev.* **38**, 1759-1782 (2009).

17. Patra, C.R., Bhattacharya, R., Mukhopadhyay, D. & Mukherjee, P. Fabrication of gold nanoparticles for targeted therapy in pancreatic cancer. *Adv. Drug Deliv. Rev.* **62**, 346-361 (2010).

18. Soppimath, K.S., Aminabhavi, T.M., Kulkarni, A.R. & Rudzinski, W.E. Biodegradable polymeric nanoparticles as drug delivery devices. *J. Control. Release* **70**, 1-20 (2001).

19. Tosi, G., Costantino, L., Ruozi, B., Forni, F. & Vandelli, M.A. Polymeric nanoparticles for the drug delivery to the central nervous system. *Expert Opin. Drug Del.* **5**, 155-174 (2008).

20. Raemdonck, K., Demeester, J. & De Smedt, S. Advanced nanogel engineering for drug delivery. *Soft Matter* **5**, 707-715 (2009).

21. Singh, N. & Lyon, L.A. Au nanoparticle templated synthesis of pNIPAm nanogels. *Chem. Mat.* **19**, 719-726 (2007).

22. Pich, A. et al. Biocompatible Hybrid Nanogels. *Small* **4**, 2171-2175 (2008).

23. Raemdonck, K. et al. Biodegradable Dextran Nanogels for RNA Interference: Focusing on Endosomal Escape and Intracellular siRNA Delivery. *Adv. Func. Mater.* **19**, 1406-1415 (2009).

24. Oh, J.K. et al. Biodegradable nanogels prepared by atom transfer radical polymerization as potential drug delivery carriers: Synthesis, biodegradation, in vitro release, and bioconjugation. *J. Am. Chem. Soc.* **129**, 5939-5945 (2007).

25. Oh, J.K., Drumright, R., Siegwart, D.J. & Matyjaszewski, K. The development of microgels/nanogels for drug delivery applications. *Prog. Polym. Sci.* **33**, 448-477 (2008).

26. Jeong, J.H., Kim, S.W. & Park, T.G. Molecular design of functional polymers for gene therapy. *Prog. Polym. Sci.* **32**, 1239-1274 (2007).

27. Anderson, J.M. & Shive, M.S. Biodegradation and biocompatibility of PLA and PLGA microspheres. *Adv. Drug Deliv. Rev.* **28**, 5-24 (1997).

28. Jain, R.A. The manufacturing techniques of various drug loaded biodegradable poly(lactide-co-glycolide) (PLGA) devices. *Biomaterials* **21**, 2475-2490 (2000).

29. Lu, J.M. et al. Current advances in research and clinical applications of PLGA-based nanotechnology. *Expert Rev. Mol. Diagn.* **9**, 325-341 (2009).

30. Ferrari, M. Cancer nanotechnology: Opportunities and challenges. *Nat.Rev. Cancer* **5**, 161-171 (2005).

31. Prinzen, L. et al. Optical and magnetic resonance imaging of cell death and platelet activation using annexin A5-functionalized quantum dots. *Nano Lett.* **7**, 93-100 (2007).

32. Gindy, M.E. & Prud'homme, R.K. Multifunctional nanoparticles for imaging, delivery and targeting in cancer therapy. *Expert Opin. Drug Del.* **6**, 865-878 (2009).

33. Oishi, M., Tamura, A., Nakamura, T. & Nagasaki, Y. A Smart Nanoprobe Based On Fluorescence-Quenching PEGylated Nanogels Containing Gold Nanoparticles for Monitoring the Response to Cancer Therapy. *Adv. Funct. Mater.* **19**, 827-834 (2009).

34. Richards, C.I. et al. Optically Modulated Fluorophores for Selective Fluorescence Signal Recovery. *J. Am. Chem. Soc.* **131**, 4619-4621 (2009).

35. Debord, J.D. & Lyon, L.A. On the unusual stability of succinimidyl esters in pNIPAm-AAc microgels. *Bioconjugate Chem.* **18**, 601-604 (2007).

36. Tewes, F. et al. Comparative study of doxorubicin-loaded poly(lactide-co-glycolide) nanoparticles prepared by single and double emulsion methods. *Eur. J. Pharm.Biopharm.* **66**, 488-492 (2007).

37. Geddes, C.D., Parfenov, A., Gryczynski, I. & Lakowicz, J.R. Luminescent blinking from silver nanostructures. *J. Phys. Chem. B* **107**, 9989-9993 (2003).

38. Barkai, E., Jung, Y.J. & Silbey, R. Theory of single-molecule spectroscopy: Beyond the ensemble average. *Annu. Rev. Phys. Chem.* **55**, 457-507 (2004).

39. Garcia-Parajo, M.F., Veerman, J.A., Bouwhuis, R., Vallee, R. & van Hulst, N.F. Optical probing of single fluorescent molecules and proteins. *ChemPhysChem* **2**, 347-360 (2001).

40. Gomez, D.E., Califano, M. & Mulvaney, P. Optical properties of single semiconductor nanocrystals. *Phys. Chem. Chem. Phys.* **8**, 4989-5011 (2006).

41. Patel, S.A., Richards, C.I., Hsiang, J.C. & Dickson, R.M. Water-soluble Ag nanoclusters exhibit strong two-photon-induced fluorescence. *J. Am. Chem.Soc.* **130**, 11602-11603 (2008).

42. Richards, C.I. Dynamic dark state depletion a path to high sensitivity imaging. *Ph. D thesis.* Georgia Institute of Technology (2009).

43. Burd, A. et al. A comparative study of the cytotoxicity of silver-based dressings in monolayer cell, tissue explant, and animal models. *Wound Repair Regen.* **15**, 94-104 (2007).

44. Hamiltonmiller, J.M.T., Shah, S. & Smith, C. Silver sulfadiazine - a comprehensive in-vitro reassessment. *Chemotherapy* **39**, 405-409 (1993).

45. Hollinger, M.A. Toxicological aspects of topical silver pharmaceuticals. *Crit. Rev. Toxicol.* **26**, 255-260 (1996).

46. Hussain, S., Anner, R.M. & Anner, B.M. Cysteine protects Na,K-ATPase and isolated human-lymphocytes from silver toxicity. *Biochem. Biophys. Res. Commun.* **189**, 1444-1449 (1992).

47. Ratte, H.T. Bioaccumulation and toxicity of silver compounds: A review. *Environ. Toxicol. Chem.* **18**, 89-108 (1999).

CHAPTER V

Easily Prepared, Photostable, DNA-Encapsulated Gold Nanodots

In this chapter, we describe the creation of ssDNA-protected, water-soluble luminescent gold nanodots. Among the sequences examined, poly-cytosine exhibits strong ability to protect gold nanodots. These nanodots with a 640 nm emission show high quantum yield in red emission among these gold nanodots reported, long lifetime, large Stokes shift as well as chemical and photophysical stability. As a proof of concept, cells were co-stained with gold nanodots and a commercial organic dye. In this application, nanodots display not only bright emission, but also extreme photostability. Since their luminescence lifetimes are 4 μs, it is possible that the gold nanodots could be a useful biomarker for time-gated imaging.

5-1. Introduction

In vivo imaging has attracted lots of attention in the last decade, in the effort to develop non-invasive imaging techniques.[1, 2] While magnetic resonance imaging (MRI) has been widely used as a diagnostic tool,[3] optical imaging system is just being developed for this purpose,[2, 4] giving the higher sensitivity, resolution and

efficacy when light is used as an information medium.[2, 5] The key to successful extraction of useful information from imaging is to increase the signal to noise ratio. One solution is to develop highly bright fluorophores. Studies on fluorophores such as quantum dots and noble nanoparticles have also been spotlighted.[6-8] Unlike conventional organic dyes, quantum dots (QDs) exhibit 10-100 fold higher extinction coefficient, enabling efficient absorption of photons in the dim environments.[9] However, QDs still have drawbacks such as cytotoxicity and large size hindering its wide biological application.

Of noble metal nanoparticles, beyond the previously mentioned silver nanodots, gold nanoparticles have been actively developed due to relatively easy synthesis, accessible modification of their surface by conjugating biomolecules, low toxicity as well as size-tuned optical and electronic properties.[10-15] In the past two decades, a broad range of emissive Au(I) complexes,[16-19] Au nanodots, and nanoparticles [20-29] were synthesized by using organic ligand or combination peptides. In general, a thiol group is one of the most widely used protection group to produce gold nanoclusters by sodium borohydride ($NaBH_4$) reduction. However, the study of water soluble Au nanodots with high luminescence quantum yield (Φ_L) in red region was rarely reported, mostly with very low Φ_L (0.001% - 3%).[20-22] Recently, Ying group reported fluorescent gold nanodot directly synthesized in protein protection, such as bovine serum albumin (BSA), in sodium hydroxide (NaOH) solution.[30] The gold nanoclusters emitted 640 nm excited at 480 nm, and their quantum yield (Φ_L) is about 6%.[30] They successfully approached green chemical synthesis without $NaBH_4$ to produce gold nanoclusters, but the BSA used in the above research may be large

size (66 kDa) for cellular imaging. Also, their photophysical study is not enough. Chang group reported carbohyrated protected gold nanodots. They used tetrakis(hydroxymethyl)phosphonium chloride as a reducing agent and capping materials to prepare gold nanodots, having 618 nm red emission excited at 375 nm.[31] The final gold nanodots were produced by surface modification with 11-mercapto-3,6,9-trioxaundecyl-r-D-mannopyranoside.[31] The resulting nanodots emitted 545 nm excited at 375 nm and quantum yield is 8.6%.[31] So far, this quantum yield is the higher than that of currently available water soluble and alkanethiol-protected gold nanodots. However, the emission was shifted from 618 nm to 545 nm, which means the quantum yield is for green emission. Also, their synthesis is not simple. We have applied single strand DNA (ssDNA) as a scaffold to protect silver nanodots.[32-34] The good affinity of DNA to metal ions, the small size and single-point-modification ability of ssDNA inspired us to apply ssDNA to protect Au nanodots. Herein, we report bright and water-soluble DNA-encapsulated Au nanodots in the red region (640 nm) with a reasonable size, remarkable chemical and photo-physical stability, and high Φ_L (7%) among reported gold nanodots. This unique photophysical property makes them a good promising candidate for biomedical applications and biological imaging.

5-2. Experimental section

Materials

All oligonucleotides were purchased from Bioneer (South Korea) and purified with standard desalting by the manufacturer. All other reagents were purchased from Sigma-Aldrich. Gold (III) chloride trihydrate was used with ≥99.9% purity and sodium borohydride with 98% purity.

Synthesis and characteration of Au nanodots

Most experimental conditions are similar as described in Chapter 2. The DNA-encapsulated Au nanodots were prepared by mixing 53 μM of 20 mer polycytosine (5′-CCCCCCCCCCCCCCCCCCCC-3′; C20) with $HAuCl_4 \cdot 3H_2O$ with a 2:1 molar ratio of base:gold. This solution was kept in dark at room temperature for 60 hours, followed by reduction with two equivalents of aqueous $NaBH_4$ solution (versus gold) under vigorous stirring. A week later, this solution was centrifuged at 100,000 rpm for two hours at 20^{o}C and then the light yellowish brown supernatant was collected for characterization and *in vitro* study.

Luminescence lifetime measurement was performed with an Edinburgh Instruments Lifespec-ps system with a Hamamatsu multi-channel plate photomultiplier tube detector. 10 kHz 532 pulsed laser or 476 diode laser operated at 10 kHz was used for lifetime measurement as the excitation source.

5-3. Results and discussion

Gold nanoparticles have been applied for *in vivo* imaging due to their low toxicity, which partially indicates that gold atoms might have weak binding to biological molecules.[35-37] Most gold nanoparticles and nanodots were prepared under the protection of thiol derivatives.[22, 27, 38] In many applications involving gold and DNA, gold mostly does not interfere with the function of DNA.[39-43] It was not clear if gold ions would interact with ssDNA to form emissive nanodots. Polyadenine (poly A), polyguanine (poly G), polythymine (poly T) and polycytosine (poly C) were mixed with $HAuCl_4$ respectively, followed by sodium borohydride reduction. However, only polycytosine solution shows red emission. Sequences consisting of a combination of varying bases failed to give strong red emission as well. Au nanodots produced under 12 mer polycytosine (5′-CCCCCCCCCCCC-3′, C12), 20 mer polycytosine (5′-CCCCCCCCCCCCCCCCCCCC-3′, C20), or 24 mer polycytosine (5′-CCCCCCCCCCCCCCCCCCCCCCCC-3′, C24), exhibiting similar photophysics, with main emission at 640 nm. The excitation spectrum has a peak at 450 nm. However, the absorption spectrum shows weak broad absorption between 400 and 500 nm, with a small peak merged into the large absorption of DNA (Figure 5-1). However, there is no plasmon absorption from Au nanoparticles (~ 520 nm), indicating that all nanoparticles can be removed after spinning down. Corrected absorption spectrum can be obtained by subtracting the absorption of [DNA + Au^{3+} solution] (before reduction) from [DNA + Au^{3+} + $NaBH_4$ solution] (after reduction), which clearly corresponds to the excitation spectrum of Au nanodots. Control experiments performed under the exact same conditions shows no emission in the

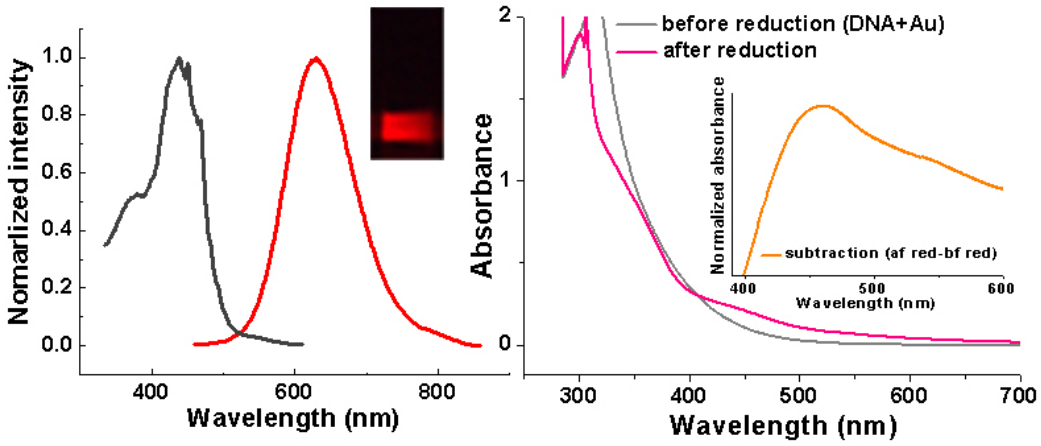

Figure 5-1. Emission and excitation spectra and absorption of C20 Au nanodots. Left, Emission (red) and excitation (black) spectra of C20 Au nanodots. Inset, emission picture of C20-Au nanodots solution under 450 nm excitation; Right, UV-Vis absorption spectra of [DNA + Au^{3+} solution] (gray, before reduction) and [DNA + Au^{3+} + $NaBH_4$ solution] (pink, after reduction). Inset, spectrum after subtraction of absorption spectra (after reduction – before reduction). C20, 5′-CCCCCCCCCCCCCCCCCCCC-3′.

absence of any of these components: gold ions, ssDNA, and chemical reduction, suggesting that emissive Au nanodots are formed. The Au nanodots are extremely stable. The luminescence intensity of this aqueous Au nanodot solution shows almost no change even after more than one year storage at room temperature. In addition, Au nanodots are quite chemically stable in biological environmental including PBS. The DNA-Au nanodots synthesized in deionized water were put into PBS, and checked at room temperature. As shown in Figure 5-2, the emission is quite stable. The Au nanodots in PBS just 14% decreased than that in deionized water.

Our DNA-encapsulated Au nanodots have a long lifetime (4 μs), large Stokes shift, and moderate quantum yield (7%), similar to gold(I) complexes[17] and europium complex reported recently.[44] The long excited-state lifetime can be applied for lifetime imaging in which emission from the longer lifetime of Au nanodots is distinguished from nanosecond autofluorescence by time-gated microscopy, resulting in higher signal to noise ratio.[45-47] Furthermore, the large Stokes shift enables more compatible multi-color staining together with conventional organic dyes which often exhibit very small Stokes shifts.

The great advantage of our Au nanodots over either Au (I) complexes or europium complexes is they are oxygen-insensitive. For instance, luminescence from Au(I) or Eu complexes involve either the triplet excited state of gold (I) complexes or the sensitization of europium complexes by triplet excited state sensitizer, which will be greatly interfered with oxygen, and consequently the generation of harmful activated oxygen is also undesirable in biological

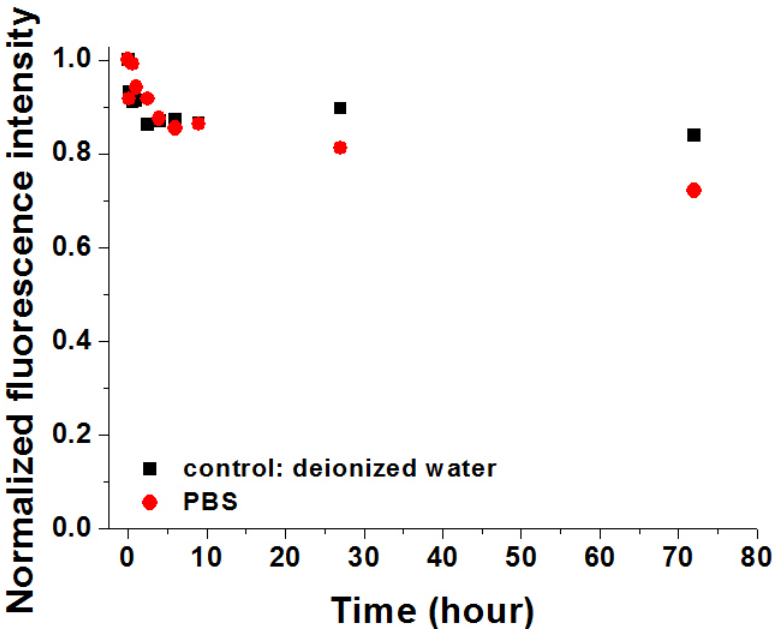

Figure 5-2. Stability of DNA-Au nanodots in PBS (red) and deionized water (black, control) at room temperature. Emission was monitored at 650 nm with 450 nm excitation.

applications.[48] However, DNA-encapsulated Au nanodots are oxygen-insensitive; removal of oxygen from the Au nanodot solution did not change the luminescence intensity. Moreover, our Au nanodots can be efficiently excited with 458 nm and even 488 nm of Ar-laser which is equipped generally for confocal microscopy. Whereas, europium complexes require sensitizers with absorption near 405 nm, a wavelength that may generate high auto-fluorescence level and may damage cells.[49]

Different from ssDNA-protected silver nanodots, the emission wavelength of Au nanodots does not shift much when adjusting the sequence of protection ssDNA. Therefore, we tried to tune the Au nanodot emission by mixing Au with other metals, as reported previously.[15, 50] The results indicate that emission from the Au nanodots was affected by other metals, but the emission wavelength was not adjusted well. Here we used C12 as an example. The addition of Ag(I) ions to the C12-Au (III) solution with a Ag/Au of 1:1, followed by sodium borohydride reduction, yielded similar 640 emission. However, the new Au/Ag nanodots (Au/Ag ND-1) exhibit about 2.5-fold lower emission intensity (Figure 5-3) but similar lifetime (5 μs).

On the contrary, the addition of Au (III) to a mixture of Ag (I) and DNA prior to reduction showed no emission. It may indicate that Au (III) has a stronger affinity to C12 than Ag (I). The first-added Au (III) binds to ssDNA firmly and then forms Au nanodots well. However, the first-added Ag (I) interfered with the subsequently added Au (III) and could not form regular DNA-protected Ag nanodots. This phenomenon can also be demonstrated by adding Au (III) ions to DNA-protected Ag nanodots, which leads to the disappearance of regular red emission of Ag nanodots, and the generation of blue emission likely as a consequence of oxidation of Ag

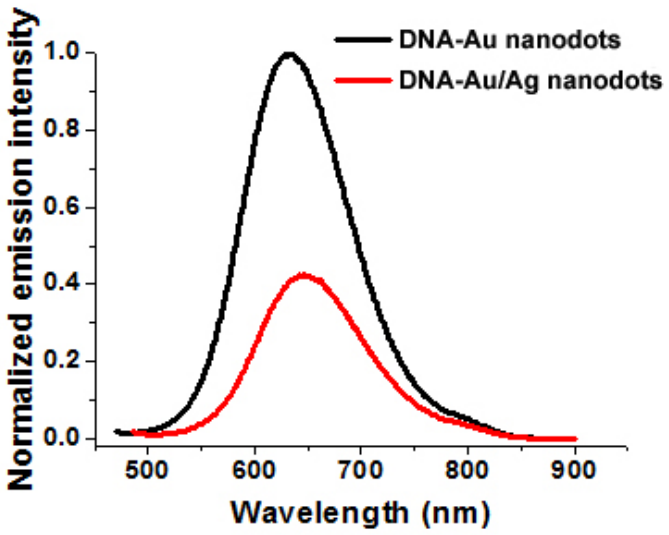

Figure 5-3. Emission intensity comparison. Emission intensity of DNA-Au nanodots (black) is much higher than that of DNA-Au/Ag (added Ag+ into Au3+ before reduction, Au/Ag of 1:1) nanodots (red). Samples were excited at 450 nm.

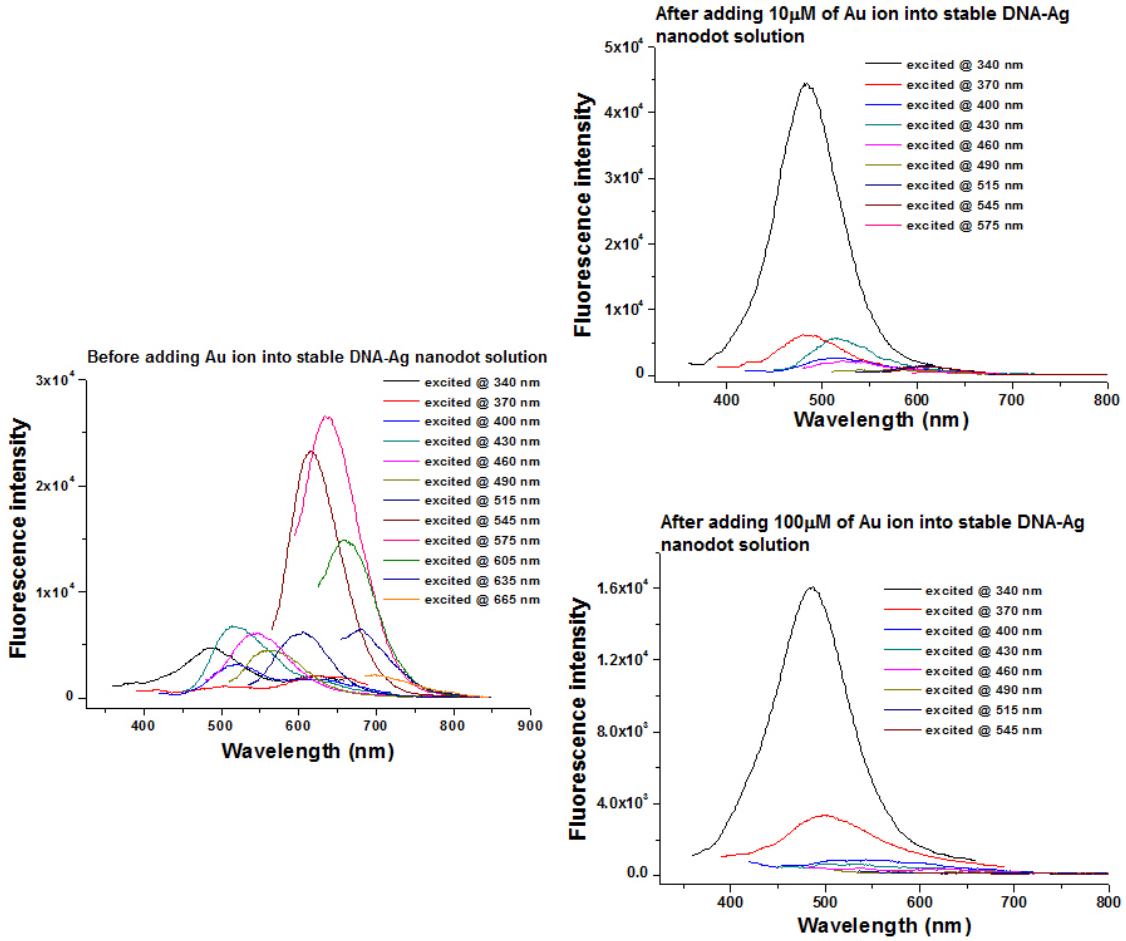

Figure 5-4. Full-scanned emission spectra of gold/silver nanodots solution. Stable DNA-encapsulated Ag nanodots before Au(III) added (left), in-situ emission after adding 10 μM of Au (III) into stable DNA-Ag nanodots (upper right), in-situ emission after adding 100 μM of Au (III) into stable DNA-Ag nanodots (lower right).

nanodots by Au (III) as shown in Figure 5-4. Reduction of the above mixture by sodium borohydride results in a mixture of emissions from both Ag nanodots and Au nanodots as indicated by their characteristic excitation wavelengths (though both have 640 nm emissions, Au nanodots are excited at 458 nm while Ag nanodots at 560 nm.) and lifetimes as shown in Figure 5-5. The emission from Ag nanodots is gradually replaced by Au nanodots and the final less photostable Au/Ag nanodots exhibit a lifetime of 1.8 μs, which is different from either the pure Au nanodots or the Au/Ag ND-1. However, in a reverse case (adding Ag ions into DNA-Au nanodots), Au emission is not much influenced (Figure 5-6a), with a blue shift of about 20 nm. This may indicate the Au(III) /Au(0) has stronger binding affinity to cytosine compared to Ag(I)/Ag(0). However, Cu(II) has stronger influence on the stability of gold nanodots. At low Cu(II) concentration (10 μM), the emission of nanodots decreases 30%, but disappeared at higher Cu(II) concentration (100 μM) as shown in Figure 5-6b. Since the redox potential of Cu(II)/Cu(0) is 0.34, while Ag(I)/Ag(0) is 0.80, it is not likely Au nanodots are oxidized by Cu(II) because the higher redox Ag(I)/Ag(0) does not interfere with the gold nanodot emission. The quenching of the emission of Au nanodots might be due to stronger binding of Cu(II) to cytosine. There are reports on the binding to Cu(II) to DNA sequence, but no available data on their exact binding affinity.[51]

The gold nanodots exhibit not only good chemical stability but also good photostability. Methanol-fixed NIH 3T3 cells were incubated with C20-encapsulated Au nanodot solution (3 μM) overnight, and then stained with Sytox Green nucleic acid stain (Invitrogen) which selectively stains the nuclei of cells. The large Stokes

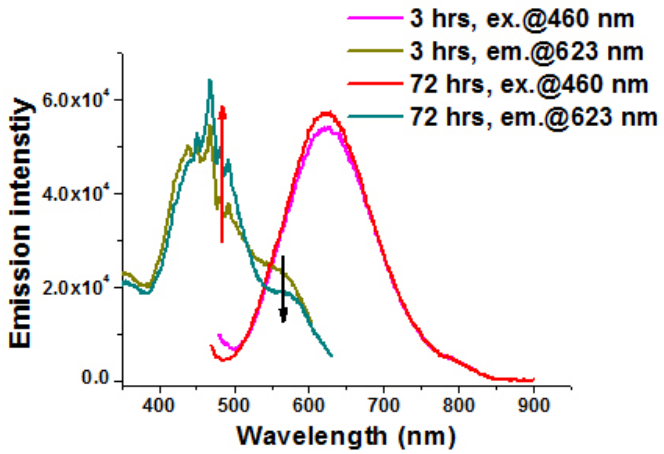

Figure 5-5. Emission and excitation spectra of Au/Ag nanodots after reduction by $NaBH_4$ to a mixture of Au (100 μM) and stable DNA-Ag nanodots solution (50 μM). As indicated by arrows, the excitation spectra showed increase at 450 nm region (more Au nanodots formed) but decrease at 560 nm region (fewer Ag nanodots left).

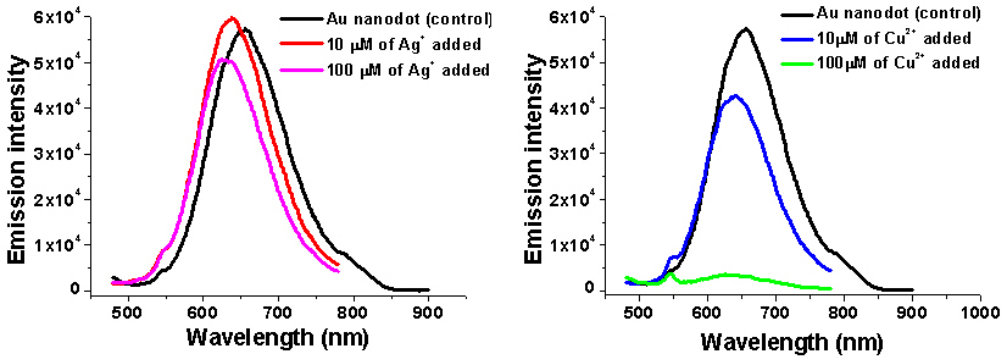

Figure 5-6. Emission spectra trace after adding different concentrated metal. (a) After adding 10 μM (red) or 100 μM (pink) of Ag (I) into stable DNA-Au nanodots. (b) After adding 10 μM (blue) or 100 μM (green) of Cu (II) into stable DNA-Au nanodots. Stable DNA-Au nanodots solution was used for a control in both (a) and (b) (black).

shift of Au nanodots enable multicolor staining with Au nanodots and Sytox Green with the same excitation at 458 nm, but detection at BP 505-550 nm for Sytox Green and BP 590-690 nm for Au nanodots. As shown in Figure 5-7, the Au nanodots display diffuse staining of the cytoplasm, and Sytox Green localizes in the nuclei. Compared to Sytox Green (green), the gold nanodots (red) are extremely photostable. After more than two hours with continuous confocal scanning (2 min 5s/full scan), the gold nanodots were still bright and the mean intensity of Au nanodots decreased only 25%. However, Sytox Green quickly bleached after a few scans. Other organic dyes may show better stability than Sytox green. However the excellent photostability of gold nanodots suggests that these nanodots can be potentially useful for long time imaging. Together with their large Stokes shift and long lifetime, the Au nanodots might be quite useful for biological labeling, *in vitro* staining, and lifetime imaging. Furthermore, DNA can be readily single-point-conjugated to other target molecules by modification of ssDNA, so more specific applications with live cell and antibody-conjugated Au nanodots for specific cell staining are currently underway

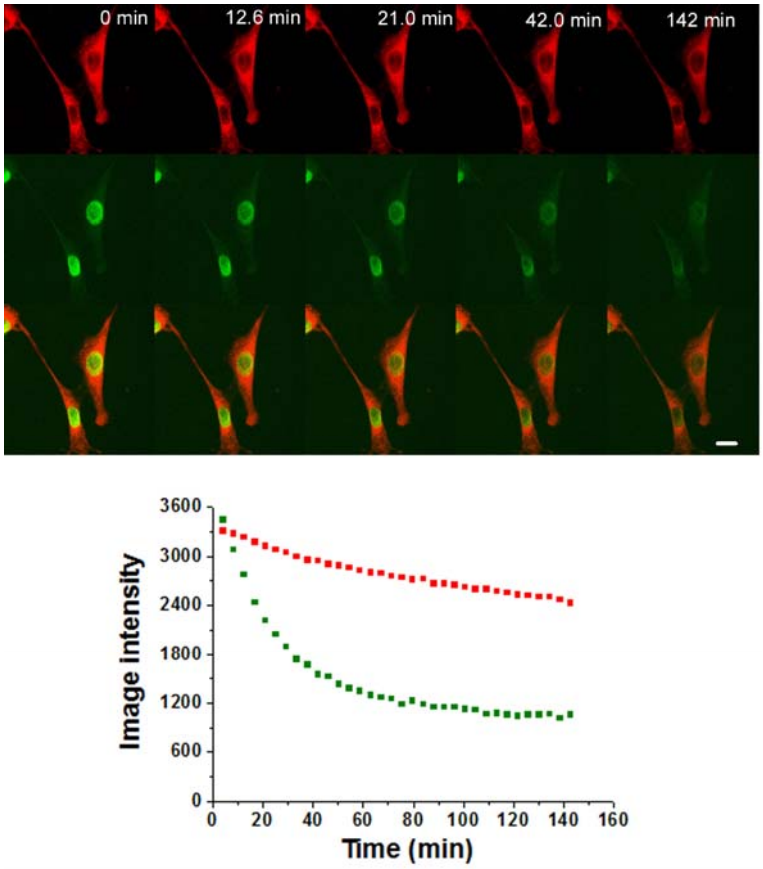

Figure 5-7. (a) The confocal images of NIH 3T3 cells loaded with C20-Au nanodots and Sytox ® Green nucleic acid stain were shown with different time trace. Emission images from Au nanodots (up) and Sytox ® Green nucleic acid stain (middle) were merged in bottom row. All images were taken by Carl Zeiss Inc. LSM 510 UV confocal microscope (both were excited at 458 nm, the emission form C20-Au nanodots were detected between 590-690 nm, and the emission from Sytox ® Green nucleic acid stain were detected between 505-550 nm). Scale bar: 30 μm. (b) The time profiles (survival time vs. intensity) of above confocal images (mean distribution). C20, 5′-CCCCCCCCCCCCCCCCCCCC-3′.

5-4. Conclusions

In summary, with DNA scaffold we easily synthesized bright and water-soluble luminescent gold nanodots. These nanodots also have excellent photostability, large Stokes shift, long lifetime, and moderate quantum yield among these long lifetime chromophores. These photophysical properties give DNA-encapsulated Au nanodots good advantages for biological applications including cell staining. Due to their long lifetimes, it might not be ideal for single molecule imaging. However, when employing time-gated imaging techniques, the gold nanodots could be a useful biomarker for biological applications.

5-5. References

1. Pierce, M.C., Strasswimmer, J., Park, B.H., Cense, B. & de Boer, J.F. Advances in optical coherence tomography imaging for dermatology. *J. Invest. Dermatol.* **123**, 458-463 (2004).

2. Ntziachristos, V., Ripoll, J., Wang, L.H.V. & Weissleder, R. Looking and listening to light: the evolution of whole-body photonic imaging. *Nat. Biotechnol.* **23**, 313-320 (2005).

3. Sun, C., Lee, J.S.H. & Zhang, M.Q. Magnetic nanoparticles in MR imaging and drug delivery. *Adv. Drug Deliv. Rev.* **60**, 1252-1265 (2008).

4. Frangioni, J.V. In vivo near-infrared fluorescence imaging. *Curr. Opin. Chem. Biol.* **7**, 626-634 (2003).

5. Bastiaens, P.I.H. & Squire, A. Fluorescence lifetime imaging microscopy: spatial resolution of biochemical processes in the cell. *Trends Cell Biol.* **9**, 48-52 (1999).

6. Bruchez, M., Moronne, M., Gin, P., Weiss, S. & Alivisatos, A.P. Semiconductor nanocrystals as fluorescent biological labels. *Science* **281**, 2013-2016 (1998).

7. Medintz, I.L., Uyeda, H.T., Goldman, E.R. & Mattoussi, H. Quantum dot bioconjugates for imaging, labelling and sensing. *Nat. Mater.* **4**, 435-446 (2005).

8. Boisselier, E. & Astruc, D. Gold nanoparticles in nanomedicine: preparations, imaging, diagnostics, therapies and toxicity. *Chem. Soc. Rev.* **38**, 1759-1782 (2009).

9. Chan, W.C.W. & Nie, S.M. Quantum dot bioconjugates for ultrasensitive nonisotopic detection. *Science* **281**, 2016-2018 (1998).

10. Connor, E.E., Mwamuka, J., Gole, A., Murphy, C.J. & Wyatt, M.D. Gold nanoparticles are taken up by human cells but do not cause acute cytotoxicity. *Small* **1**, 325-327 (2005).

11. Ghosh, P., Han, G., De, M., Kim, C.K. & Rotello, V.M. Gold nanoparticles in delivery applications. *Adv. Drug Deliv. Rev.* **60**, 1307-1315 (2008).

12. Hainfeld, J.F. & Powell, R.D. New frontiers in gold labeling. *J. Histochem. Cytochem.* **48**, 471-480 (2000).

13. Lin, C.-A. et al. Synthesis of Fluorescent Metallic Nanoclusters toward Biomedical Application: Recent Progress and Present Challenges. *J. Med. Biol. Eng.* **29**, 8 (2009).

14. Zheng, J., Nicovich, P.R. & Dickson, R.M. Highly fluorescent noble-metal quantum dots. *Annu. Rev. Phys. Chem.* **58**, 409-431 (2007).

15. Huang, C.C. et al. Synthesis of wavelength-tunable luminescent gold and gold/silver nanodots. *J. Mater. Chem.* **19**, 755-759 (2009).

16. Che, C.M. et al. Spectroscopy, photoredox properties and x-ray crystal-structures of triangular gold(i) and silver(i) phosphine complexes. *J. Chem. Soc.-Dalton Trans.*, 427-433 (1992).

17. Wang, Q.M. et al. Intensely luminescent gold(I)-silver(I) cluster complexes with tunable structural features. *J. Am. Chem. Soc.* **126**, 9488-9489 (2004).

18. Xiao, H., Weng, Y.X., Wong, W.T., Mak, T.C.W. & Che, C.M. Structures and luminescent properties of polynuclear gold(I) halides containing bridging phosphine ligands. *J. Chem. Soc.-Dalton Trans.*, 221-226 (1997).

19. Zhang, T.L., Drouin, M. & Harvey, P.D. Preparation, spectroscopic characterization, and frontier MO study of the heteronuclear luminescent [Pt2Au2(dmb)(2)(PPh3)(4)] (PF6)(2) cluster (dmb=1,8-diisocyano-p-menthane). A cluster with a formal Au-0-Au-0 bond encapsulated inside a "Pt-2(dmb)(2)(2+) " fragment. *Inorg. Chem.* **38**, 4928-4936 (1999).

20. Bigioni, T.P., Whetten, R.L. & Dag, O. Near-infrared luminescence from small gold nanocrystals. *J. Phys. Chem. B* **104**, 6983-6986 (2000).

21. Huang, T. & Murray, R.W. Visible luminescence of water-soluble monolayer- protected gold clusters. *J. Phys. Chem. B* **105**, 12498-12502 (2001).

22. Link, S. et al. Visible to infrared luminescence from a 28-atom gold cluster. *J. Phys. Chem. B* **106**, 3410-3415 (2002).

23. Negishi, Y. & Tsukuda, T. Visible photoluminescence from nearly monodispersed Au-12 clusters protected by meso-2,3-dimercaptosuccinic acid. *Chem. Phys. Lett.* **383**, 161-165 (2004).

24. Yang, Y.Y. & Chen, S.W. Surface manipulation of the electronic energy of subnanometer-sized gold clusters: An electrochemical and spectroscopic investigation. *Nano Lett.* **3**, 75-79 (2003).

25. Wilcoxon, J.P., Martin, J.E., Parsapour, F., Wiedenman, B. & Kelley, D.F. Photoluminescence from nanosize gold clusters. *J. Chem. Phys.* **108**, 9137-9143 (1998).

26. Negishi, Y. et al. Magic-numbered Au-n clusters protected by glutathione monolayers (n=18, 21, 25, 28, 32, 39): Isolation and spectroscopic characterization. *J. Am. Chem. Soc.* **126**, 6518-6519 (2004).

27. Negishi, Y. & Tsukuda, T. One-pot preparation of subnanometer-sized gold clusters via reduction and stabilization by meso-2,3-dimercaptosuccinic acid. *J. Am. Chem. Soc.* **125**, 4046-4047 (2003).

28. Schaaff, T.G., Knight, G., Shafigullin, M.N., Borkman, R.F. & Whetten, R.L. Isolation and selected properties of a 10.4 kDa Gold : Glutathione cluster compound. *J. Phys. Chem. B* **102**, 10643-10646 (1998).

29. Lin, C.A.J. et al. Synthesis, Characterization, and Bioconjugation of Fluorescent Gold Nanoclusters toward Biological Labeling Applications. *Acs Nano* **3**, 395-401 (2009).

30. Xie, J.P., Zheng, Y.G. & Ying, J.Y. Protein-Directed Synthesis of Highly Fluorescent Gold Nanoclusters. *J. Am. Chem. Soc.* **131**, 888-889 (2009).

31. Huang, C.C., Chen, C.T., Shiang, Y.C., Lin, Z.H. & Chang, H.T. Synthesis of Fluorescent Carbohydrate-Protected Au Nanodots for Detection of Concanavalin A and Escherichia coli. *Anal. Chem.* **81**, 875-882 (2009).

32. Petty, J.T., Zheng, J., Hud, N.V. & Dickson, R.M. DNA-templated Ag nanocluster formation. *J. Am. Chem. Soc.* **126**, 5207-5212 (2004).

33. Richards, C.I. et al. Oligonucleotide-stabilized Ag nanocluster fluorophores. *J. Am. Chem. Soc.* **130**, 5038-5039 (2008).

34. Ritchie, C.M. et al. Ag nanocluster formation using a cytosine oligonucleotide template. *J. Phys. Chem. C* **111**, 175-181 (2007).

35. Lee, S. et al. A near-infrared-fluorescence-quenched gold-nanoparticle imaging probe for in vivo drug screening and protease activity determination. *Angew. Chem.-Int. Edit.* **47**, 2804-2807 (2008).

36. Mei, B.C., Susumu, K., Medintz, I.L. & Mattoussi, H. Polyethylene glycol-based bidentate ligands to enhance quantum dot and gold nanoparticle stability in biological media. *Nat. Protoc.* **4**, 412-423 (2009).

37. Murphy, C.J. et al. Gold Nanoparticles in Biology: Beyond Toxicity to Cellular Imaging. *Accounts Chem. Res.***41**, 1721-1730 (2008).

38. Huang, C.C., Yang, Z., Lee, K.H. & Chang, H.T. Synthesis of highly fluorescent gold nanoparticles for sensing Mercury(II). *Angew. Chem.-Int. Edit.* **46**, 6824-6828 (2007).

39. Dubertret, B., Calame, M. & Libchaber, A.J. Single-mismatch detection using gold-quenched fluorescent oligonucleotides. *Nat. Biotechnol.* **19**, 365-370 (2001).

40. Lu, Y. & Liu, J.W. Functional DNA nanotechnology: emerging applications of DNAzymes and aptamers. *Curr. Opin. Biotechnol.* **17**, 580-588 (2006).

41. Nel, A.E. et al. Understanding biophysicochemical interactions at the nano-bio interface. *Nat. Mater.* **8**, 543-557 (2009).

42. Pissuwan, D., Cortie, C.H., Valenzuela, S.M. & Cortie, M.B. Functionalised gold nanoparticles for controlling pathogenic bacteria. *Trends Biotechnol* **28**, 207-213 (2010).

43. Schultz, D.A. Plasmon resonant particles for biological detection. *Curr. Opin. Biotechnol.* **14**, 13-22 (2003).

44. Yu, J.H., Parker, D., Pal, R., Poole, R.A. & Cann, M.J. A europium complex that selectively stains nucleoli of cells. *J. Am. Chem. Soc.* **128**, 2294-2299 (2006).

45. Alpturk, O. et al. Lanthanide complexes as fluorescent indicators for neutral sugars and cancer biomarkers. *Proc. Natl. Acad. Sci. U. S. A.* **103**, 9756-9760 (2006).

46. Connally, R.E. & Piper, J.A. in Fluorescence Methods and Applications: Spectroscopy, Imaging, and Probes, Vol. 1130. (ed. O.S. Wolfbeis) 106-116 (2008).

47. Wu, J. et al. Luminescent europium nanoparticles with a wide excitation range from UV to visible light for biolabeling and time-gated luminescence bioimaging. *Chem. Commun.*, 365-367 (2008).

48. Montgomery, C.P., Murray, B.S., New, E.J., Pal, R. & Parker, D. Cell-Penetrating Metal Complex Optical Probes: Targeted and Responsive Systems Based on Lanthanide Luminescence. *Accounts Chem. Res.* **42**, 925-937 (2009).

49. Pandya, S., Yu, J.H. & Parker, D. 2757-2766 (Royal Soc Chemistry, 2006).

50. Larochelle, C.L. & Patterson, H.H. Tunable photoluminescence for a novel silver-gold mixed metal system. *Chem. Phys. Lett.* **429**, 440-444 (2006).

51. Geierstanger, B.H., Kagawa, T.F., Chen, S.L., Quigley, G.J. & Ho, P.S. Base-specific binding of copper(II) to Z-DNA. *J. Biol. Chem.* **266**, 20185-20191 (1991).

CONCLUSIONS AND FUTURE OUTLOOK

Though as a emerging field, silver nanodot has been shown to be a new type of promising fluorophore with excellent photophysics, potentially useful for single molecule imaging and *in vivo* imaging. Its spectral purity, as a requisite for imaging agents, has been greatly improved by engineering the protective ssDNA sequence as well as preparation conditions. The introduction of hairpin structure of the DNA was one of the strategies, leading to the synthesis of outstanding silver nanodots with highly spectral purity, decent fluorescence quantum yield and much higher fluorophore concentration. However, different from organic fluorophores that are constructed with relatively stable covalent bonds, silver nanodots are protected partially by coordination bonds. In other words, any component having stronger affinity to silver in the solution will compete with the DNA protection group, resulting in destabilization of silver nanodots. Building up a strong protection group for silver nanodots, for example, increasing the melting temperature of hairpin DNA, can delay the deterioration of silver nanodots in harsh conditions.

A stable silver nanodot can be therefore applied to cellular imaging. Though the nonspecific staining still appears to be an issue, multi-color staining by multi-silver nanodot emitters was achieved in fixed cells. Moreover, the stability and brightness of silver nanodots in live cells were also examined to be best so far. However, it would be still a challenge to prepare the highly pure silver nanodot-DNA complex, considering that the current synthetic yield of DNA-protected silver nanodots is less than 3%, and the

applied silver nanodots are actually a mixture of free DNA, non-reduced silver-DNA complex, and silver nanodot-DNA complex. Once the purer silver nanodots are obtained, the total amount of [silver + DNA] will be much less and consequently non-specific staining will be lessened.

Nevertheless, the chemical stability of silver nanodots in drug delivery vehicles is not always a problem. For nanogel, however, it is a relatively open system, and the chemical and thermal stability of silver nanodots are still critical for their applications. When encapsulated in PLGA, DNA-protected silver nanodots retain their photophysics in hydrophobic PLGA particles, promising application to *in vivo* imaging. Combined with fluorescence modulation technique, silver nanodots will be strong candidates as imaging agents to obtain high signal to noise ratio.

The development of perfect silver nanodots requires reasonable scaffold design and laborious ligand screening. There has been a good start via DNA microarrays to screen better silver nanodots. With the contributions of more and more research groups, it will not be far away from the robust silver nanodots ideal for biological applications.